



**HAL**  
open science

# Experimental investigation of the relationship between noise occurrence and the load-bearing area in dry sliding contact

Narinder Singla

► **To cite this version:**

Narinder Singla. Experimental investigation of the relationship between noise occurrence and the load-bearing area in dry sliding contact. Mechanics [physics]. Ecole Centrale de Lille, 2019. English. NNT : 2019ECLI0020 . tel-02926969

**HAL Id: tel-02926969**

**<https://theses.hal.science/tel-02926969v1>**

Submitted on 1 Sep 2020

**HAL** is a multi-disciplinary open access archive for the deposit and dissemination of scientific research documents, whether they are published or not. The documents may come from teaching and research institutions in France or abroad, or from public or private research centers.

L'archive ouverte pluridisciplinaire **HAL**, est destinée au dépôt et à la diffusion de documents scientifiques de niveau recherche, publiés ou non, émanant des établissements d'enseignement et de recherche français ou étrangers, des laboratoires publics ou privés.

**N° d'ordre : 389**

**CENTRALE LILLE**

**THESE**

Présentée en vue d'obtenir le grade de

**DOCTEUR**

En

**Spécialité : Mécanique**

Par

**Narinder SINGLA**

**DOCTORAT DELIVRE PAR CENTRALE LILLE**

Titre de la thèse

Etude expérimentale de la relation entre l'occurrence de bruit et  
l'aire de portance dans un contact sec glissant

Soutenue le 20 decembre 2019 devant le jury d'examen:

<b>Président</b>	Aurélien SAULOT, Professeur à l'INSA Lyon
<b>Rapporteur</b>	Mohamed ICHCHOU, Professeur à Centrale Lyon
<b>Examineur</b>	Caroline RICHARD, Professeur à l'Université de Tours
<b>Encadrant</b>	Jean-François BRUNEL, Maitre de Conférences à l'Université de Lille
<b>Encadrant</b>	Alexandre MEGE-REVIL, Maitre de Conférences à Centrale Lille
<b>Directeur de thèse</b>	Yannick DESPLANQUES, Professeur à Centrale Lille

Thèse préparée au Laboratoire de Mécanique, Multiphysique et Multiechelle - LaMcube  
Univ. Lille, CNRS, Centrale Lille, FRE 2016, F-59000, Lille, France  
Ecole Doctorale SPI 072 (Université de Lille, Université d'Artois, ULCO, UPHF, Centrale Lille)

**Order N° : 389**

**CENTRALE LILLE**

**THESIS**

Presented in view to obtain the degree of

**PhD**

In

**Specialty: Mechanics**

by

**Narinder SINGLA**

**DELIVERED BY CENTRALE LILLE**

Title of the thesis

Experimental investigation of the relationship between noise occurrence and the load-bearing area in dry sliding contact

Defended on 20<sup>th</sup> December 2019

PhD Committee:

<b>President</b>	Aurélien SAULOT, Professor (INSA of Lyon)
<b>Reviewer</b>	Mohamed ICHCHOU, Professeur (Centrale Lyon)
<b>Examiner</b>	Caroline RICHARD, Professor (University of Tours)
<b>Examiner / Tutor</b>	Jean-François BRUNEL, Associate Professor (University of Lille)
<b>Examiner / Tutor</b>	Alexandre MEGE-REVIL, Associate Professor (Centrale Lille)
<b>Thesis Director</b>	Yannick DESPLANQUES, Professor (Centrale Lille)

Thesis prepared in the Laboratoire de Mécanique, Multiphysique et Multiechelle - LaMcube  
Univ. Lille, CNRS, Centrale Lille, FRE 2016, F-59000, Lille, France  
Ecole Doctorale SPI 072 (Université de Lille, Université d'Artois, ULCO, UPHF, Centrale Lille)

# ACKNOWLEDGEMENT

---

This thesis is made possible with the assistance of several persons to whom I would like to express my deep gratitude.

The work presented in this thesis was carried out at the “Laboratoire de Mécanique, Multiphysique, Multiéchelle” (LaMCube), France. Here, I had the opportunity to meet exceptional people both scientifically and humanely. I would like to thank all the professors, research engineers and technicians from LaMCube (Centrale Lille and PolyTech Lille), who helped me, advised me and provided me with the necessary tools to carry out my research work.

I would like to express my sincere thanks to my thesis director Professor Yannick DESPLANQUES for trusting me in leading this thesis. I am proud to have been part of his team. The accuracy of his comments, his desire to always go further, a lot of discussions, has made this work an exciting life experience. His scientific and human qualities have allowed me to surpass myself on many occasions and for that, I am grateful.

I also extend my deep gratitude to my supervisors, Dr. Jean-François BRUNEL and Dr. Alexandre MÈGE-RÉVIL for their help, advice and encouragement, and especially for their availability to lead relevant and fruitful discussions throughout my process. They have put a lot of effort for me to ensure the smooth running of this study from its preparation to its completion.

I am grateful to Professor Aurélien SAULOT and Professor Mohamed ICHCHOU, to accept as the rapporteurs (reviewers) of the thesis and for their interest in my work. I would also like to thank Professor Caroline RICHARD for agreeing to serve as examiner in my thesis jury. It is an honor to have a jury of this scientific quality.

My thanks also go to Dr.- Ing Werner ÖSTERLE and his team members in Department 5.1 of Federal Institute for Materials Research and Testing (Bundesanstalt für Materialforschung und –prüfung) BAM, Berlin for the FIB/SEM characterization of the post-friction materials.

I would like to thank Philippe DUFRENOY, Anne-Lise CRISTOL and Vincent MANGNIER for their expertise, which enabled me to polish my skills.

A special thanks goes to Dr. Edouard DAVIN and Dr. Florent BRUNEL, for technical guide, help with the instrumentations for the experimental part, with their valuable advice and many times with language. I would also like to thank Igor PASZKIEWICZ, François LESAFFRE and Arnaud BEAURAIN for help with the measuring equipment and professional advice. I am thankful to all the persons and friends, especially Nora DAHDAH and Fatma MAKNI, who made my working environment at LaMCube stimulating and pleasant.

I express my gratitude to the friends of all time, from France to India or elsewhere who have provided me with their moral and intellectual support throughout this journey. I would like to express my gratitude to Mohit, Pushpendra, Debarun, Raghav, Ankita and kanika for their help and invaluable support. I want to mention as well my special friends Sumit, Mayank, Parampreet and Shreya for all time encouragement.

A sincere gratitude and regard to my family – Mom, Dad and Dr. Gupta, who have always supported me during my studies and allowed me to carry out whatever I want to do in my life. I got here because of you.

This acknowledgment would not be completed without my full gratitude to Neetu, who shared with me these years, wherever we were, permitting me to forget any distance. You always have been there to back up and shown me, through your love and unconditional support, that I can do it.

# ABSTRACT

---

Friction brakes can induce vibrations and noise, including squealing, which is a major public health concern. Squeal results from dynamic instabilities, leading to high amplitude vibrations and intense noise emissions. Although the phenomenon is well known, the origin of squealing occurrences remains poorly understood. It is recognized that squealing is related to many factors, including the wear of the friction parts. However, the multi-scale nature of physical couplings, the complexity of friction materials and the closed nature of contact are all obstacles to understanding its appearance.

This experimental work is based on the third-body approach and the notion of a tribological circuit to explore the mechanisms originating squeal, considering that flows of third body at the interface continuously change the friction surfaces and thus the load-bearing area during the slip.

The objective of the work is to examine the link between the change of the third body, that of the tribological triplet and the appearance of noise in dry friction conditions. For this purpose, an elementary tribometer dedicated to the analysis of contact vibrations is used, the experiment allowing a monitoring of the interface through a transparent disc and a control of the tribological circuit by the use of an artificial third body and an appropriate contact configuration. The results show in particular that the appearance of squealing is strongly related to the densification and redistribution of the third-body layer in the contact during sliding.

Keywords : Brake squeal, Friction induced vibrations, Tribological circuit, Third-body flows

# RESUME

---

Les freins à friction peuvent induire des vibrations et du bruit, notamment le crissement, qui constitue un enjeu de santé publique majeur. Le crissement résulte d'une instabilité dynamique, responsable de vibrations de grande amplitude et d'émissions sonores intenses. Si le phénomène est bien connu en soi, l'origine des occurrences de crissement demeure mal comprise. Il est reconnu que le crissement est lié à de nombreux facteurs, parmi eux notamment l'usure des organes de friction. La nature multi-échelle des couplages physiques, la complexité des matériaux de friction et la nature fermée du contact, sont cependant autant d'obstacles à la compréhension de son apparition.

Ce travail expérimental s'appuie sur la tribologie à trois corps et la notion de circuit tribologique pour explorer les mécanismes source de crissement, considérant que les écoulements du troisième corps modifient continuellement les surfaces de frottement et donc l'aire de portance pendant le glissement.

L'objectif des travaux est d'examiner le lien entre l'évolution du troisième corps, celle du triplet tribologique et l'apparition du bruit en condition de frottement sec. Pour cela, un tribomètre élémentaire, dédié à l'analyse vibratoire d'un contact est utilisé, l'expérimentation permettant l'observation de l'interface à travers un disque transparent et un contrôle du circuit tribologique par l'usage d'un troisième corps artificiel et d'une configuration de contact appropriée. Les résultats montrent en particulier que l'apparition du crissement est fortement liée à la densification et à la redistribution de la couche de troisième corps dans le contact au cours du glissement.

Mots-clefs : Crissement de frein, Vibrations induites par frottement, Circuit tribologique, Circulation de troisième corps

# TABLE OF CONTENTS

---

<b>ACKNOWLEDGEMENT</b> .....	<b>I</b>
<b>ABSTRACT</b> .....	<b>III</b>
<b>RESUME</b> .....	<b>IV</b>
<b>TABLE OF CONTENTS</b> .....	<b>V</b>
<b>LIST OF FIGURES</b> .....	<b>VIII</b>
<b>LIST OF TABLES</b> .....	<b>XIII</b>
<b>INTRODUCTION</b> .....	<b>2</b>
<b>1 STATE OF THE ART</b> .....	<b>6</b>
1.1 Disc brake system .....	6
1.1.1 Disc brake systems .....	6
1.1.2 Rotor .....	8
1.1.3 Friction materials .....	8
1.2 Brake noises .....	9
1.2.1 Classification of brake noises .....	9
1.2.1.1 Judder .....	10
1.2.1.2 Groan.....	10
1.2.1.3 Low frequency squeal .....	11
1.2.1.4 High frequency squeal .....	11
1.3 Brake squeal measurements .....	11
1.3.1 Experiments .....	11
1.3.2 Parametric influence .....	12
1.3.2.1 Disc thickness variations.....	12
1.3.2.2 Contact surface heterogeneities .....	13
1.3.2.3 Operating conditions .....	13
1.3.3 Analytical models for instability mechanisms .....	15
1.3.3.1 Stick-slip and Negative damping .....	15
1.3.3.2 Sprag-slip .....	15
1.3.3.3 Mode lock-in.....	16
1.3.4 Numerical modeling.....	18



1.4	Tribology & Braking.....	19
1.4.1	The third-body concept.....	19
1.4.2	Load-bearing contact plateaus .....	20
1.4.3	Tribological circuit involved in braking .....	22
1.5	Wear goes in favor of squeal?.....	26
1.5.1	Friction or wear inducing vibration?.....	26
1.5.2	Relationship between morphology of the surface and the squeal.....	29
1.6	Motivation.....	30
<b>2</b>	<b>EXPERIMENT BASE .....</b>	<b>34</b>
2.1	Description of setup & Materials .....	34
2.1.1	Experimental test-rig.....	34
2.1.2	Instrumentation .....	36
2.1.2.1	Disc displacement .....	36
2.1.2.2	Pad displacement and normal load.....	37
2.1.2.3	Frictional torque .....	38
2.1.2.4	Acoustic measurements .....	39
2.2	<i>In-situ</i> contact observation.....	40
2.2.1	First-bodies material .....	41
2.2.2	Experimental approach .....	41
2.2.2.1	Mastery of the apparent area.....	41
2.2.2.2	Introduction of an artificial body .....	43
2.2.3	Observations of the interface evolution .....	44
2.2.4	Limit set for normal load and disc rotational speed.....	45
2.3	Procedure and trial of <i>in situ</i> observation (preliminary tests).....	46
2.3.1	Reference test.....	46
2.3.2	Third-body test.....	47
2.4	Results and discussion .....	48
2.4.1	Noise results and visual description of the LBA (load-bearing area).....	48
2.4.1.1	Reference test.....	48
2.4.1.2	Third-body test.....	50
2.4.2	Influence of the disc undulation.....	54
2.5	Conclusions.....	56

<b>3</b>	<b>DEFINITION OF THE EXPERIMENT PROTOCOL .....</b>	<b>59</b>
3.1	Limit set for normal load and disc rotational speed.....	59
3.2	Experimental configurations:.....	60
3.2.1	Contact on the upper side of the disc (Preliminary tests) .....	60
3.2.2	Contact on the underside of the disc (main tests): .....	61
3.3	Parametric analysis towards criteria for experimental configuration selection	63
3.3.1	Trapping of the third body .....	63
3.3.1.1	Leading-edge design .....	64
3.3.1.2	Pad tilt .....	65
3.3.2	Effect of the third-body recirculation flow .....	69
3.3.3	Effect of the amount of third body.....	70
3.3.4	Test repeatability.....	79
3.4	Synthesis of the protocols for experimental configuration 2 .....	79
3.5	Conclusions.....	84
<b>4</b>	<b>TOWARDS THE EARLY STAGE OF SQUEAL .....</b>	<b>87</b>
4.1	System behavior .....	87
4.2	Experimental procedure .....	88
4.3	Results and discussion .....	90
4.3.1	Normal load and sound pressure.....	90
4.3.2	Friction and pad tilt.....	95
4.4	Characterization of the third-body layer .....	99
4.5	Noise appearances vs third-body layer change .....	102
4.6	Conclusions.....	106
	<b>CONCLUSIONS AND PERSPECTIVES .....</b>	<b>109</b>
	<b>BIBLIOGRAPHY .....</b>	<b>113</b>
	<b>APPENDIX - A.....</b>	<b>122</b>
	<b>RESUME ETENDU.....</b>	<b>124</b>

# LIST OF FIGURES

---

Figure 1.1: Dynamics of braking (Suchal et al. 2013).....	7
Figure 1.2: Brake noise classification (Akay 2002).....	10
Figure 1.3: <b>(a)</b> Fieldhouse and Newcomb’s reconstructed hologram of a squealing disc braking system (the rotor is rotating at 10 rpm, the vibration of the rotor has 8 ND, the frequency of vibration is 10750 Hz and the ND are rotating about the center of the rotor at ~1344 Hz) (Fieldhouse et al. 1993); <b>(b)</b> 3D laser vibrometry measurement (normal displacements) of a squealing disc brake system, the squeal frequency is around 3600 Hz (Duboc et al. 2013).....	12
Figure 1.4: Percentage occurrence of brake squeal having different frequencies for various brake pressures and temperatures (Papinniemi et al. 2002).....	14
Figure 1.5: Friction-velocity slope. stick-slip phenomenon. ....	15
Figure 1.6: Sprag-slip phenomenon (Kinkaid et al. 2003).....	16
Figure 1.7: Mode coupling mechanism (Hoffmann et al. 2002).....	17
Figure 1.8: Mode coupling behavior of the system (Hoffmann et al. 2002).....	18
Figure 1.9: Schematic of the contact situation between an organic brake pad and a brake disc, involving contact plateaus with primary (lighter) and secondary parts, and a flow of debris, partly piling up against the plateaus (Eriksson et al. 2000).....	21
Figure 1.10: Overview - the mechanisms for the contact surface variations (Eriksson et al. 2002). ....	22
Figure 1.11: Flows involved in the tribological circuit (Berthier 2001).....	23
Figure 1.12: FIB cut of a third-body layer and TEM analysis (Österle et al. 2009)....	24
Figure 1.13: Tribological circuit involved in braking: third-body flows <b>(a)</b> at the micro and nano-scales of the friction mechanisms; <b>(b)</b> at the macro scale of contact surfaces, activated by the disc rotation. ....	25
Figure 1.14: Synthetic diagram of the coupling between tribological mechanisms, third-body flows and thermo-mechanical localizations involved during braking (Desplanques et al. 2008).....	25

Figure 1.15: Evolution of the coefficient of friction and accumulated number of registered squeals with the number of braking for two test configurations (Bergman et al. 1999). .....	26
Figure 1.16: Investigation of squeal occurrence for high, low and no copper content brake lining formulation: correlation with (right) average coefficient of friction, and with (left) Disc weight loss (Sriwiboon et al. 2016). .....	27
Figure 1.17: Correlation between weight loss and occurrences of squeal (S. Lee et al. 2015). .....	28
Figure 2.1: Experimental set-up ‘CrisMat’: <b>(a)</b> general view; <b>(b)</b> schematic (Rapontchombo et al. 2019). .....	35
Figure 2.2: Disc/pad contact configurations: <b>(a)</b> Normal loading; <b>(b)</b> Normal loading and sliding friction with perfect disc rotation; <b>(c)</b> Normal loading and sliding friction including disc undulation effect. Arrows indicate the controlled displacement applied to the flexible thin plate. ....	36
Figure 2.3: Placement of strain gauges on the flexible thin plate to calculate the force exerted by it. ....	38
Figure 2.4: Torque-meter mounted below the disc in experimental configuration 2. .	39
Figure 2.5: Schematic representation of the modified experimental set-up with a glass disc, a pad, an artificial third body, an optical camera and a light source. ....	41
Figure 2.6: Measurement of the contact distribution using a Tek-Scan pressure-film sensor: <b>(a)</b> set-up; <b>(b)</b> example of pad-disc pressure field measurement, black zones corresponds to open areas. ....	43
Figure 2.7: Contact observation: <b>(a)</b> Set-up including camera, glass-disc and light source; <b>(b)</b> example of image captured during the experiment. ....	45
Figure 2.8: Experimental set-up: <b>(a)</b> general view and <b>(b)</b> schematic diagram. ....	46
Figure 2.9: <b>(a)</b> Contact distribution (after friction parts adjustment) before starting the friction test; <b>(b)</b> Typical optical view of the interface through the glass disc during the ‘Reference test’; and <b>(c)</b> during the ‘Third-body test’. ....	48
Figure 2.10: Schematic of third body trapping process: contact <b>(a)</b> open and <b>(b)</b> closed. ....	48

Figure 2.11: Reference test without introducing artificial third-body: **(a)** time variation of the normal load and the sound pressure; **(b)** Optical images of the contact area at different times of the test. ....50

Figure 2.12: Third-body test: **(a)** time variation of the normal load and the sound pressure; **(b)** time evolution of the third-body layer and contact localization (optical images taken at same angular position of the disc, light reflection - bright zones - corresponds to lead-bearing area localization).....54

Figure 2.13: Optical images of the contact localization, taken just before and after the first small transitory vibration (bright zones - corresponds to lead-bearing area localization). The fringes represent the opening of the contact on the leading side at time 18.9 s and on the trailing side at 19.1 s.....54

Figure 2.14: Quasi steady state test stage: **(a)** cyclic time evolution of sound pressure and out-of-plane disc displacement; **(b)** related frequency-time diagrams; **(c)** cyclic change of load-bearing area localization (taken during stage  $c_2$  of Figure 2.12a).....56

Figure 3.1: Set-up instrumentation for pad contact on the upper side of the disc: **(a)** general view of instruments; **(b)** schematic illustration of the optical instrumentation. ....60

Figure 3.2: Set-up instrumentation for pad contact on the underside of the disc: **(a)** disc/pad interface; **(b)** powder spread on the pad surface before experiment; **(c)** schematic illustration of the optical instrumentation; **(d)** general view of instruments used to capture the experimental data. ....62

Figure 3.3: Optical view of the disc/pad interface during the powder deposition and approach phases in configuration 1 (contact above the disc): **(a)** Standard run with sharp edged pad at the entrance that restricts the flow of third body; **(b)** Experiment with slightly rounded edge at the entrance that allows the flow of third body; **(c<sub>1</sub>)** disc/pad contact distribution (shown in blue) without powder and before the friction test and **(c<sub>2</sub>)** powder captured at the pad valley zones. ....65

Figure 3.4: Schematic diagrams for capturing the artificial third body in configuration 1: **(a)** pad surface parallel to the disc surface; **(b)** Tilted pad with respect to the disc surface; (1) open contact area, (2) closed contact area. ....66

Figure 3.5: Schematic diagrams for capturing the artificial third body in configuration 2: **(a)** pad surface parallel to the disc surface; **(b)** Tilted pad with respect to the disc surface; (1) open contact area, (2) closed contact area. ....67

Figure 3.6: Configuration 1: **(a)** pad surface parallel to the disc surface; **(b)** pad is tilted with respect to the disc surface. (1) disc/pad contact distribution (blue in color) without powder, before the experiment and (2) the captured powder in the interface in the respective cases. ....68

Figure 3.7: Configuration 2: **(a)** pad surface parallel to the disc surface; **(b)** pad is tilted with respect to the disc surface. (1) disc/pad contact distribution (except black color) without powder, before the experiment and (2) the captured powder in the interface in the respective cases. ....69

Figure 3.8: Optical pictures of the recirculation flow of the artificial third body during the approach phase of the pad in configuration 1. The third body visibly accumulates by forming primary plateaus. ....70

Figure 4.1: Pad-disc contact accommodation: **(a)** open contact; **(b)** contact closed, third-body layer bearing the load applied by the thin-plate bending; **(c)** contact closed, sliding friction involving a pad tilt allowed by the thin-plate bending; **(d)** contact closed, rotational undulation of the disc involving cyclic variation of the pad-disc clearance in thickness and tilt. ....88

Figure 4.2: Pressure film measurements of the disc/pad contact distribution: **(a)** without pad tilting; **(b)** with pad tilting (pressure film measurement: low to high pressure from dark to light).....89

Figure 4.3: Temporal analysis of the experiment: variation of the normal load and the sound pressure, and frequency-time diagram of the noise emission. ....92

Figure 4.4: Successive scenes of the apparent contact area related to particular times, (i) to (vii), in the test chronology, as shown in Figure 4.3.....94

Figure 4.5: Contact scene during the last noisy event of the experiment (stage c3): fragmentation and de-cohesion of the third-body layer along the leading side of the contact area. ....94

Figure 4.6: Variation of friction and pad tilt as a function of time. ....96

Figure 4.7: Cyclic mobility of the load-bearing area: a), c), e) towards the leading when the pad tilt is opening, b), d) f) towards the trailing when the pad tilt is closing. ....98

Figure 4.8: **(i)** Optical image of pad with third-body layer illustrated the load-bearing area as dark part, captured during the friction test; **(ii)** Colored image of the third-body layer to distinguish the grey level. .... 100

Figure 4.9: 3D optical profilometer images of **(i)** zone ‘a’; **(ii)** zone ‘b’ ..... 101

Figure 4.10: FIB-SEM characterizations of **(i)** zone ‘a’; **(ii)** zone ‘b’ ..... 102

Figure 4.11: Measure the load-bearing extent using Digital Image Analysis, at low (t = 52.1 s) and high (t = 53.1 s) pad tilt. Results are indicated in fraction of the total extent of the third-body layer. .... 103

Figure 4.12: Correlation between noise emission and load-bearing area extent. .... 104

Figure 4.13: Frequency-time diagram corresponding to stage {c<sub>3</sub>} of the friction experiment (see in Figure 4.3). .... 105

# LIST OF TABLES

---

Table 3.1: Experimental details: physical conditions of disc and pad; amount of powder spread on rotating disc of 5 different experiments of configuration 1.....	72
Table 3.2: In relation to the Table 3.1, disc/pad contact distribution, amount of powder spread on rotating disc and amount of powder captured in the interface for configuration 1. ....	73
Table 3.3: In relation to the Table 3.2, noise spectrum of 3 experiments.....	74
Table 3.4: Experimental details: physical conditions of disc and pad; amount of powder spread on rotating disc of 3 different experiments of configuration 2.....	76
Table 3.5: In relation to the Table 3.4, Disc/pad contact distribution, amount of powder spread on the pad and amount of powder captured in the interface for configuration 2. ....	77
Table 3.6: In relation to the Table 3.5, noise spectrum of 3 experiments.....	78
Table 3.7. Synthesis of the protocols for the configuration 2. ....	82
Table 3.8: In relation to the Table 3.7, optical images of the artificial third-body distribution just before the tests and after each step of the protocol for the respective tests. ....	83
Table 3.9: In relation to Table 3.7, noise spectrum of experiments 3 (no tilt) and 5 (tilt). ....	84
Table 4.1. Roughness parameters obtained by 3D optical profilometer for zone (a) and zone (b) .....	101



# LIST OF ABBREVIATIONS

---

ND	Nodal Diameter
FEM	Finite Element Method
FFT	Fast Fourier Transform
SEM	Scanning Electron Microscopy
FIB	Focused Ion Beam
TEM	Transmission Electron Microscopy
SAE	Society of Automotive Engineers
NAO	Non-Asbestos Organic
LBA	Load-Bearing Area
CPR	Compressed Polyurethane Resin
TBL	Third-body Layer
$R_a$	Average roughness
$R_z$	Average maximum height
$R_k$	Core roughness depth
$R_{pk}$	Reduces peak height
$R_{vk}$	Reduced valley depth

---

# INTRODUCTION

---

# INTRODUCTION

---

Braking is an energy dissipation mechanism used to restrict the movement of vehicles. Rubbing contact is a frequent cause of self excited vibrations and noise occurrence. These friction-induced vibrations are generally CLASSIFIED according to their frequency and the associated physical mechanisms. This study focuses on squeal, which is a sharp noise involving frequencies between 1 kHz and 10 kHz and is often encountered in automotive and rail braking systems. It causes a significant acoustic emission that can exceed 80 dB and is unpleasant for users. For this reason, over the past forty years or so, this phenomenon has been the subject of numerous studies to find solutions to alleviate or eliminate it. The understanding of the phenomenon is still incomplete, which limits the solutions.

From a scientific point of view, the squeal phenomenon is complex to study due to its multi-physical and multi-scale nature. Indeed, acoustic emissions come from vibrations of the whole structure, but are generated because of local phenomena between the contact surfaces. Thus, the study of brake squealing involves the fields of tribology, structural dynamics, materials and also thermodynamics.

Different approaches are possible to study this phenomenon: the experimental approach with scale 1 or reduced scale benches or the numerical approach with finite element simulations or analytical models. But very often, studies on squealing rarely take into account several phenomena and focus on one or two parameters such as the links between structural dynamics and friction coefficient. Similarly, many studies are limited to the use of a single approach, experimental or numerical. Recent work has begun to involve phenomena on several scales showing strong interactions between surfaces, structures and systems. Stochastic analyses based on parameter variability are beginning to emerge to understand the nature of squealing. Nevertheless, shortcomings remain both in the modeling, for example on the introduction of non-linearity, and in the identification of the phenomena involved. Many researchers are also adopting theoretical approaches i.e. the discrete element method or cellular automata to model the tribofilm at the disc/pad interface as well as to describe the surface topography. Despite the recent significant progress in processing techniques,

characterization tools and computational algorithms, fundamental understanding of physical conditions leading to squeal is still incomplete, since it is inevitably affected by many different factors on both the micro and macro scales.

The “classical” experimental studies related to squeal issues in particular and to tribology in general, imply worn surface post-friction observation. The shortcoming of such observations resides in the fact that after opening the contact much vital information related to the dynamic interface are definitively lost. If one has to understand the squeal, then it is important to be able to measure *in-situ* the involved parameters and to follow their time-space variation during the experiment. It is also established that the particles flowing in the contact are able to change continually the friction surface and thus the load bearing area. Considering the internal situation, the flow of particles is very complex, involving far too many factors. It is thus very difficult from an experimental point of view to access much information in the tribological circuit.

In view of this complexity and in order to better understand the squeal phenomenon, it is proposed to develop a small-scale test method capable of involving the interactions encountered in a brake. In line with the simplification of the system, it is also proposed to use plain materials which allow the *in-situ* observations while giving the possibility to “control” somehow the internal flow instead of undergoing it by using controlled artificial third-body instead of uncontrolled natural third-body.

This thesis is divided into five parts:

**Chapter 1** presents a state of the art of the various researches carried out in the field of friction contact and vibration instabilities. This bibliography is mainly oriented towards squealing problems in brake mechanisms. Particular attention was paid to experimental studies which cover multi-scale and multi-physics phenomena along with the bibliography linked to wear-induced squeal. At the end of this chapter, we will focus on positioning this work in relation to the bibliography and specifying the objectives and methodology used.

**Chapter 2** establishes step by step friction experimentation on a simplified customized pin-on-disc test-rig “CrisMat”. This setup allows for the instrumentation of the operational conditions leading to the occurrence of squeal. This bench, on a

reduced scale, has a simplified architecture. This simplification is achieved by limiting the number of parts and connections as much as possible. The purpose of this simplification is to control its dynamics. A focus is made on materials selection for the first body materials and the artificial third-body to allow *in-situ* observations. Finally, an experiment which allows for the validation of the setup is presented. It does leads to squeal and provide access to *in-situ* observations.

**Chapter 3** discusses about the two test configurations used in the said experimentation. The chapter also includes the techniques used to trap the artificial third-body at the disc/pad interface. The effects of different parameters in the two experimental configurations are discussed. The complete set of parameters of the final experiment is thus determined.

**Chapter 4** deals with the final detailed protocol and the execution of the experiment. The study deals with the evolution of the load bearing area in order to determine its influence on the occurrence of squealing. Normal load, sound pressure and friction torque results are analyzed in the light of the *in-situ* observations of the contact and its load bearing area. Different material characterizations will also be presented as interpretive elements for different load bearing areas. In the end, the general conclusions have been given which highlight the main results of the study.

---

# **Chapter 1: STATE OF THE ART**

---

# 1 STATE OF THE ART

---

Brakes represent one of the most important safety and performance components of a vehicle. They are important in terms of reliability, braking power, as well as in a smooth operation of the vehicles. One of the unwanted side effects of braking is its occasional noise emissions. Especially brake squeal is a current problem of automotive industry because customers understand this strange noise as a defect of functionality of the brake system. This results in high warranty payouts and in enormous money loss of carmakers and contributing component producers. Among the different braking technologies used in transport (friction, eddy current, rheostatic, etc.), braking by friction (considered the most effective, particularly in cases of emergency) is still the most commonly used. Although friction brakes have been improved considerably over the years, certain fundamental problems related to their use remain unresolved. The most frequent of these problems are cracking within brake discs due to thermal fatigue (Dufrénoy et al. 2002), friction instabilities (K. Lee et al. 1994), wear (Österle et al. 2009; Haytam Kasem et al. 2007; Ozcan et al. 2005) and noise emissions among them squeal (Mortelette et al. 2009; Massi et al. 2008).

The literature review focuses on the historical background and the developments in brake squeal in terms of experiments & analytic models for instability mechanisms. Thereafter, the literature regarding tribology in braking, disc/pad contact interface & wear that induced vibrations has been presented.

## 1.1 Disc brake system

Disc brakes have been developed since 1890s. Even if many various designs exist, the major components of a disc brake are the rotor, the caliper, the brake pad assemblies and the pneumatic or hydraulic actuation system. Further information has been reported in the review papers of brake squeal (Papinniemi et al. 2002; Kinkaid et al. 2003; Ouyang et al. 2005).

### 1.1.1 Disc brake systems

Generally disc brakes are composed of two basic parts; the disc and brake caliper assemblies. The disc is rigidly mounted on the axle hub and rotates with the wheel.

The caliper assemblies contain one or more hydraulic pistons which push against the back of the brake pads, pressing them together on both sides of the disc.

When the brake pedal is pressed, the hydraulic pressure in the piston housed inside the caliper is increased. The master cylinder converts the brake pedal motion into hydraulic pressure and forces the hydraulic oil (brake fluid) through a series of tubes and hoses to the braking unit at each wheel. The fluid from the master cylinder is forced into a caliper where it presses against a piston. The piston presses the pads against the disc causing the vehicle to reduce its translational speed.

The two main functions of the brake rotor are the transmission of mechanical force and the dissipation of heat, produced when functioning at both medium and high temperature. This means that the materials used for brake discs must be able to support high temperatures.

The braking surface is the area on which the braking action of the friction material takes place. Normal load is a result of actuated brake and generates an in-plane friction force at the disc-pad interface. This in turn produces a brake torque about the center of rotation of the wheel (Figure 1.1).

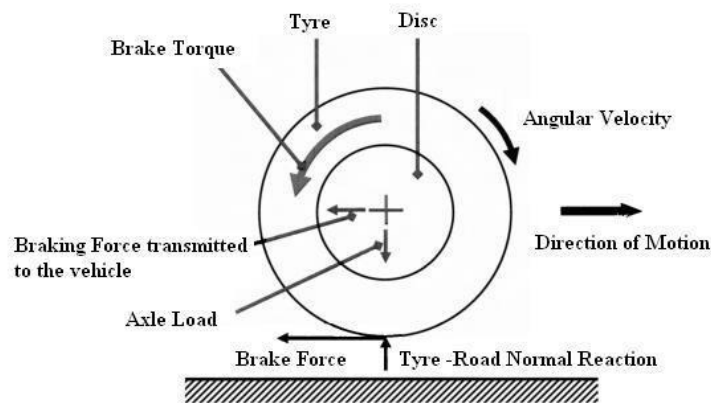


Figure 1.1: Dynamics of braking (Suchal et al. 2013)

The brake pad is designed to rub against the disc surface leading to a diminution of the vehicle speed, thereby converting mechanical work into thermal energy. The brake pad assemblies consist of a friction material which is mounted to a back plate (with high rigidity compared to the friction material). There is a variety of manners to achieve mounting between the friction material and the backing plate.



### **1.1.2 Rotor**

The majority of disc brake rotors are made of grey cast iron or iron with highly machined surfaces. Grey cast iron is cheap and relatively wear resistant. There are many designs of brake rotors; top hat shaped, with ribs connecting two contact surfaces or rotors with holes. Hollowed disc are usually used for high performance brakes for faster heat dissipation. Disc brakes with connecting ribs enhance better cooling abilities and the top hat shaped protect the wheel bearing from becoming too hot, since the path that heat must travel is longer and the surface is larger.

### **1.1.3 Friction materials**

Friction materials may be classified as organic, carbon-based and metallic. The first one is predominantly used and is an organic matrix composite which can content dozen of components. These components can be divided in five categories (Bergman et al. 1999; Kinkaid et al. 2003):

- A matrix which is composed of a thermosetting polymer binder with some possible additions of rubber and cashew nuts resin;
- Fibers (organic, resin bonded metallic and mineral);
- Friction modifiers including metallic and ceramic particulates;
- Mineral fillers;
- Solid lubricants.

Due to health issues, the replacement of asbestos fibers leads to complex formulation with an increased number of components. The mixture of the components depends on the performances required (wear, thermal range, friction level). In a general way, the metallic particulates help to control the wear and the thermal properties, the mineral fillers improve the manufacturability and the lubricants serve as stabilizers for the friction coefficient. The manufacturing process is also very important on performances with various kinds of pressure level and cooking temperature. Formulation of the friction materials and operating conditions of manufacturing remain generally secret and are based on empirical developments.

## **1.2 Brake noises**

Noise emissions are generally linked to the vibration of the components inducing sound propagation. However the dynamic behavior of the global braking system has to be considered, knowing that the components are linked together and that contact conditions (effective contact surface, pressure distribution, surface topology and third body layer interface) may strongly affect the dynamic behavior as far as the history evolution of the friction material. Considering that several kind of noise may occur, associated with various origins, a classification is presented in the following.

### **1.2.1 Classification of brake noises**

There are several categories of brake noise distinguished according to the frequency range at which they tend to occur or according to the mechanism of generation. In the literature, many studies offer different classifications of brake noise, such as judder, hum, groan, squeal, squeak, wire-brush, chatter, moan and other (Akay 2002).

Applying a load on the pads as well as friction lead to normal and tangential forces at the contact interface. Even if assuming that these forces are uniformly distributed during stationary contact, which is not realistic, they develop a non-uniform distribution during their relative motion. Tangential forces may develop in-plane vibrations and even under assumed constant-friction properties, the moment arm induced by friction force leads to oscillations of the pads. These oscillatory normal forces excite bending waves in the rotor and pads. Geometric instabilities can result and lead to rigid-body oscillations of the pads but can also lead to vibrations within the pads. These vibrations may travel to brake caliper and cause resonances providing other sources of excitation for the bending waves of the rotor. Other parameters may superpose other sources as time-dependant nature of friction parameters, non-perfect flatness and parallelism of rotor surfaces, heterogeneity of materials. This large amount of sources explains the variety of brake noise types as illustrated in Figure 1.2.

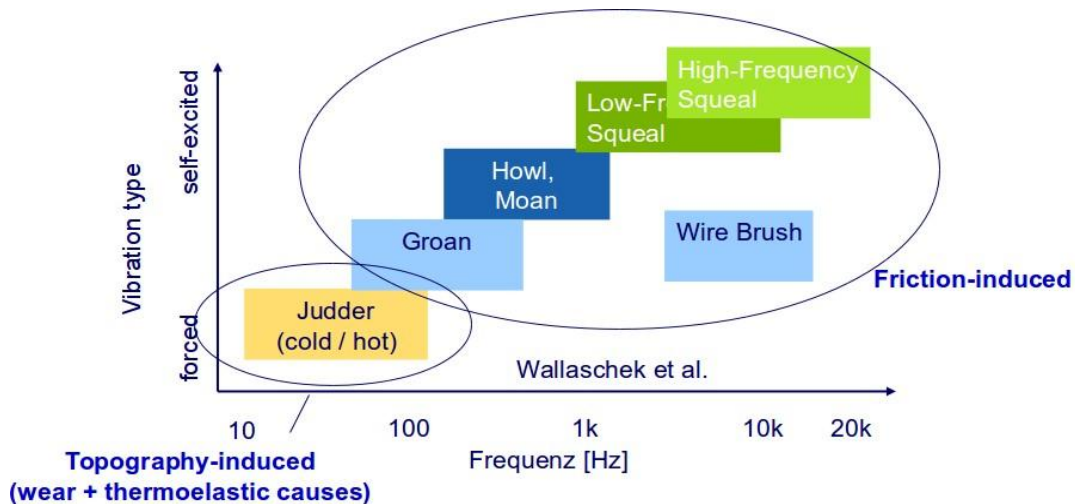


Figure 1.2: Brake noise classification (Akay 2002)

Numerous designations describe automotive brake noises and vibrations; it is now assumed that a physical-based classification may be done considering the vibration type and the frequency range.

Self-excited vibrations correspond to sources close to the contact as oscillations of the pads leading to high frequency noises.

Forced vibrations correspond to more macroscopic excitations with non-uniform friction forces coming for example from deformations of the surface as circumferential thickness variation, thermal dilatations due to hot spotting. It leads to vibration and harshness at low frequencies.

According to Akay (Akay 2002), the brake-noise mechanisms could be summarized as follow:

### 1.2.1.1 Judder

It develops from pulsations between the rotor and pads with low-frequencies that are integer multiplies of the rotational speed. It results from non-uniform friction forces due to non-perfect geometry and surfaces (disc thickness circumferential variations, hot spotting).

### 1.2.1.2 Groan

It has a typical spectrum between 10 to 30 Hz with harmonics reaching 500 Hz and occurs at low speeds under moderate braking conditions. It appears to result from

instabilities of pads giving rise to stick-slip which excites low frequencies of the brake system. In particular resonances of the rigid-body rotation mode of the caliper and local suspension parts develop and radiate sound without the participation of the rotor.

#### **1.2.1.3 Low frequency squeal**

It involves disc modes with few nodal diameters and with nodal spacing larger than the pad length. Squeal frequency may be slightly shifted from natural frequency of the rotor. Modal shape is strongly affected by the coupling with the pads and the brake assembly (caliper) leading to intermediate nodal diameter shape.

#### **1.2.1.4 High frequency squeal**

It involves the higher-order out-of-plane disc modes with 5 to 10 nodal diameters (ND). Mode shapes remain stationary with respect to the ground indicating constraining effects of the pads, even if they do not always alter the mode shapes. It exhibits the modal coupling between the components called mode lock-in phenomenon.

### **1.3 Brake squeal measurements**

Brake squeal is troublesome for both people as well as the environment. Since squeal is a noise with a frequency, above 1 kHz, and acoustic pressure more than 80 dB (Akay 2002). It may be associated with high frequency and large amplitude vibrations under sliding conditions (Massi et al. 2007). Sound propagation is mainly from the vibrations of the disc. Other components of the brake system are also involved with numerous assembly conditions. Squeal frequencies and its propensities are varying with various parameters i.e. contact pressure, temperature, materials, history effects, boundary conditions etc.

#### **1.3.1 Experiments**

During dry friction sliding, two types of energy arise namely; dissipation of the energy and deformation energy. Relative speeds of the first bodies cause dissipation of the energy and friction force generates the deformation energy. If the amount of dissipated energy is lower than the deformational one, instability may arise at the rubbing interface. This instability can lead to system vibrations (Oberst et al. 2011a).

A review of experimental studies on brake squeal can be found in (Kinkaid et al. 2003). Also, a summary has been listed for all the experimental setups considering friction induced vibrations (Oberst et al. 2011b). Natural basic measurements refer to the vibrations of the components. In Figure 1.3a, holographic interferometry illustrates these vibrations at discrete frequencies, whereas, laser vibratory measurements are able to give precise amplitudes (see in Figure 1.3b). Different works have explicitly correlated the vibrations measured to the acoustic radiation.

As discussed before in the case of high frequency squeal, hologram of Figure 1.3a shows unconstrained disc mode shapes associated with high-frequency squeal sounds, suggesting that the pads do not act everywhere within their nominal contact areas.

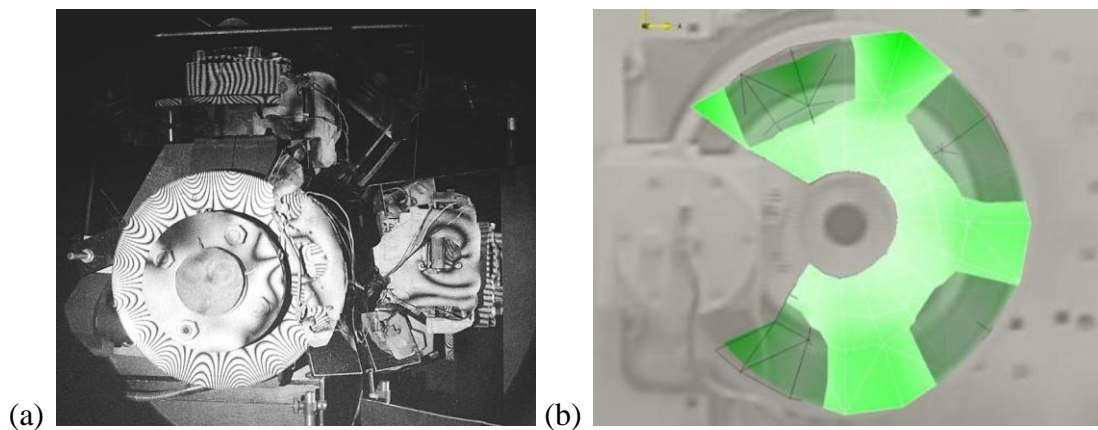


Figure 1.3: **(a)** Fieldhouse and Newcomb's reconstructed hologram of a squealing disc braking system (the rotor is rotating at 10 rpm, the vibration of the rotor has 8 ND, the frequency of vibration is 10750 Hz and the ND are rotating about the center of the rotor at  $\sim 1344$  Hz) (Fieldhouse et al. 1993); **(b)** 3D laser vibrometry measurement (normal displacements) of a squealing disc brake system, the squeal frequency is around 3600 Hz (Duboc et al. 2013)

## 1.3.2 Parametric influence

### 1.3.2.1 Disc thickness variations

A numerical study by Bonnay (Bonnay et al. 2015) on the effect of contact's geometric imperfections on the propensity for squealing. They concluded that 'disc thickness variations' as well as 'surface-layer distribution' have a strong influence on the dynamic behavior and the mode lock-in.

### **1.3.2.2 Contact surface heterogeneities**

Heussaff (Heussaff et al. 2012) worked with semi-metallic brake linings experimentally and with the use of FEM. They developed a methodology for finite element model by introducing the variability of brake lining surfaces in terms of contact pressure, velocity and temperature. The impact of stochastic processes (e.g.random variables and random fields) of geometrical and structural properties of the brake lining surfaces, introduced in the model, has shown a good correlation with the experimental results, in terms of contact pressure profiles. A highly dependency of friction coefficient on the contact pressure, velocity and temperature is also concluded.

Magnier (Magnier et al. 2014) developed an analytical model for pin-on-disc frictional contact. The analysis depicts the influence of contact distribution on squeal phenomenon by introducing the stiffness heterogeneities of the disc/pad contact surface. In the study, it is concluded that stiffness heterogeneities may change the system dynamics that further leads to squeal. The similar results also presented in the study (Sherif 1991) for the establishment of self excited vibrations.

Magnier (Magnier et al. 2017) proceeded their work by introducing the local mechanical properties in a modeling for complex modal analysis. These local mechanical properties of friction pad were identified experimentally at various locations by indentation tests (Ramasami et al. 2014). Various friction tests have also been performed to identify the influence of brake history effect by interrupting at different number of test stops. A global decrease in equivalent bulk Young Modulus is observed that depends on the friction history of the materials. The history effect, also, has an impact on the roughness that changes the local stiffness (Heussaff et al. 2012).

### **1.3.2.3 Operating conditions**

For the same set of operational conditions, a brake system may not always squeal. Squeal may occur with different propensities or frequencies with a small change in friction coefficient, rotor velocity or operating temperature. To relate or to make some relationship for the characteristics of the brake squeal, Papinniemi (Papinniemi et al. 2002), perform a range of experiments at various brake pressures and temperatures.

Figure 1.4 shows the percentage occurrence of brake squeal having different frequencies for various brake pressures and temperatures respectively. It is concluded that the influence of temperature and pressure variation is quite complex in relation to both the percentage occurrence and frequency of the brake squeal.

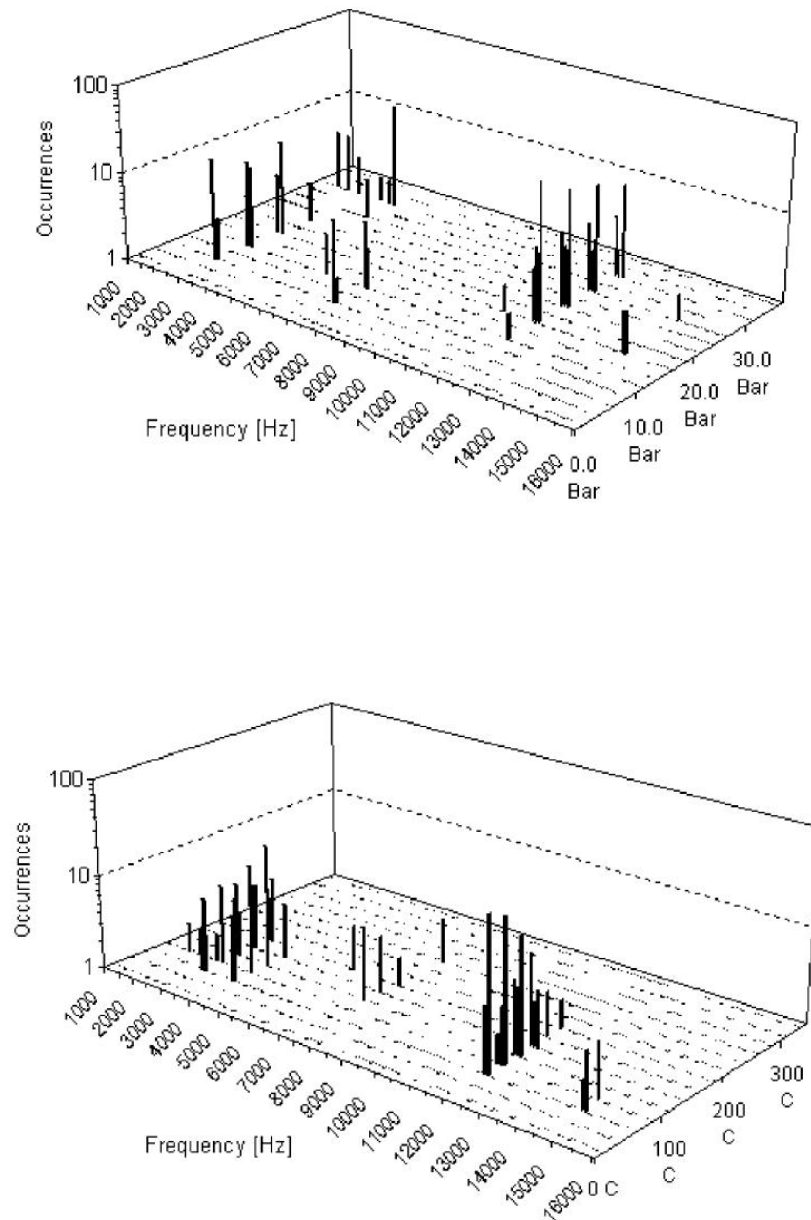


Figure 1.4: Percentage occurrence of brake squeal having different frequencies for various brake pressures and temperatures (Papinniemi et al. 2002).

### 1.3.3 Analytical models for instability mechanisms

Squeal has been understood as instability due to friction. Considering the non-conservative aspects of friction, several mechanisms have been discussed in the bibliography.

#### 1.3.3.1 Stick-slip and Negative damping

A first experimental investigation discovered in 1938 that squeal could have been caused by the variation of friction coefficient  $\mu$  at the contact interface. In this study, Mills claimed that squeal was associated with the negative gradient characteristics of dynamic friction coefficient against the sliding velocity  $v$  (Mills 1938). Later on, the stick-slip phenomenon had been described ‘unstable’ because the static coefficient of friction  $\mu_s$  (stick) was higher than the dynamic  $\mu_d$  (sliding) and this led to ‘friction induced vibration’ instability at low sliding speed (see in Figure 1.5). Both mechanisms led to unstable oscillations and provoked self-excited vibration in the system.

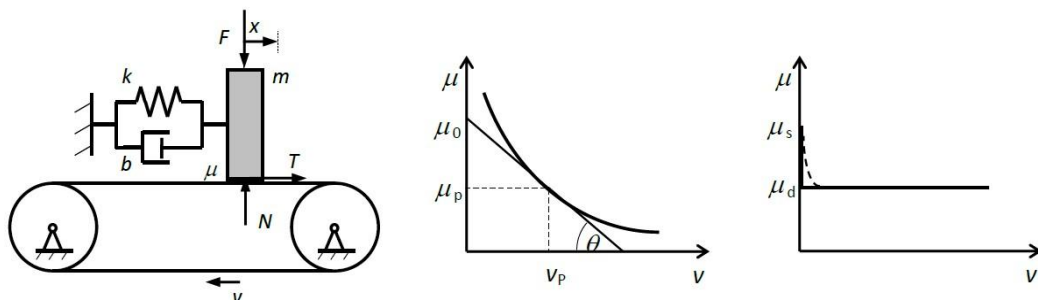


Figure 1.5: Friction-velocity slope. stick-slip phenomenon.

#### 1.3.3.2 Sprag-slip

Subsequent experiments proved that brake squeal could occur even though the friction coefficient was constant or even with a slight increase of relative velocity in the contact surface.

In 1961 Spurr came up with the sprag-slip model, which claimed that unstable friction induced oscillations occur even with a constant friction coefficient (Spurr 1961). To demonstrate this type of instability, he developed a model that consists of a mass-less rod in contact with a moving plane (Figure 1.6).



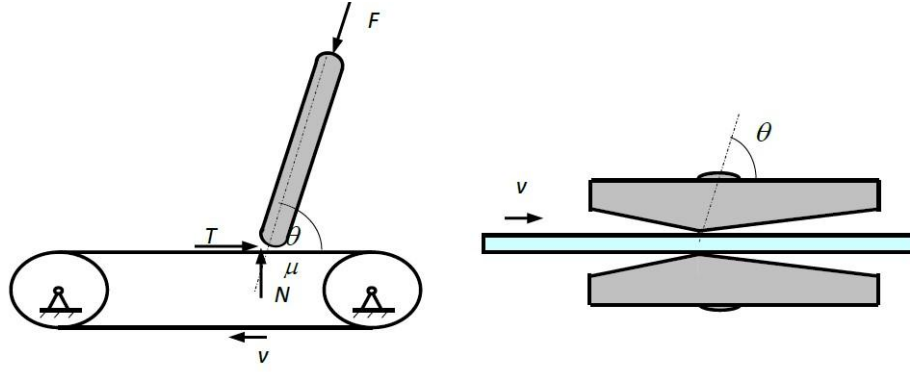


Figure 1.6: Sprag-slip phenomenon (Kinkaid et al. 2003)

This type of instability arises from locking action of the slider into the moving surface. This model links the magnitude of the friction coefficient  $\mu$  and the angle  $\theta$  between the rod and the moving plane, according to the following relationships:

$$F \cos\theta = \mu N; \quad N \leq F \sin\theta; \quad \mu \geq \cot\theta$$

Due to elasticity of interacting materials this system could oscillate, and for certain system parameters this system could give an unstable oscillatory motion.

During squeal the friction material is deflected elastically along the disc surface by the frictional force. This deflection causes a second deflection with a component normal to the surface of the pad which reduces the friction and the stored elastic energy returns the system to the first configuration, and the cycle is repeated.

### 1.3.3.3 Mode lock-in

As a response to many tests and analysis, further studies were concerned to describe brake squeal, as a friction induced self-excited mode coupling vibration, with constant friction coefficient  $\mu$ . North (North 1976) is the first to propose an analytical model illustrating such instability. The simplified Hoffman's model (Figure 1.7) (Hoffmann et al. 2002) describes the friction induced instability (binary flutter) caused by the coalescence of Eigen modes of a two degree of freedom system with friction, where the governing equation in matrix form is:

$$\begin{bmatrix} m & 0 \\ 0 & m \end{bmatrix} \begin{bmatrix} \ddot{x} \\ \ddot{y} \end{bmatrix} + \begin{bmatrix} k_{11} & k_{12} - \mu k_3 \\ k_{21} & k_{22} \end{bmatrix} \begin{bmatrix} x \\ y \end{bmatrix} = 0$$

where particular stiffness are:

$$k_{11} = k_1 \cos^2 \alpha_1 + k_2 \cos^2 \alpha_2$$

$$k_{12} = k_{21} = k_1 \sin \alpha_1 \cos \alpha_1 + k_2 \sin \alpha_2 \cos \alpha_2$$

$$k_{22} = k_1 \sin^2 \alpha_1 + k_2 \sin^2 \alpha_2 + k_3$$

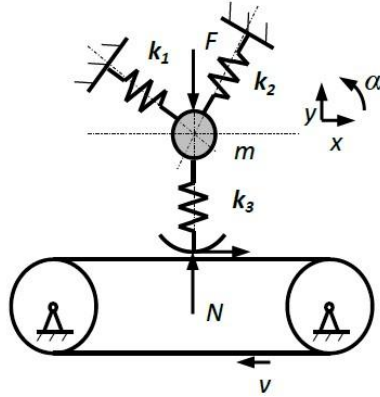


Figure 1.7: Mode coupling mechanism (Hoffmann et al. 2002).

Due to the asymmetry of the stiffness matrix this system may present an unstable behavior. Using complex Eigen value analysis, this system can be rewritten as:

$$\begin{bmatrix} k_{11} + ms^2 & k_{12} - \mu k_3 \\ k_{21} & k_{22} + ms^2 \end{bmatrix} \begin{pmatrix} x \\ y \end{pmatrix} = 0$$

Where  $s = \lambda + i\omega$  are Eigen values of the system. As stiffness matrix is not symmetrical, that shows the limit of stability: the real part of  $s$  is zero and the 2 imaginary parts are equal. While a positive real part of Eigen vectors indicates the instability of the system, this analysis can be used to define a range of system parameters for which this system is stable. The analysis introduces a control parameter  $D = \mu k_3$ .

Figure 1.8 shows the dependency between the real and imaginary part of 's' as a function of control parameter 'D' and the friction coefficient  $\mu$ . A characteristic of this instability is that the oscillations of two Eigen modes of the system come as function of a control parameter to a very close proximity until they merge and a pair of an unstable and a stable mode results. This is a type of oscillation, when the energy between two modes of vibration is exchanged within each other in a way that it feeds additional energy into the system.

Using complex Eigen value analysis, it is possible to obtain the dependency of Eigen values, which indicates the instability of such system as a function of various parameters, for instance force, relative velocity, particular stiffness as well the friction coefficient.

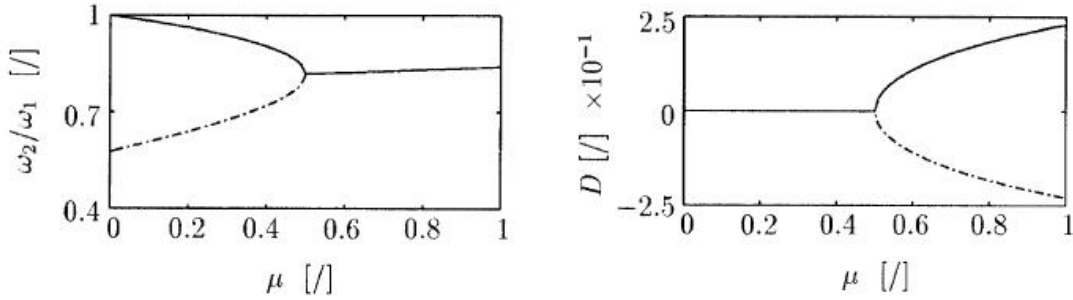


Figure 1.8: Mode coupling behavior of the system (Hoffmann et al. 2002).

### 1.3.4 Numerical modeling

For first bodies, the FEM is used with two possible analyses; (i) Stability analysis for the sliding equilibrium following a similar approach to that presented above: it is a linear analysis with Eigen-values (Papinniemi et al. 2002; Massi et al. 2007; Renaud et al. 2012), (ii) A transient analysis that allows taking into account the non-linearity of contact (Brunel et al. 2006; Massi et al. 2007). The dynamic responses are calculated in the time domain and can be converted to frequency domain using FFT (Loyer et al. 2012). The modes involved in squealing are mainly the modes of the braking system under contact conditions. On the other hand, the conditions under which this type of instability occurs seem to be related to local phenomena in the contact interface.

When focusing on the interface that separates two bodies in contact, flows of the latter can be observed under certain conditions (high pressures and shear rates). Two kinds of approaches are commonly used to model the third body flow: continuous and discrete approaches. Continuous approaches offer extensions of models derived from continuum mechanics and are essentially used in applications involving lubrication powder, i.e. using an artificial third body. In the case of a natural third body (resulting for the most part from the bodies in contact), continuity hypotheses cannot be retained and, under such conditions, it is necessary to verify whether this approach is still valid

and what its limits are. This is the main reason for using discrete element approaches to describe the evolution of a discontinuous medium and to infer rheological behavior (Mathieu Renouf et al. 2011). For third body flows, a unified discrete element approach is used for the multi-physical modeling of discrete assemblies (M. Renouf et al. 2011). This approach is well-suited to modeling the multi- physical behavior of third-body flows. After several validations and comparisons (in static and dynamic situations), the thermal model allows linking velocities and temperature profiles during shearing processes: maximal temperature localizations and asymmetric temperature profiles can be directly correlated to the cohesion value used in a simulation for a given interaction law.

## **1.4 Tribology & Braking**

Tribology, the science of lubrication, friction, and wear, deals with a variety of man-made and natural systems of interacting bodies in relative motion. Friction between sliding surfaces is a main cause of wear and energy dissipation with regard to the magnitude of relative motion between them. It plays a dual role by transmitting energy from one surface to the other and by dissipating energy related to the relative motion.

### **1.4.1 The third-body concept**

It is well known that a brand new brake pad does not perform well. It needs a running-in period until a stable coefficient of friction of the order of 0.3–0.5 is reached. This behavior can be attributed to the formation of a so-called third-body layer at the interface of pad and disc (Österle et al. 2004). Jacko (Jacko et al. 1989) stated: “when stable friction films, commonly called glaze, are readily formed for a given friction couple, a stable friction level and low wear rates can be maintained at various temperatures, as long as the friction film is not destroyed”.

The basic configuration of the mechanical approach of tribology stipulates that the two contacting parts, namely the “first bodies”, are not in a direct contact, being separated by a third one, the “third body”, constituted by detached particles (Godet 1984; Berthier 1996; 2001). The third body corresponds to a volume of material that

separates the first bodies and transmits the load while accommodating the greater part of their relative sliding velocity.

In the framework of braking by friction, the third-body approach suggested by (Godet 1984) implies that wear particles compaction plays a major role during formation of such surface layers. From the experimental works, it is identified that in the third body layers, induced by braking, there are several species like iron, iron oxides, copper oxide, copper sulfide, barium sulfate, carbonaceous products and several other phases. Thus, the formation of the third-body layer results of a complex combination of physico-chemical and mechanical processes which are activated by high thermal and thermo-mechanical stresses. From a mechanical point of view, 2 main ideas drive the third-body layer involved in braking: contact plateaus constituting load-bearing areas, and the flows of third-body particles through the contact, able to feed the contact plateaus.

#### **1.4.2 Load-bearing contact plateaus**

Introduced by Eriksson (Eriksson et al. 2000; 2002), the concept of contact plateaus aims at explaining the load-bearing capacity of the contact at the microscopic scale during the braking process. The mean idea relies on a life cycle of the local areas of contact, by the formation and the disintegration of primary and secondary contact plateaus, introduced in the case of organic composite lining materials, having hard fibers or abrasive particles. As the metal fibers have high wear resistance, during the running conditions the less wear-resistant matrix material will wear out at a greater pace than the fibers (Axén et al. 1994). Hence, the largest portion of the load will be carried by the fibers, which protects the matrix material from further wear. Thus, the contact situation is dominated by contact on emerging fibers, known as primary plateaus, allowing the formation of flat contact plateaus on the composite pad surface by third-body particle accumulation and compaction, known as secondary plateaus (Figure 1.9).

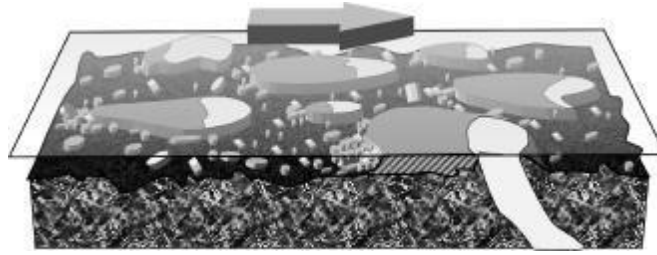


Figure 1.9: Schematic of the contact situation between an organic brake pad and a brake disc, involving contact plateaus with primary (lighter) and secondary parts, and a flow of debris, partly piling up against the plateaus (Eriksson et al. 2000).

During steady state wear, the removal rate must concern both the contact plateaus as well as the matrix part surrounding the contact plateaus. However, after analysis of the pad topography, no sign of a sliding contact can be found on the matrix, which remains below the rubbing surface. According to Eriksson, the removal of material of lower area may be due to either wear debris trapped between pad and the disc causing the mechanical crushing or the fragmentation preceded by decomposition of the organic pad constituents.

The size of the contact plateaus on the pad will grow due to the frictional energy, which helps to agglomerate and compact the wear debris around the primary plateaus and form the secondary plateaus, which depends upon the humidity, temperature and the state of normal as well as shear pressures. The secondary contact plateaus will shrink as there is the removal of this compacted debris when the contact situation changes. The removal of compacted debris may be due to the adhesive particle or surface defect on the passing disc or to the three-body abrasion and erosion. Now, if the later wear mechanisms dominate over the formation mechanisms, the secondary plateaus degrade and finally primary contact plateaus disintegrate as soon as the fiber wears out. As said above that the fibers are of a higher wear resistance than the matrix, these plateaus have longer life than other plateaus and repeated inspection of the same area of the pad shows the same plateaus with different size and shape. In spite of pad topography, the disc exhibits very smooth profile parallel to the sliding, but is a wavy profile perpendicular to sliding direction.

The size of the real contact area between the pad and the disc and the composition of the outermost surface layers within this area are not constant. They are affected by

pressure, temperature, deformation and wear. The contact pressure may vary on different time scales and both locally and globally, due to various processes which are shown in Figure 1.10.

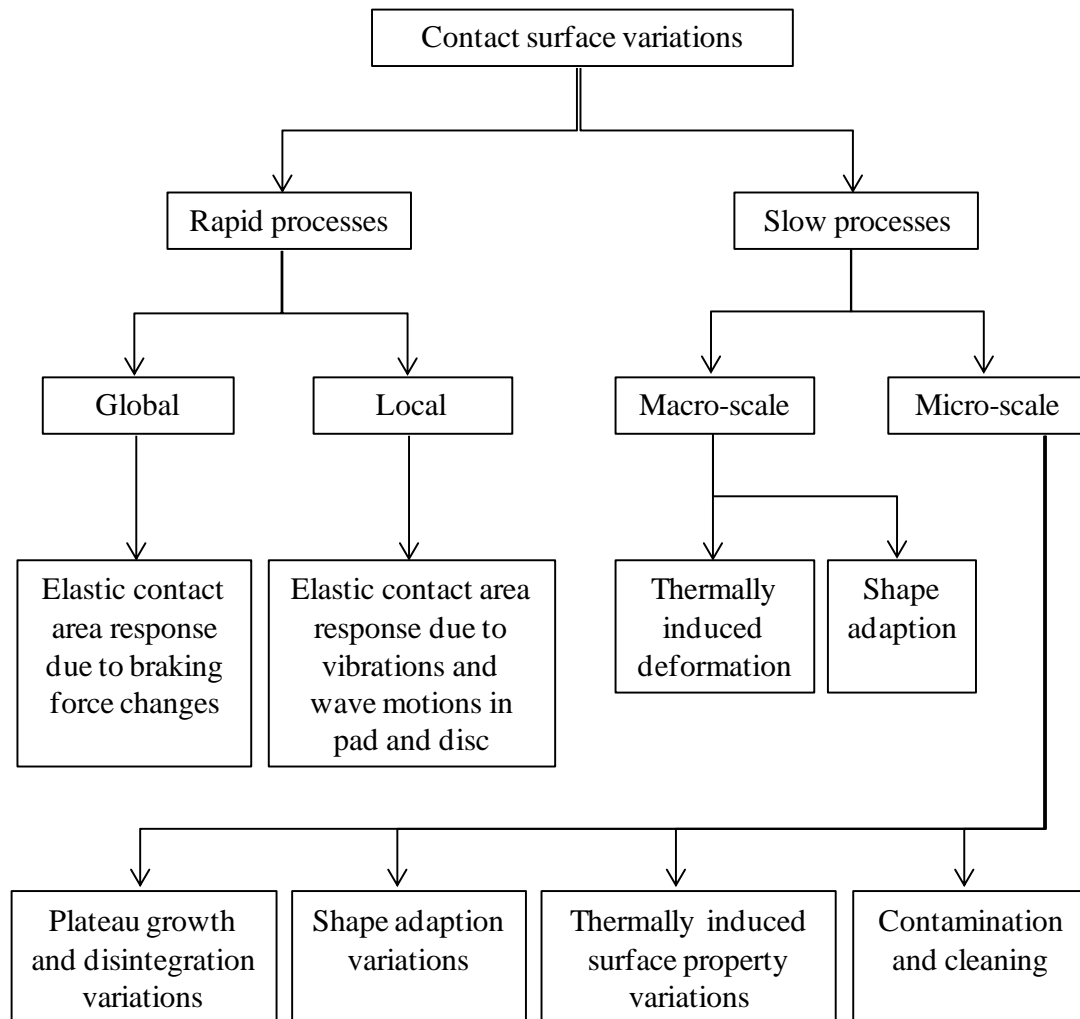


Figure 1.10: Overview - the mechanisms for the contact surface variations (Eriksson et al. 2002).

### 1.4.3 Tribological circuit involved in braking

The concept of tribological circuit has been proposed by Berthier (Berthier 1996; 2001). It aims at defining a material balance involved at the rubbing interface of the two first bodies, in particular to defend the idea that wear must be considered as a balance between the matter supplied to the contact and the matter lost by the contact. According to this approach, five types of flows of materials are defined, namely the third-body flows, as illustrated in Figure 1.11.

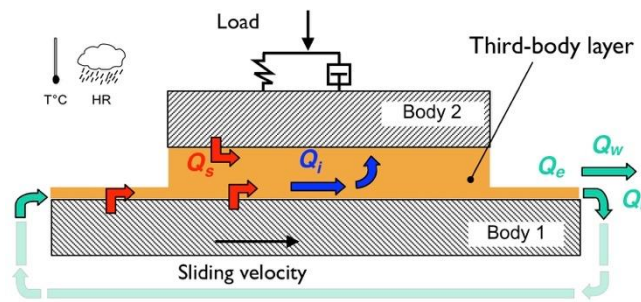


Figure 1.11: Flows involved in the tribological circuit (Berthier 2001).

The source flows  $Q_s$  correspond to the matter supplying the circuit. These flows can be provided by the first bodies, due to their damage and wear, these are the internal flows. The source flows can also come from outside the contact, due to interactions of the first bodies with the environment for instance, or by artificially introducing them into the contact as is often the case in lubrication.

The internal flows  $Q_i$  describe how the third body is moving inside the contacting area. In particular, these flows are involved in the development of the load-bearing area as well as the accommodation of the sliding velocity. They are of major importance since they are driving how the contact is working. They contribute to friction physical mechanisms.

The external flow  $Q_e$  corresponds to the part of third body leaving the contact, which inevitably occurs in the case of an open rubbing system, such as pad-on-disc configurations. It is relevant to divide this flow into two parts, taking into account the ability of the rubbing system to reuse the material leaving the contact. Thus, the recirculation flow  $Q_r$  corresponds to the part of the exiting matter that can be reintroduced into the contact, while the wear flow  $Q_w$  corresponds to the rate of material leaving the tribological circuit, permanently lost to the contact.

In the case of braking by friction, the interfacial layers formed in the contact are composed of a mixture of metallic oxides and ingredients of pad materials, most of the studies referring to organic composite lining materials (Eriksson et al. 2000; 2002; Cho et al. 2005; Österle et al. 2007; Cristol-Bulthé et al. 2008). Some authors have shown the very high proportion of iron oxide particles contained in the third body layer (over 90 wt%), and whose origin is the oxidative wear of the disc. Österle (Österle et al. 2009) studied the nano-metric nature of the third body layer (Figure



1.12). It consists locally of a very thin layer, a few hundred nanometers thick, essentially composed of ultrafine iron oxide particles, which concentrates the shear of the third body necessary to accommodate the sliding of the first bodies.

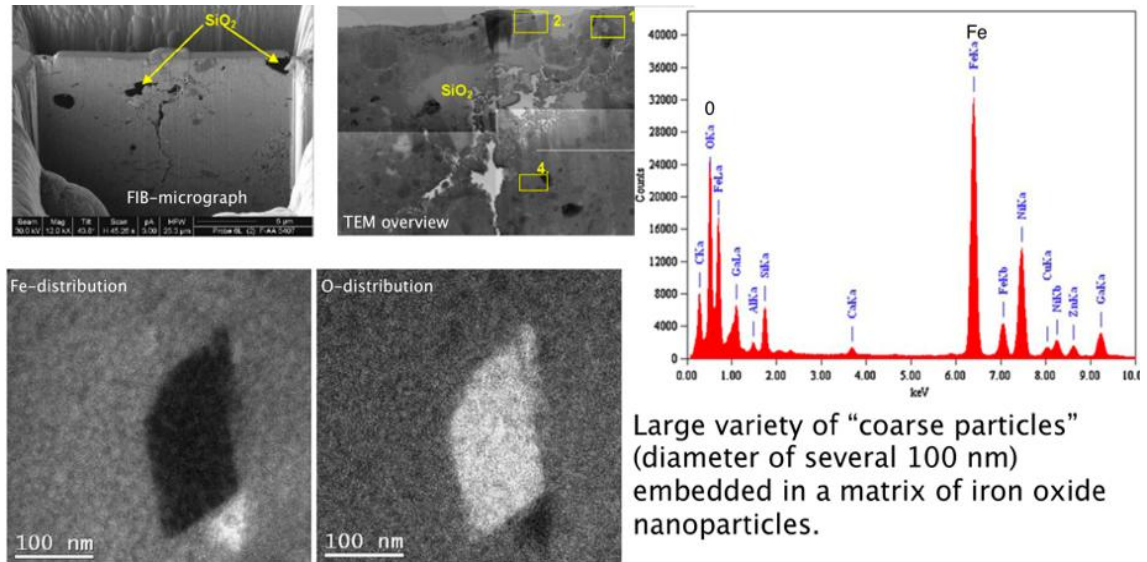


Figure 1.12: FIB cut of a third-body layer and TEM analysis (Österle et al. 2009).

Thus, during braking, the third body ensures the accommodation of the load-bearing capacity by the formation of contact plateaus at the micro-metric scale, and the accommodation of the sliding velocity within the topmost nano-metric layers of the third body, that develop on the surface of the plateaus. Figure 1.13 illustrates the contribution of third body flows that makes this contact operation possible (Desplanques et al. 2009a). Large amount of powder layers flows through the contact, enabling plateaus development by particles accumulation and compaction. At the macro scale, the disc rotation works as the engine of the tribological circuit, allowing a large part of exiting third body to be reintroduced into the contact. Although, this circulation of the third body can occur because of large openings of the apparent contact area during friction. In fact, pad-disc contact localizes in small and moving areas as a result of couplings between thermo-mechanical distortion and wear of the first bodies (pad and disc), as illustrated in Figure 1.14 in the case of hot-band migration (Cristol-Bulthé et al. 2007; Desplanques et al. 2008a).

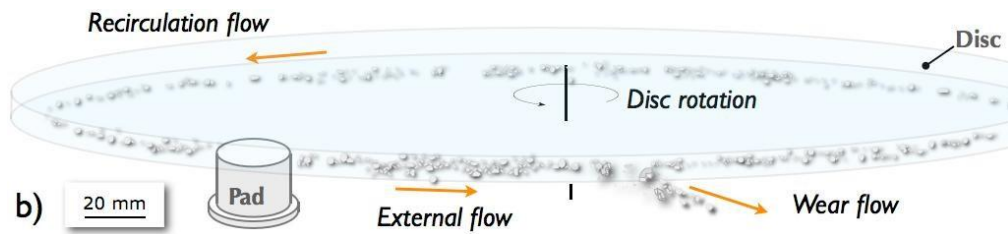
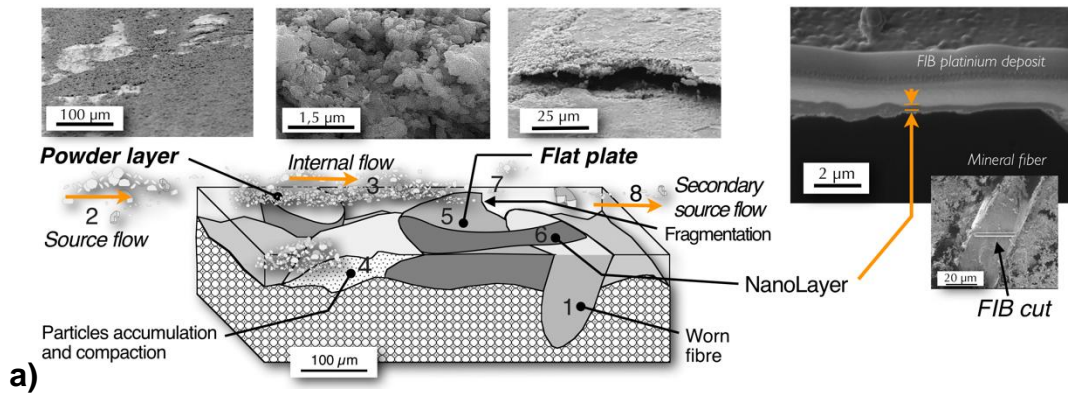


Figure 1.13: Tribological circuit involved in braking: third-body flows (a) at the micro and nano-scales of the friction mechanisms; (b) at the macro scale of contact surfaces, activated by the disc rotation.

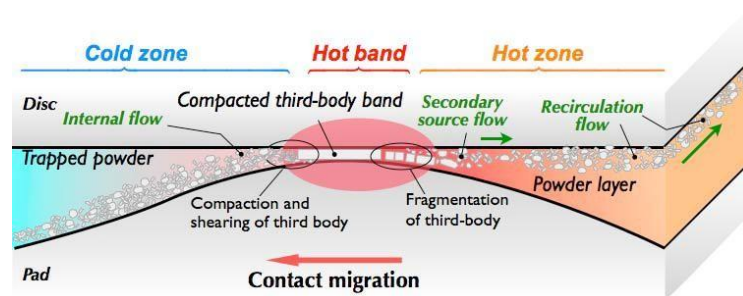


Figure 1.14: Synthetic diagram of the coupling between tribological mechanisms, third-body flows and thermo-mechanical localizations involved during braking (Desplanques et al. 2008a).

## 1.5 Wear goes in favor of squeal?

The influence of friction on squealing has been studied for many years, nevertheless some studies show contradictory results and the question of the role of wear has become an issue. As we have seen in the previous section, the wear of the first bodies, as a source flow of third body, shapes the contact interface, which is likely to modify its vibratory behavior. Rhee, who studied the influence of the third body on squeal generation (Rhee et al. 1991), seems to be a precursor of the effect of wear on brake squeal.

### 1.5.1 Friction or wear inducing vibration?

The formation of friction interface films between pad and rotor can increase friction until a steady level, and that brake squeal does not occur until the films are formed. Bergman (Bergman et al. 1999) examined the surface of the disc brake rotors and examined the change in the friction coefficient as the braking system was running-up. It increased, and after over one thousand braking applications, began to stabilize. As the friction coefficient increased beyond a critical value, it has been observed that the squealing behavior sharply increased (Figure 1.15).

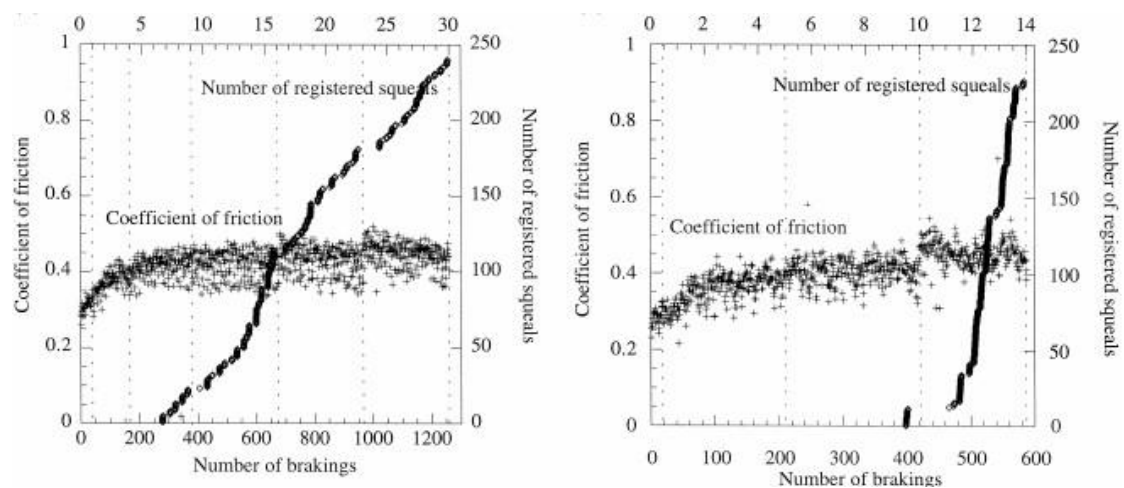


Figure 1.15: Evolution of the coefficient of friction and accumulated number of registered squeals with the number of braking for two test configurations (Bergman et al. 1999).

Bergman investigated the change in microscopic friction conditions on the generation of brake squeal by using a disc having a shot blasted sector. It is concluded

that the disc surface topography play a very crucial role in the macroscopic coefficient of friction, which in turn, affects the generation of brake squeal. The tribological system with a shot-blasted brake disc has a lower coefficient of friction than with a normal regular disc. The low initial friction in each individual braking and the low friction against the shot-blasted surface, in general, are proposed to be due to the reduced real contact area. It is found that there is always a critical value, below which, there is no squeal generation and beyond that value, there is huge increase in occurrence of squeal generation. It is also proposed that there is a decrease in coefficient of friction with the reduction of the real area of contact. Hence, reduction in generation of brake squeals.

Sriwiboon (Sriwiboon et al. 2016) analyzed squeal occurrence applying the SAE J2522 performance procedure to a pick-up truck brake equipped of a twin piston caliper. They investigated the number of brake squeal events versus friction and disc wear rate. 14 brake pads were tested for 3 different organic composite formulations, more than one hundred of stops overall. No correlation was found between friction and squeal occurrence, whatever average, maximal or variation of the coefficient of friction was considered. On the contrary, authors have shown a clear correlation between disc weight loss and squeal (Figure 1.16). They conclude to a threshold disc wear rate for a given test procedure below which squeal remains minimal.

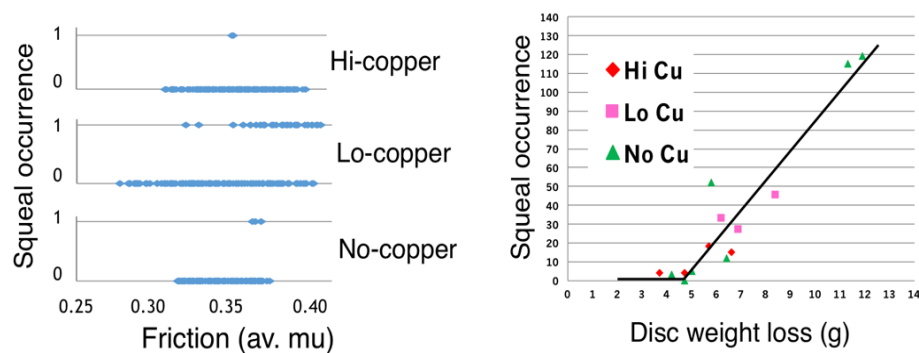


Figure 1.16: Investigation of squeal occurrence for high, low and no copper content brake lining formulation: correlation with (right) average coefficient of friction, and with (left) Disc weight loss (Sriwiboon et al. 2016).

Lee (Seongjoo Lee et al. 2015) did an extensive study of squealing following a chassis noise dynamometer testing procedure, for rear disc brakes of a car. The two

brakes were equipped with the same friction materials, a grey cast-iron disc, and a NAO formulation for pads. Left and right rear brakes shown different behaviors, noise emission been correlated with the wear of each brake, the higher the wear, the higher the number of squeal occurrences (Figure 1.17).

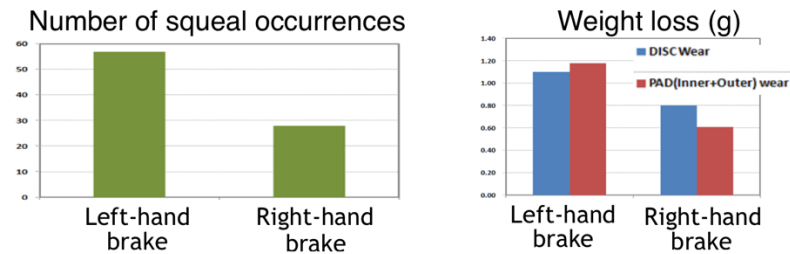


Figure 1.17: Correlation between weight loss and occurrences of squeal (Seongjoo Lee et al. 2015).

Authors investigated the third-body distribution on the pad rubbing surface, considering the amount of iron as a maker of the third-body layer, since the NAO lining formulation was iron-free. The mapping of measurements shows higher third-body concentrations on the outer and on the leading sides of the pad surfaces, which is a comprehensive result, considering the source and re-circulating flows of third body provided by the disc and its rotation. Quantification showed a higher content of third body for the left-hand brake pads, suggesting a relationship between the amount of third body and the propensity to squeal.

Jessie (Rapontchombo et al. 2019) worked experimentally to observe the squealing propensity of friction tests using several friction materials. Through these tests, it can be observed that there is no obvious relationship between the friction coefficient and the squeal. The friction coefficient should be seen as an overall result of the system but not as an excitation parameter. Each of the materials generates particular induced vibrations due to their own wear mechanisms. It is mentioned that the tribological circuit has a major influence on the excitations that cause the squealing. The hypothesis is that an established third body, with relatively large bearing plates, would facilitate the appearance of squealing, while a third body less distributed and especially less compact or powdery would limit its occurrence.

Davin (Davin et al. 2019) performed friction experiments in dry air and in an inert atmosphere of argon. It is observed that a modification in the surrounding atmosphere of the sliding interface (from dry air to inert atmosphere of argon) leads to change in the tribological and vibrational behavior because of the inert atmosphere changes the nature of the third body flows by restricting oxidation.

### **1.5.2 Relationship between morphology of the surface and the squeal**

Eriksson (Eriksson et al. 1999) performed experimental work to characterize their brake pads after squealing as well as non-squealing experiments. It is observed that during the sliding contact of a brake disc, there is formation of plateaus that affect brake squeal depending upon the size and the number of plateaus. Squeal is more prone with small contact plateaus than a few large ones. At low pressure, which is the squealing pressure interval, pressure has little effect on the growth in size of the contact plateaus but there is a huge increase in size with the increase in pressure during the non-squealing pressure interval. The effect of disc temperature is almost negligible for the size of contact plateaus and the generation of brake squeal.

Massi (Massi et al. 2008) works experimentally to draw attention to contact stresses and to contact surface topography during the dry friction sliding with and without squeal. During this work, it is observed that when there is no squeal then there are no cracks or detachment of the surface of pad but the existence of cracks and material exfoliations of third body are observed during squeal. This is because of the oscillations of the contact stresses caused by high frequency vibrations, which leads to fatigue. The same predictions are given by Massi et al. (Massi et al. 2007) in their non-linear transient numerical analysis of contact stresses. Conversely, squeal does not affect the disc surface topography but some grooves at the disc periphery are observed due to the contact with highest points of pad surface. It is declared that the whole condition of the topography of the contact surface is just an effect and not the cause of the squeal generation.

Mo (Mo et al. 2013) observed experimentally how friction induced vibrations and noise change from a disc with a smooth surface to a disc with a groove-textured surface with different widths and pitches during dry friction sliding. It is observed that squeal generation is affected by width to pitch ratio instead of individual dimensions

of grooved surface. At fixed width to pitch ratio, which is  $\frac{1}{2}$ , with different pitch or widths there is no brake squeal at all. Furthermore, it is also observed that if squeal occurred, it is produced at 1500 Hz irrespective of the disc topography, which is very close to the natural frequency of the whole tribo-system. Squeal occurs due to the high frequency fluctuations of friction force as well as vibration, which further depends upon the microscopic irregularities of the worn surface i.e. wear debris or detachment. As the grooved surfaces give way to wear debris to escape from contact zone, there is reduction in the irregularities and hence, the suppression of squeal occurrence.

Wang (Wang et al. 2013) correlate the experimental observations with that of numerical simulations. The Eigen-value analysis shows that the first flexural mode of vibration takes place on the ball holder. The second and third modes of vibration come closer to each other with the increase in coefficient of friction and give rise to mode coupling, which is the cause of unstable vibration and hence the squeal occurrence. The effect of sliding direction is also studied and it is observed that the ball sliding across the grooves has more propensities to squeal than sliding along the groove length. All the observations made from the numerical simulation are in good agreement with those obtained from experimental work.

Wang (Wang et al. 2014) further extended their experimental and numerical work using dynamic transient analysis along with Eigen value analysis and a self-excited vibration model with three degrees of freedom. It is concluded that the impact behavior between the ball and the grooves reduces the self-excited vibrations and consequently the generation of brake squeal. This theory explains their previous work (Mo et al. 2013) that at fixed width to pitch ratio, which is  $\frac{1}{2}$ , some impact is observed and there is no brake squeal at all at this ratio but at other ratios, no impact is observed and hence, there is the occurrence of squeal at the frequency close to the natural frequency of the whole tribo-system.

## **1.6 Motivation**

The published works allow the conclusion that the contact is affected by the phenomena occurring at the small scales related to space (microscopic contact effects) and time (high-frequency vibrations) on the one hand, and on the other hand, at large

scales (wear, behavior of the tribological triplet and dynamics of the whole brake system). As a consequence, it is clear that squeal is a complex problem involving strongly interdisciplinary issues, which requires an adequate approach that should combine both tribological and dynamic analyses.

The present work aims at defining an experimental approach and the related methodology to analyze in a comprehensive way the relationship between the load-bearing area, its changes along with sliding friction, because of the third-body layer, and the propensity of the rubbing system to lead to vibrations and squeal. The proposed work is therefore intended to improve the link between the local dynamic visualization of contacts already made in non-squealing configurations (Krick et al. 2012; H. Kasem et al. 2011; Mathieu Renouf et al. 2014) with those made without optical interface (Massi et al. 2008; Eriksson and Jacobson 2001) in brake squeal configurations.

“Classic” experimental studies, related to squeal issues in particular and tribology in general, imply worn surface observation post-friction (Haytam Kasem et al. 2010). The shortcoming of such observations resides in the fact that after opening the contact, much vital information related to the interface is definitively lost. If one has to understand squeal, then it is important to be able to measure *in-situ* the parameters involved and follow their time-space variation during the experiment. This is especially true if we consider the complex tribological circuit of the third body in general proposed by Berthier and particularly in braking systems proposed by Desplanques. It is admitted that the tribological circuit is able to continually change the friction surface and thus the load bearing area. In addition, it is constantly affected by many factors such as (i) external sources, (ii) internal sources of third body, including adhesion and chemical reactions (Haytam Kasem et al. 2007), (iii) ejection and reintroduction of third-body particles in the contact. Considering all these factors, it is clear that gaining access to information by following the tribological circuit is a very complex task from an experimental point of view, particularly due to the inaccessibility of the contact during friction.

Therefore, a realistic approach needs to be simplified as much as possible while allowing the possibility to introduce somehow an artificial, controlled third body instead of undergoing uncontrolled natural wear particles coming from the first bodies



(i.e., pad and disc). In addition, the approach should allow the *in-situ* observation of the interface and measurement of its time-space variation along with investigation of the influence of contact conditions (contact distribution) on squeal occurrence.

The following chapters present the developed experimental approach, which is based on an elementary tribometer specifically dedicated to the analysis of friction materials and surfaces on squeal, defined by Duboc (Duboc et al. 2013). The experiment is designed to master the tribological circuit and to allow *in-situ* monitoring of the contacting area during sliding.

In this way, the tribological system involves a glass disc, through which one can visualize and observe the contact conditions. The third body, which consists of pure alumina powder, and the defined experimental protocols allow a third-body layer thick and wide enough for optical observation of the load-bearing area and the monitoring of its mechanical quantities. The definition of the testing conditions is driven in such a way that friction must not damage the first body and there should be very little or approximately no wear.

The experiment is conducted with dynamic and acoustic instrumentation to determine the vibration evolution of the system in adequacy with the change of the friction layer. The identification of determining factors of the dynamical behavior is carried out jointly with a *post-mortem* analysis of the morphological characteristics of the third-body layer.

---

## **Chapter 2: EXPERIMENT BASE**

---

## 2 EXPERIMENT BASE

---

The objective of this chapter is to present the development of the setup and parameters of the experiment that will be subsequently used for the study of evolution of third-body layer and its relation to squeal occurrence. An experimental device with a simplified architecture was designed in a previous study (Duboc et al. 2013) by reducing the number of parts and minimizing the complex links between the different components of the system. This experimental device was further developed to meet the requirements of this study. A glass/quartz disc has been chosen to retrieve the *in-situ* information of the third-body flow at the disc/pad interface with a camera.

The chapter will begin with the description of the system dealing with the instrumentation and by illustrating the methodology and materials used. The next part will discuss preliminary tests results (without and with artificial third-body). An analysis of the dynamic behavior of the tribological system will be presented, linking the behavior to the evolution of the load bearing area (LBA). The chapter will conclude with the validation of the experiment.

### 2.1 Description of setup & Materials

#### 2.1.1 Experimental test-rig

Friction tests have been performed on a customized test rig ‘CrisMat’ built on the basis of a pin-on-disc configuration. The tribosystem, having an elementary architecture, has been designed for the studies of influential parameters. It is especially focused on the influence of materials of friction, contact parameters and temperature effect in relation with brake squeal phenomenon. Figure 2.1 gives a general view and a schematic of the test-rig that is extensively described in the references (Duboc et al. 2013; Suchal et al. 2013; Rapontchombo et al. 2019).

Many other systems have been proposed in the bibliography to study vibrations induced by friction e.g. (Massi et al. 2006a) and a summary has been listed for all the experimental setups considering friction induced vibrations (Oberst et al. 2011b). This confirms the interest of working on simplified experimental devices.

The present tribosystem is designed to study sliding contact induced vibrations in a well-known dynamical environment. The number of parts is intentionally reduced to minimize joints between parts of the system to simplify the overall friction-induced vibrations problem. This pin-on-disc setup contains a flexible, elastic thin plate made of steel, on which the pad (friction material) is affixed at its center by means of pad housing. A controlled displacement applied to the two extremities of the thin plate pushes down the pad and brings it into contact; the normal loading of the contact is obtained due to the bending of the thin plate as illustrated in Figure 2.1.

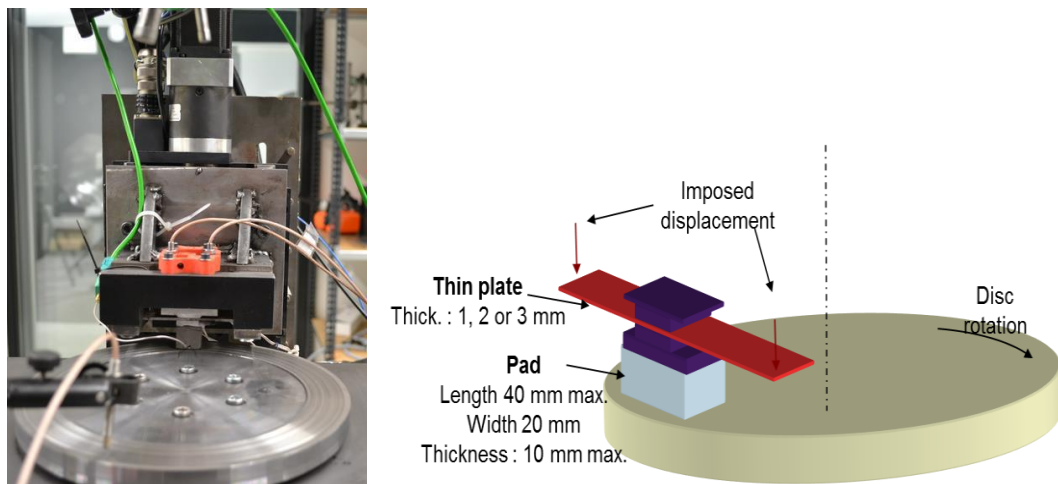


Figure 2.1: Experimental set-up ‘CrisMat’: (a) general view; (b) schematic (Rapontchombo et al. 2019).

As soon as the disc rotates and the disc/pad contact is established, due to the friction, the pad tilts (inwards at leading edge and outwards at trailing edge as shown in Figure 2.2). Consequently, there is a reduction in the contact area. Furthermore, the disc never rotates perfectly in a plane due to some undulation of the disc (discussed later in this chapter section 2.2.2.1). Thus, the apparent contact area is always subjected to dual effect, which alternately decreases and increases the contact area in comparison with the contact area due to the pad tilt only (due to friction). The contact localization may change from leading to trailing edge of the pad surface due to the disc undulation. This experimental setup has the flexible blade, which allows the pad to tilt and translate in vertical direction during friction.

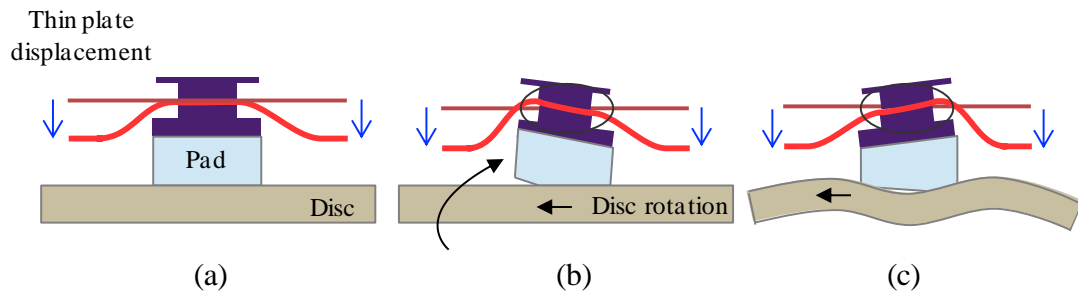


Figure 2.2: Disc/pad contact configurations: **(a)** Normal loading; **(b)** Normal loading and sliding friction with perfect disc rotation; **(c)** Normal loading and sliding friction including disc undulation effect. Arrows indicate the controlled displacement applied to the flexible thin plate.

## 2.1.2 Instrumentation

The system is made as simple as possible but its behavior is not fully understood. To observe the friction test and to link the interface conditions (or test data) with the system, it is necessary to follow the system behavior and how it is changing in terms of disc displacement (undulation as well as displacement due to load), disc tilt, pad tilt, normal load exerted by the pad, tangential load and vibrational frequencies that arise in the system. Thus, the existing setup has been equipped with complementary instrumentation to provide information on these parameters.

### 2.1.2.1 Disc displacement

#### 2.1.2.1.1 Dial gauge

As the mounted disc cannot be perfectly set in a parallel plane to the friction surface of the pad, an undulation occurs during the disc rotation. A dial gauge has been used to check the disc undulation before the friction tests, and the undulation has been corrected to be as low as possible (down to a maximum of 10  $\mu\text{m}$ ). The dial gauge has been used in preliminary experiments (experimental configuration 1, discussed in chapter 3).

#### 2.1.2.1.2 Laser sensors

The lasers sensors have also been used to measure the disc undulation before the tests but for experimental configuration 2 (discussed in chapter 3). During the friction

tests, these sensors also facilitate to determine the disc displacement (slight bending due to the application of the normal load) during disc/pad contact loading and unloading, at different angular locations of disc. Keyence LK-H022 and LK-H082 having wavelength 650 nm are used for the disc displacement in axial direction. The characteristics of the lasers sensors used are as follows:

Model	Diffuse reflection mounting		Specular reflection mounting	
	Reference distance	measured range	Reference distance	measured range
LK-H022	20 mm	+ - 3 mm	16.1 mm	2.8 mm
LK-H082	80 mm	+ - 18 mm	76.7 mm	17.6 mm

### 2.1.2.2 Pad displacement and normal load

During friction, as explained earlier, there is a tilt of the pad and it is varying with the disc angular position due to undulation. So, it is very important to have a measure of the pad normal displacement on the leading as well as on the trailing sides of the pad, along with the force exerted by the pad during the tests.

#### 2.1.2.2.1 Strain gauges

The thin plate bends with the pad tilt due to normal loading and friction, as the pad has been rigidly attached to the thin plate as shown in Figure 2.2. This bending has been used to calculate the pad displacement and the force exerted by it, with the help of strain gauges. A total of four strain gauges has been used, two of which have been glued on the upper part of the thin plate, one on each side of the pad as shown in Figure 2.3 and the other two on the bottom side of the thin plate.

The four strain gauges have been calibrated during a test on a compression machine (or with force sensor) to determine the force as a function of the strain measure and the bending of thin plate. The calibration has been done in static conditions i.e. without considering the disc rotation and friction. These gauges are mounted either in two half-bridges (a half-bridge on each side of the pad) or in one quarter-bridge. When there is no force acting on the pad, both strain gauges of the

half-bridge have the same resistance and the bridge circuit is balanced. In case a force is exerted on the pad, causing the bending of the thin plate, the upper strain gauge will be stretched while the lower strain gauge will be compressed. During a dynamic friction test, either because of the frictional load and/or of the disc undulation, there is a tilt of the pad and hence, of the thin plate. Hence, the measured voltage is higher on a side of the thin plate than on the other. This difference allows us to calculate the bending of the plate on both sides of the pad, and thus to estimate the load and the pad displacement.

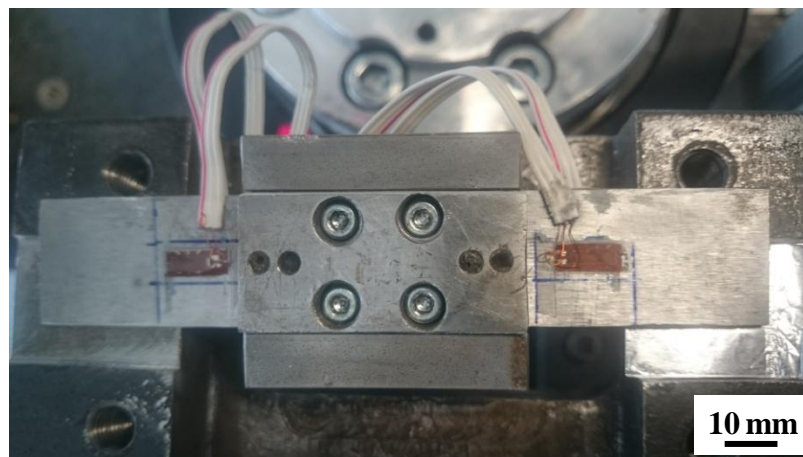


Figure 2.3: Placement of strain gauges on the flexible thin plate to calculate the force exerted by it.

#### 2.1.2.2.2 Eddy current sensors

Eddy current sensors have also been used to calculate the normal load exerted by the pad and the displacement of the pad. Two sensors have been placed adjacent to the pad but on the thin plate to observe the displacement of the plate before, during and after the friction test for experimental configuration 2 (chapter 3). These sensors are very precise non-contact sensors to measure the displacement. Like strain gauges, these sensors have also been calibrated with compression machine (or with force sensor).

#### 2.1.2.3 Frictional torque

To measure the tangential force during friction tests (used in for experimental configuration 2, chapter 3), a torque-meter (T40) has been used. The torque meter

operates with a magnetic rotational speed measuring system, which enables to monitor the direction of rotation and the torque. Torque measurement device with Nominal (Rated) Torques from 50 Nm to 10 kNm. The torque transducer features 0.03% accuracy in terms of linearity including hysteresis, as well as high temperature stability. This digital torque transducer has been mounted on the disc rotor, below the glass disc as shown in Figure 2.4.

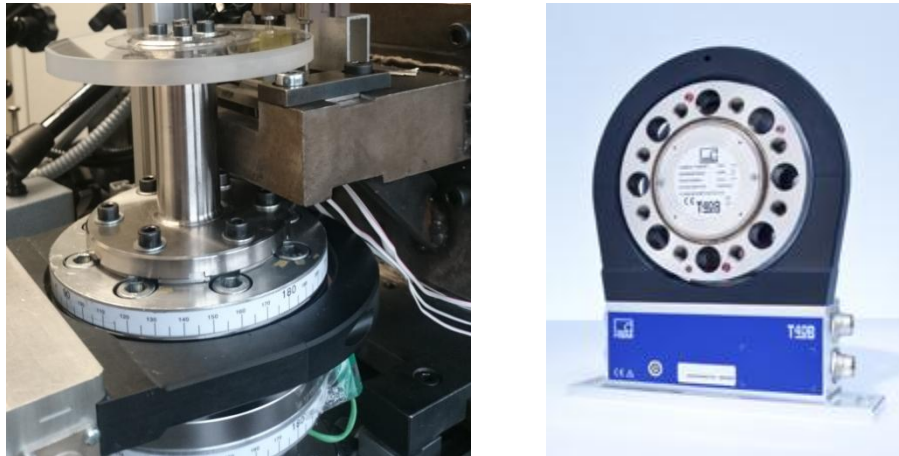


Figure 2.4: Torque-meter mounted below the disc in experimental configuration 2.

#### **2.1.2.4 Acoustic measurements**

To study brake squealing, it is necessary to know the squeal frequencies and intensities. During the tests, the sound pressure was measured by a PCB microphone, located close to the contact. The data were recorded at high frequency (50 kHz) using a Graphtec acquisition system.

##### **2.1.2.4.1 Sound frequencies and microphone**

During friction, vibrations of the experimental set-up mainly involve the deformation of the thin plate, the pad and the disc, the other parts can be considered perfectly rigid. For each occurrence of squeal, the frequencies have been calculated by means of FFT of noise signals given by the microphone. These frequencies can be related to the vibrational mode shapes of the disc, pad or thin plate that are known from numerical analysis.



## 2.2 *In-situ* contact observation

As explained in the chapter 1, considering the tribological circuit, the flows of third-body through the contact is able to continually change the friction surface. These flows are affected by many factors such as (i) external sources, (ii) internal sources of third-body, including adhesion and chemical reactions, (iii) ejection and reintroduction of third-body particles in the circuit. To access information, it is clear that following the tribological circuit is a very complex task from an experimental point of view, particularly due to the inaccessibility of the contact, closed by definition during friction.

Therefore, a comprehensive approach to a squealing system needs to simplify the tribological triplet as much as possible. The first step consists in introducing an artificial and controlled third-body instead of undergoing natural and uncontrolled production of wear particles coming from the first bodies (i.e., pad and disc). In addition, the approach should allow the *in-situ* observation of the interface and following its time-space variation along with an investigation of the influence of contact conditions (contact distribution) on the squeal occurrence. A schematic representation of the modified experimental set-up is presented in Figure 2.5

It is very important to have a good choice of materials for the two first bodies and the artificial third body. For this, one of the first bodies – namely the disc – should be transparent in order to allow the observation of the contact during friction. The second first body – the pad – should be chosen in such a way to minimize wear and damage, i.e. to cut off the source flow of natural third body.

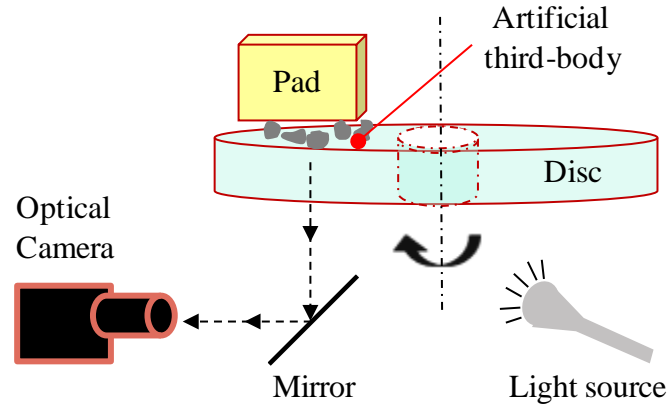


Figure 2.5: Schematic representation of the modified experimental set-up with a glass disc, a pad, an artificial third body, an optical camera and a light source.

### 2.2.1 First-bodies material

- Disc: The use of glass and quartz discs enables us to observe clearly the contact interface because of its optical transparency. The disc with internal diameter 40 mm, outer diameter 120 mm, and thickness 10 mm was mounted on the tribometer.
- Pad: Nylon and compressed polyurethane resin (CPR) were used as a pad material. Various preliminary friction tests showed that nylon was more prone to wear than CPR., thus the nylon pad was discarded. Also, the yellow color of CPR makes easier the observation of the white artificial third-body. The rubbing surface of the pad is  $20 \times 20 \text{ mm}^2$  and its height is 10 mm.

### 2.2.2 Experimental approach

The experimental study has been approached in two steps: the adjustment of the relative position of the disc and the pad surfaces, which define the apparent surface area of the contact, followed by the introduction of the artificial third body at the interface.

#### 2.2.2.1 Mastery of the apparent area

The first task of the experiment is to make the entire friction surface of the pad very closed to the one of the disc. The objective is to make as much as possible uniform the apparent contact area by reducing the sources of contact localizations.

This would also increase the contact area size between the pad and the glass disc. All the sources of relative position and orientation deviations from the assembly have been considered in order to minimize their effects.

On the one hand, it has to be noticed that the small deviation of the flatness of the glass disc (less than 1  $\mu\text{m}$ ) allows considering its surface perfectly flat compared to other sources of deviation. On the other hand, the assembly of the disc on the set-up axle and the rotation of the axle itself introduce deviations in orientation that cause the disc to undulate as it rotates. Machined pad samples were rectified to limit flatness and parallelism deviations. The final shape of the surface results in a concavity of a few micrometers deep. In addition, as for the disc mount, the assembly of the pad in the test-rig during the installation introduces orientation variations. While mounting the disc, the assembly introduces an undulation defect which one seeks to minimize.

Firstly, the disc assembly on the set-up axle has been adjusted to reduce the disc undulation. The mounting was considered satisfactory when the disc rotation induced out-of-plane displacement lower than 10  $\mu\text{m}$ , i.e. by an order of magnitude smaller than the thickness of the third-body layer.

Secondly, the pad, a pressure film sensor (Tek-scan) has been used to adjust the orientation of the surface of the pad relative to the surface of the disc. Adjustments are made by inserting thin spacers between the thin plate and the pad housing. The pressure film allows observing the zone of contact distribution (size, uniformity) between the pad and the disc. Thus, the pad alignment can be adjusted accordingly. This film has been placed between the two first bodies only before the experiment as shown in Figure 2.6(a). Figure 2.6(b) represents the square-shaped disc/pad contact zone (blue in color). This adjustment was made prior to the tests. The sensor was not used after the experiment as it may spoil the surfaces of specimens.

Thirdly, a final check has been carried out by pressing the pad, at low load, against the glass disc and holding it for some time while the disc rotates. The objective is to approach the consistent contact between the friction surfaces during the sliding. The regularity of the contacting area has to be appreciated by visualization through the glass disc thanks to an optical camera. At the end of this step, we consider the relative orientation of the pad and the disc as a reference for the experiment.

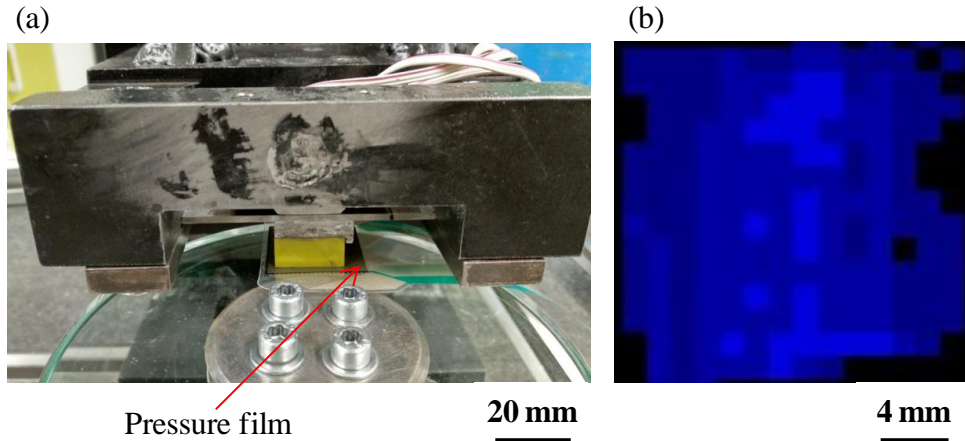


Figure 2.6: Measurement of the contact distribution using a Tek-Scan pressure-film sensor: **(a)** set-up; **(b)** example of pad-disc pressure field measurement, black zones corresponds to open areas.

### 2.2.2.2 Introduction of an artificial body

As explained earlier in chapter 1, the mastery of third-body flows and of the tribological circuit needs first to prevent from the wear of the first bodies. By introducing an artificial third body, the natural production of the third body would be neglected. The tests are thus set in more reproducible conditions. Secondly, this artificial third body has to act as a separation layer between the first bodies. It prevents wear and damage of the sliding surfaces of the first bodies. Finally, it sets a load-bearing area that can be assessed by observing the contact through the glass disc.

The chosen material for the artificial third body is alumina. Alumina was chosen to reduce many unknown phenomena occurring at the interface. Al (III) is the most oxidized form of aluminum, thus it cannot get oxidized. Its physico-chemical stability and inertness prevent any chemical (oxidative or reductive) reaction from happening at the interface. Other stable oxides can be used in place of alumina, as long as they are chemically stable and available in the range of 100 nm particle size.

At micro-scale, the size of the used alumina particles (100-150 nm) is sufficiently small to obtain good cohesion between particles, making it possible for the particles to agglomerate with each other to achieve thick third-body layers.

For macro-scale observation of the evolution of the interface, a significant thickness of the third body is needed. The choice of the particle size, considerably larger than the nano-metric size of the natural third-body particles involved in braking, helps to obtain a sufficiently thick layer of third-body able to accommodate the “flat” pad-disc contact without involving significant natural wear of first bodies. More precisely, a large thickness of the third-body layer provides the tribosystem with the necessary degrees of freedom to accommodate pad-disc flatness and alignment deviations that evolve during sliding following the disc waviness. Moreover, the “large” alumina-particle size leads to the formation of third-body plateaus sufficiently large to be observed using an optical camera.

In addition, the yellow color of the pad and the white color of the alumina powder facilitate the optical observation of the contact interface and make it possible to follow its time-space variation.

### **2.2.3 Observations of the interface evolution**

An optical camera (Nikon D7100 equipped with a 105 mm macro lens) is used to observe the *in-situ* changes at the disc/pad interface. The acquisition frequency was set at 60 frames per second. The camera recorded the contact interface through the bottom or upper part of the transparent disc depending upon the experimental configuration as will be explained in the next chapter. An experimental configuration (contact at the top of the disc surface) is illustrated in Figure 2.7(a).

Apart from camera, a light source, which is an essential part of the experimental instrumentation, is used. The changing glare and reflection of the light source make possible to follow the evolution of the load bearing area (an example of a capture picture from the video is shown in Figure 2.7(b)).

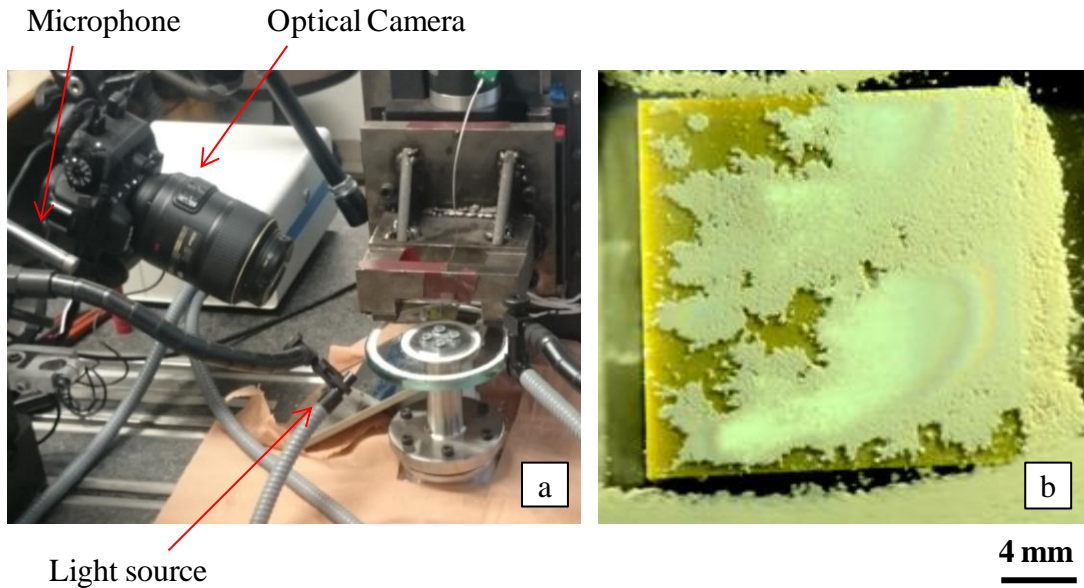


Figure 2.7: Contact observation: (a) Set-up including camera, glass-disc and light source; (b) example of image captured during the experiment.

#### 2.2.4 Limit set for normal load and disc rotational speed

The operational parameters (i.e. normal load) of the experiment have to be chosen so that the wear of first bodies has negligible effects on the tribological circuit and remains sufficiently low to maintain adequate visibility of the contact area when using a transparent disc for optical monitoring during friction. In addition, the disc rotational speed has been set with the following criteria:

- The centrifugal force has to have a negligible effect on the powder in order to avoid the powder to be expelled from the disc surface during disc rotation.
- The angular speed should be in such a way that the same angular location can be observed and recorded by the camera after each disc rotational cycle. As mentioned earlier, the acquisition frequency was set at 60 frames per second; therefore, the disc rotational speed was set at 30 rpm.

Hence, it allows 120 frames par disc revolution and the same angular disc location can be observed after every 2 seconds with negligible centrifugal effect.

## 2.3 Procedure and trial of *in situ* observation (preliminary tests)

For the first experimental configuration, the contact is made on the upper surface of the disc (see Figure 2.8). Two kinds of tests were conducted. The first test, done without introducing artificial third body, is considered as a “reference test”. The second test on the same pad and the same disc was performed with the introduction of an artificial third body and was called “third-body test”. The “reference test” is necessary to make sure that, without introducing the artificial third body, there is quasi absence of natural third body generation coming from the first bodies or any interfacial chemical reaction. Indeed, natural third body may interfere with the concept of introducing controlled artificial third body. Once it is validated that there is no other external factors influencing the system, an artificial third body has been introduced called “third-body test”. Once the different prior adjustments were made, both the “reference test” and “third-body test” were begun by driving the disc into rotation, without contact with the pad, at a constant angular velocity of 30 rpm.

The test procedures differed between the tests (Reference test and third-body test) while making the contact to take into account the presence of the artificial third body.

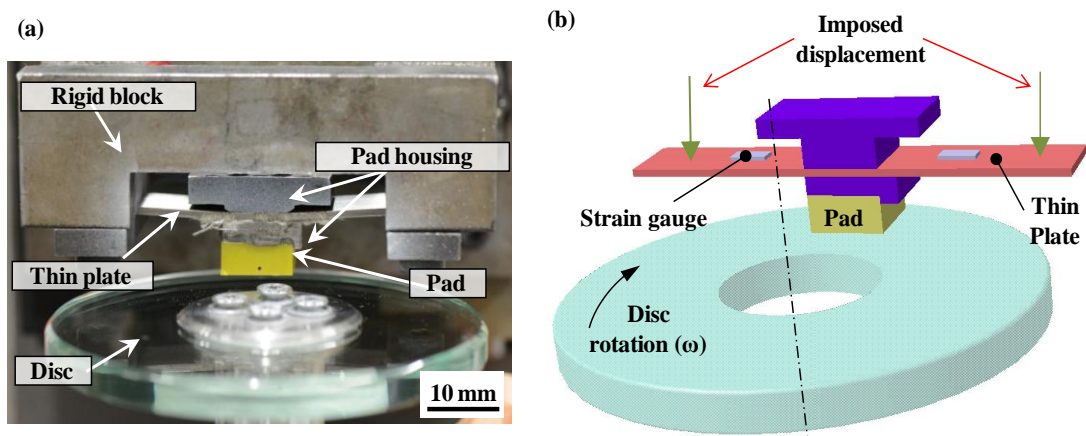


Figure 2.8: Experimental set-up: (a) general view and (b) schematic diagram.

### 2.3.1 Reference test

In the reference test, while the disc is rotating, the pad is moved down toward the disc, closing the contact without applying any normal load (zero clearance system position). The system was held in this position for two seconds (a complete rotation)

to make sure that almost zero load is attained. Then a predefined displacement of 40 micrometers was applied to the extremities of the elastic plate resulting in the application of a normal load of approx. 100 N. The duration of a test was 25 seconds, and then the test ended by stopping the disc rotation without opening the contact. Figure 2.9 illustrates (a) the contact distribution before friction test and (b) an optical view of the disc/pad interface through the transparent disc during the test. In Figure 2.9(a), the black color represents non-contact zone, the dark blue shows the disc/pad contact with less pressure and light blue shows the contact with more pressure.

### **2.3.2 Third-body test**

In the third-body test the alumina powder is spread on the rotating disc while the contact is open. Then the pad is moved down toward the disc to the same zero clearance system position defined for the reference test as illustrated in Figure 2.10. The concavity of the pad surface regarding flatness helps to trap the third body between disc and pad surfaces. As the powder is re-circulating with the disc rotation, more particles are trapped in the interface until the contact is closed. Figure 2.9(a) presents the disc/pad contact distribution assessed by pressure film. Figure 2.9(c) shows the optical view of trapped third-body in the interface. In this case, due to the presence of the third body in the pad-disc interface, the thin plate bends earlier, as a consequence of the thickness of the third-body layer, leading to a measurable normal load at 'zero clearance system position' defined above, whereas in the 'Reference test' the pad needed more displacement towards the disc to attain some normal loading. The test lasts for 25 seconds before the disc rotation is stopped without opening the contact.



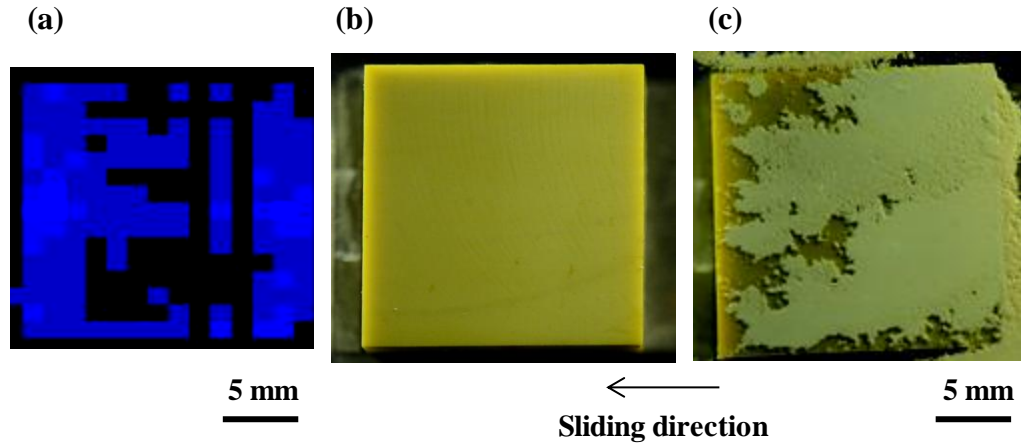


Figure 2.9: (a) Contact distribution (after friction parts adjustment) before starting the friction test; (b) Typical optical view of the interface through the glass disc during the ‘Reference test’; and (c) during the ‘Third-body test’.

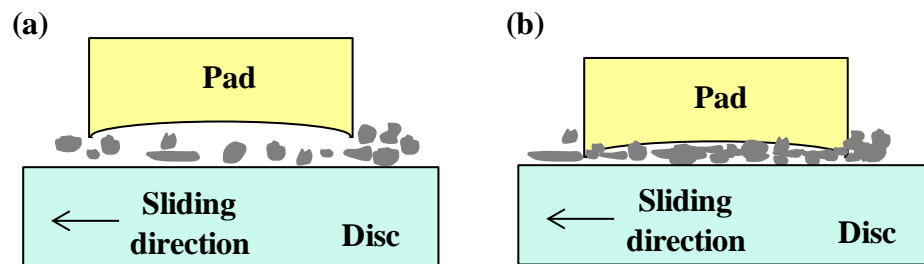


Figure 2.10: Schematic of third body trapping process: contact (a) open and (b) closed.

## 2.4 Results and discussion

### 2.4.1 Noise results and visual description of the LBA (load-bearing area)

As previously mentioned, two different cases were investigated: (1) without introduction of any artificial third body (reference test), and (2) with artificial third body introduction in the interface (third-body test).

#### 2.4.1.1 Reference test

Figure 2.11(a) shows the time variations of the normal load as well as the sound pressure for the reference test. This typical behavior can be divided into three

successive stages: (a) the first two seconds correspond to the pad contact with the disc without contact loading (zero clearance system position), (b) from time of 2 s to 7 s to the second stage sees the increase of the normal load as a result of the increase of the thin plate bending due to additional displacements applied to its extremities towards the disc, and (c) from 7 s until the end of the test, the final stage corresponds to a steady-state of the operational conditions. Stage (c) constitutes the main part of the test in which the variation of the normal load is due to disc undulation only. Due to out-of-plane displacements induced by the disc undulation, the normal load varies cyclically along with the disc revolutions, depending on the angular position of the disc. The cyclic normal load variation was close to  $\pm 3\%$  of the obtained average value for the chosen predefined displacement. This small variation cannot be avoided. Its consequences are discussed in later in the chapter (see section 2.4.2). Regarding sound pressure shown in Figure 2.11(a), no noise was detected throughout the test, meaning no squeal appears. This quiet and stable behavior can be correlated to optical observations of the pad-disc interface at different times of the test as shown in Figure 2.11(b). Indeed, at a macroscopic scale no change of the contact area can be observed, clearly showing a certain stability of the interface. This silent behavior has been observed for various testing durations and contact loading conditions, as long as the contact area remains unchanged. On the contrary, we observed the appearance of squeal, when pad wear occurred.

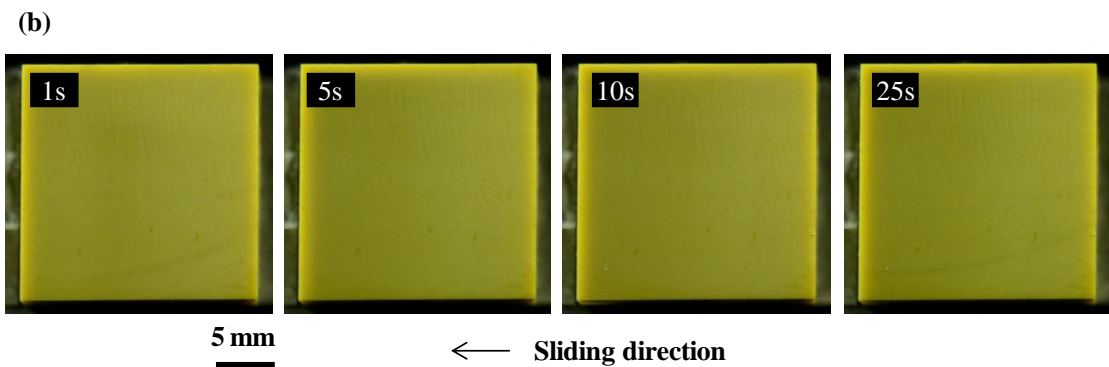
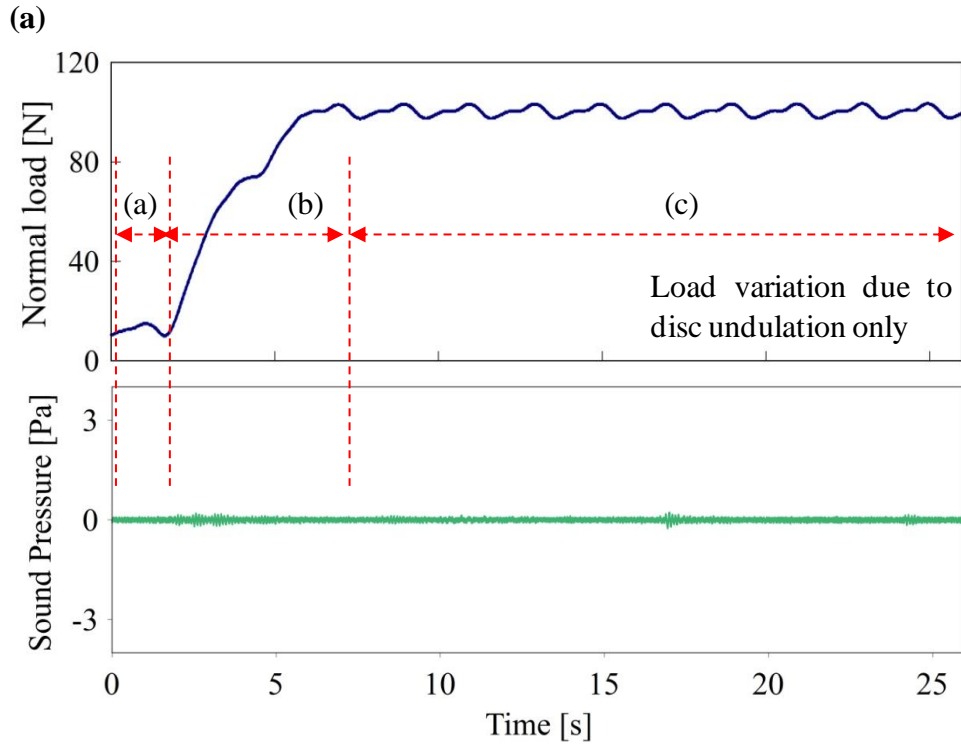


Figure 2.11: Reference test without introducing artificial third-body: (a) time variation of the normal load and the sound pressure; (b) Optical images of the contact area at different times of the test.

#### 2.4.1.2 Third-body test

Figure 2.12(a) presents the time variation of the normal load and the sound pressure recorded during the third-body test. As mentioned before in section 2.3.2, moving the pad towards the zero clearance system position causes the normal load to increase due to the bending of the thin plate induced by the formation of the artificial third-body layer in the interface. Due to the artificial third-body layer, the first bodies

had not any direct contact with each other. The final thickness of the artificial third-body layer was measured after specimen dismounting by an interferometric profilometer and was of the order of 100  $\mu\text{m}$ .

The formation of the third-body layer corresponds to the stage (a) in Figure 2.12(a) and can be easily observed with the optical images showing spread, trapping, and compacting of the third-body in the interface as shown in Figure 2.12(b). It should be clarified that the different optical images presented in Figure 2.12(b) all correspond to the same disc angular position, thus similar contact conditions with respect to the disc undulation. The angular position of the disc corresponds to the maximum normal load. Once zero clearance system displacement is achieved and the third-body layer is trapped in the interface, apart from the disc rotation, no further external intervention is made on the tribological system, and all changes in the contact behavior arise from the change of the third-body layer and internal flow of alumina particles (redistribution, expand, compaction, etc.). Stage (b) in Figure 2.12(a) corresponds to the steady state of the operational conditions. The variation of the normal load can be attributed to disc undulation and the stiffness and thickness change of the third-body layer. Two main observations can be made:

- I. A slight progressive decrease in the average normal load can be explained by the cyclic loading variation of the third-body layer due to the disc undulation, allowing progressive third-body redistribution by internal flow of alumina particles. It is strongly believed that the redistribution and compaction of the third-body layer decreases its thickness, leading to a reduced normal load.
- II. Absence of noise means that even if the third-body layer and contact conditions progressively change, favorable conditions required for squeal occurrence are still not achieved.

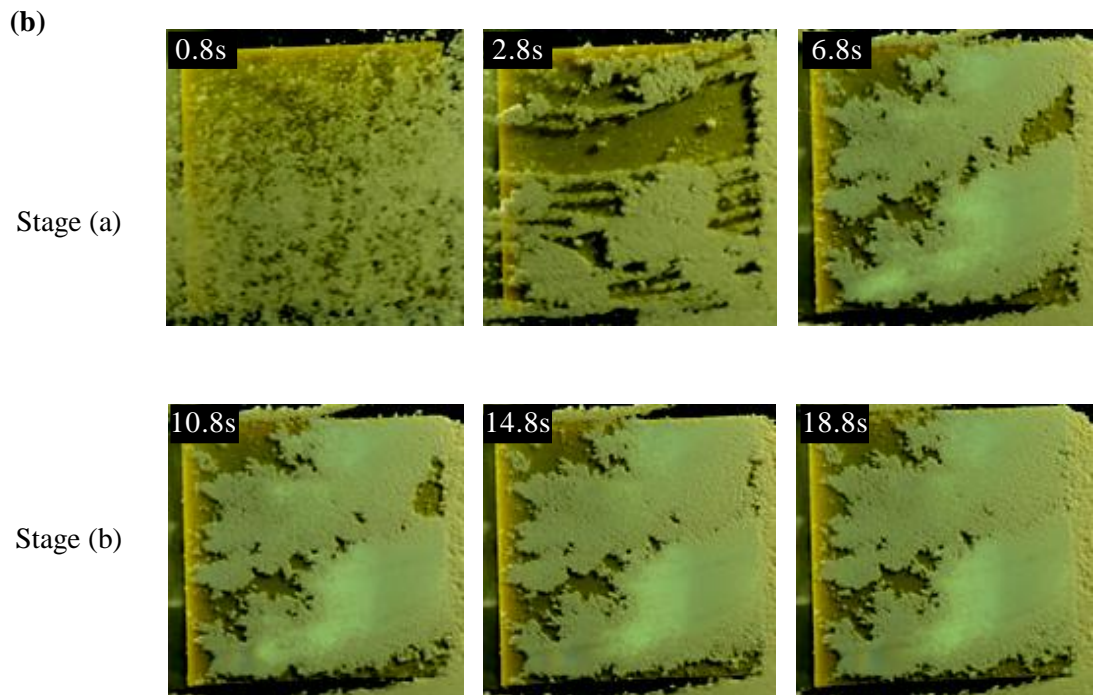
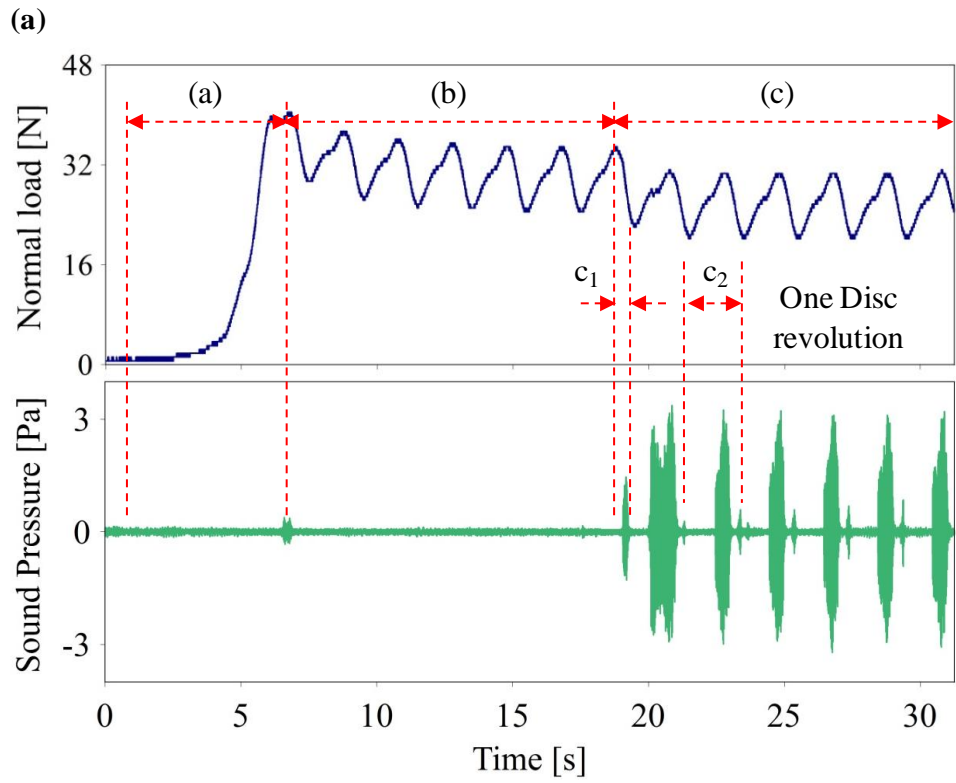
In the following stage (c) (Figure 2.12a), three main observations can be made:

- I. A small and brief transitory vibration appears at the beginning of this stage, leading to a sudden drop in the normal load. This fast reduction in normal force figures out a certain compaction of particles and hence diminution in the third-body layer thickness, as well as changes in the load-bearing contact zone. The latter can be confirmed by observing the related optical images

taken just before and after the transitory vibration (see bright zone corresponding to load bearing area in Figure 2.13). Some fringes can also be seen in Figure 2.13, which clearly represent the opening of the contact on the leading side at time 18.9 s and on the trailing side at 19.1 s. This result shows clearly the high capacity of the instrumented experimental set-up to follow and to record fine and fast variations of measured parameters, making it adequate for the study of friction-induced vibrations.

- II. A stabilization of the cyclic normal load variation is obtained after the first brief vibration, meaning that no further notable compaction and/or redistribution of the third-body in the contact occur. This behavior tends to highlight a certain “dynamic balance” reached between, on one hand, the compaction and redistribution due to disc undulation and, on the other hand the internal third-body flow.
- III. This “quasi steady state” is characterized by the periodic occurrence of squeal at the same angular position of the disc. Periodic squeal appears when adequate conditions are fulfilled. These conditions are believed to be related to the compaction ratio of the third-body in the interface (before stage  $c_2$ , which is referred to as first full disc revolution in this quasi steady state). The compaction of the third-body is apparently one of the key parameters governing the occurrence of squeal in our experimental conditions. It cannot be excluded that this compaction can influence contact interface stiffness.

It is important to note that during the quasi steady-state stage, small and very slow changes are believed to occur in contact at very small scales, however they are undetectable with the used system of optical observation due resolution limits. Preliminary experiments show that prolonging the experiment in the quasi steady-state stage leads to the occurrence of another dynamical situation (drastic changes in vibrations, forces, destruction of third-body layers, etc.). In this work, the experiment was intentionally stopped during the quasi steady-state to conserve the third-body layer. In this experiment, the main squeal frequencies are of 6,000 Hz as shown in Figure 2.14(b) and its link with disc undulation is discussed further in section 2.4.2.



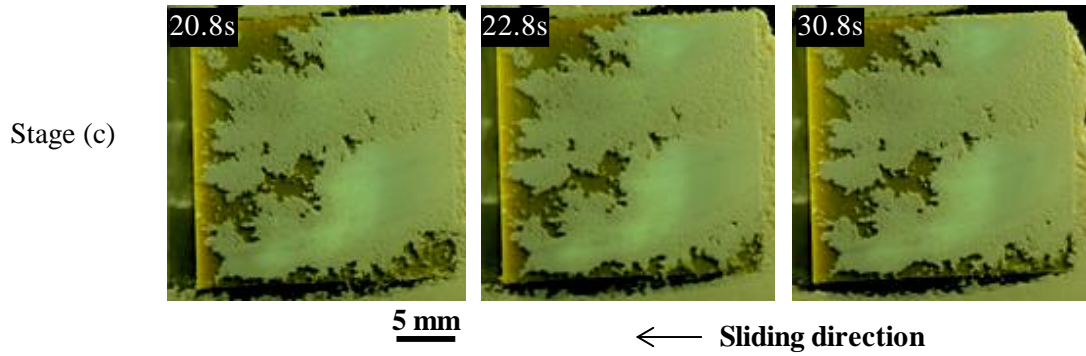


Figure 2.12: Third-body test: (a) time variation of the normal load and the sound pressure; (b) time evolution of the third-body layer and contact localization (optical images taken at same angular position of the disc, light reflection - bright zones - corresponds to lead-bearing area localization).

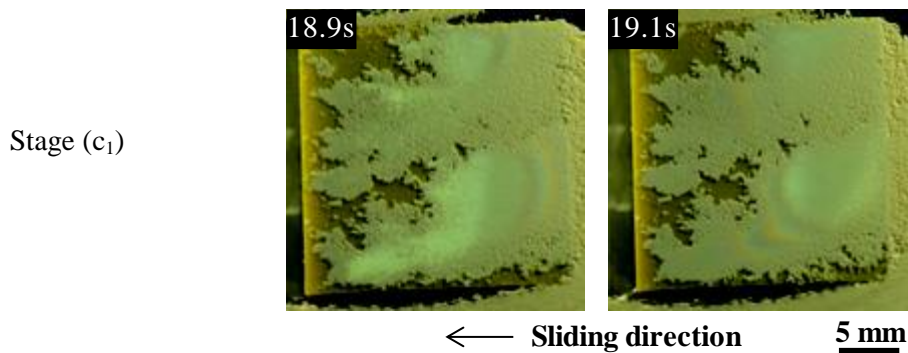


Figure 2.13: Optical images of the contact localization, taken just before and after the first small transitory vibration (bright zones - corresponds to lead-bearing area localization). The fringes represent the opening of the contact on the leading side at time 18.9 s and on the trailing side at 19.1 s.

## 2.4.2 Influence of the disc undulation

To assess the influence of the disc undulation, a focus has to be made on successive disc revolutions. Figure 2.14(a) shows the sound pressure-time evolution and the out-of-plane disc displacement for two successive disc revolutions within stage (c). Figure 2.14(b) shows a related frequency-time diagram. As can be seen, two main noise events occur periodically at each disc revolution. The frequency as well as the intensity of squeal events are very well reproducible from one cycle to the next,

confirming the quasi steady state of the tribosystem during this stage of the test. It is important to note that the high intensity squeal event appears when the out-of-plane disc displacement goes up towards a maximum (thus with an increase of the normal load), whereas the low intensity event arises when the out-of-plane disc displacement goes down towards a minimum (thus with a decrease of the normal load). It is clear that the disc undulation causes vibration occurrences. Figure 2.14(c) shows the change of the contact localization (in stage  $c_2$  of Figure 2.12a) in the friction area along a revolution of the disc. Contact localization oscillates forward and backward regarding the sliding direction, the disc undulation closing the contact towards the leading edge (from i to iii), while out-of-plane disc displacement goes up, and towards the trailing edge (from iii to iv) while out-of-plane disc displacement goes down. This results is in agreement with the dynamical relocation of load-bearing areas during friction suggested in the literature (Eriksson, Lord, et al. 2001). It can be remarked that this cyclic opening and closure of the contact should affect how third-body particles have degrees of freedom to move or not move inside the third-body layer, i.e., how internal flows of third body are able to dynamically facilitate the contact accommodation between the first bodies. This last experiment shows a clear correlation of the periodic changes of the friction interface, activated by sliding contact imperfections, with the occurrence of squeal.



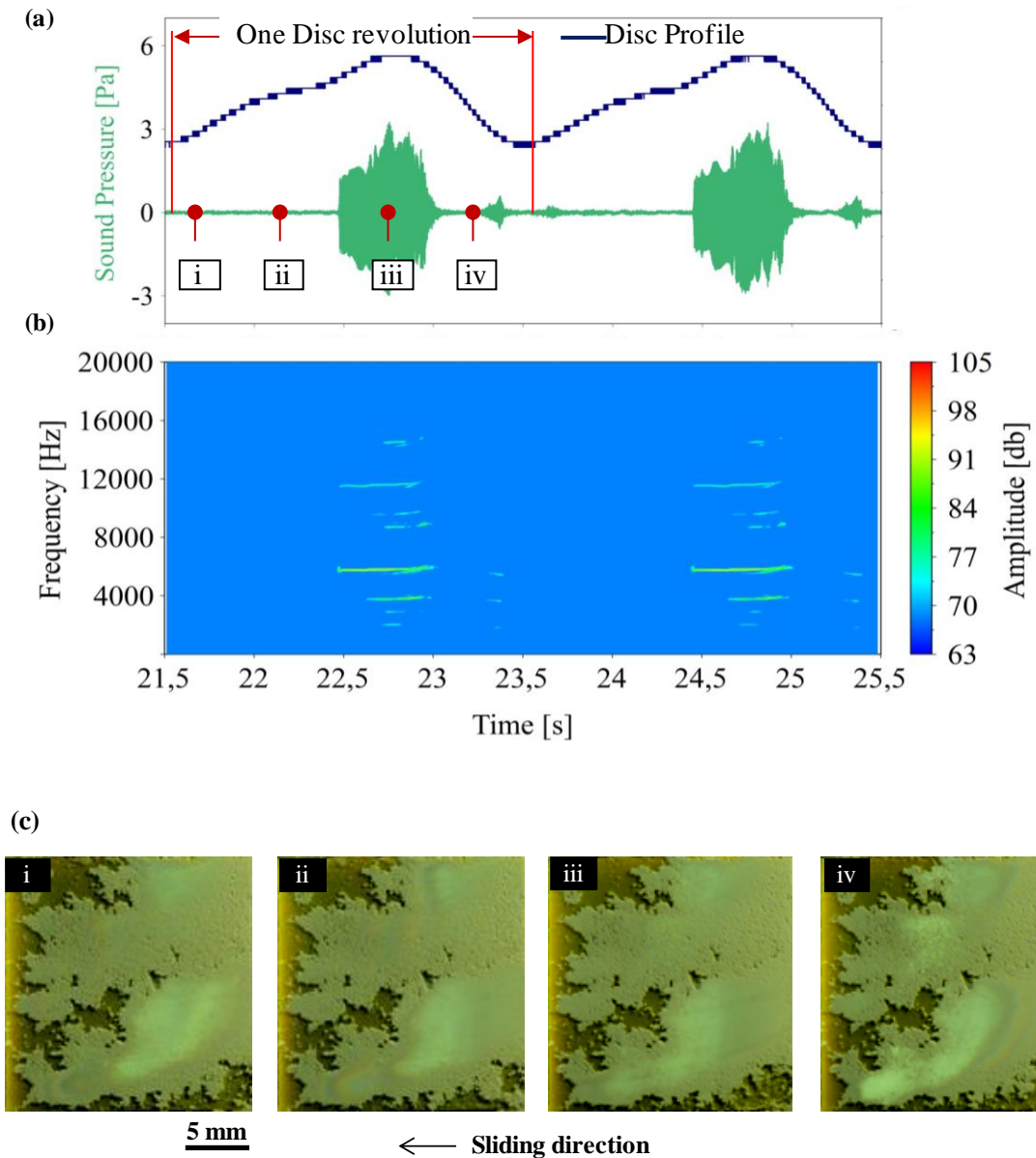


Figure 2.14: Quasi steady state test stage: **(a)** cyclic time evolution of sound pressure and out-of-plane disc displacement; **(b)** related frequency-time diagrams; **(c)** cyclic change of load-bearing area localization (taken during stage  $c_2$  of Figure 2.12a).

## 2.5 Conclusions

The experiments assess the relationship between the change of the third-body layer and the appearance of squeals in a dry sliding contact. The challenge is to identify contact accommodation mechanisms at a macroscopic scale involving internal flows of third-body particles at a microscopic scale. These mechanisms correspond to the so-called third-body plateaus in the case of real braking systems.

The third body consists of alumina particles artificially introduced inside a flat pin-on-disc interface. The third-body layer, which completely separates pad and disc, bears the load and continuously accommodates the fluctuations of the flat contact which are due to the relative out-of-plane displacements of moving parts. This accommodation is possible due to the thick artificial third-body layer, made possible by the large size of alumina particles compared to the nano-sized particles of the natural third-body obtained in braking. The time-evolution of the contact area is monitored by an optical camera through a transparent glass disc. During testing, no external action is applied to the tribosystem, except for the disc rotation. The loading of the contact is provided by bending the elastic plate in the set-up. Thus, any change of the third-body layer is expected to cause changes in the behavior of the tribosystem. The following observations were made:

- Whatever the loading or the test duration, as long as the friction interface remains unchanged, the tribosystem initially silent remains silent.
- With an artificial third-body (which acts like natural wear particles in real braking systems), a tribosystem initially silent becomes noisy.
- In a noisy tribosystem, the occurrence of squeal is apparently linked to the change in the redistribution of third-body particles in the interface, which strongly influences the location of the load-bearing area.
- The thickness variation and densification of the third-body layer can influence the interface stiffness. The tribosystem is prone to cyclic squealing according to contact closure, alternately towards the leading or the trailing in the sliding direction. This behavior suggests the existence of a relationship with the inability of the third body to flow where the load is carried.

---

## **CHAPTER 3: DEFINITION OF THE EXPERIMENT PROTOCOL**

---

# 3 DEFINITION OF THE EXPERIMENT PROTOCOL

---

In the previous chapter, an experimental approach designed to follow the evolution of the contact during friction was validated. The reflection of the light source through the glass disc and on the third body allows us to observe the evolution of load bearing area. Preliminary experiments in dry sliding contact also indicate that there is a strong relationship between changes in the third-body layer and the appearance of squeals. The third-body layer bears the load and continuously accommodates fluctuations of the flat contact due to the relative out-of-plane displacements of moving parts. Nonetheless, the bulk of the experimental configuration limits the number of measurement equipment that can be set. The main drawbacks are the absence of information regarding friction and time-variation of the disc displacement. Moreover, using mirrors to observe the contact from below reduces the visibility to monitor the interface. These shortcomings in the experimental configuration lead to improve the configuration.

The objective of this chapter is to present the development of the experimental approach for the friction test. The chapter will begin with the possible alternative to the present experimental configuration. Thereafter, it will present the techniques used for powder trapping in both configurations. The roles of different parameters will be presented for both, based on which, the final configuration and its protocol will be decided.

## **3.1 Limit set for normal load and disc rotational speed**

As explained in chapter 2, the disc rotation speed was set at 30 rpm, which is consistent with both the acquisition frequency of the camera (60 frames per second) and the dispersion of the alumina powder on the surface of the disc. According to this rotational speed, the normal-load range has been compromised. In order to limit contact heating as well as wear of the first bodies while allowing a test time of several tens of seconds, it appeared important to limit the normal load below a threshold of a hundred Newton. Conversely, the normal load must be sufficient to allow the

compaction and the trapping of the artificial third body in the contact, and to accommodate the bending decrease of the flexible blade while the third body layer is thinning. The preliminary study showed that an initial load of a few tens of Newton, typically 50 N, was appropriate for a proper conduct of the test.

### 3.2 Experimental configurations:

Two experimental configurations have been studied to obtain a large and homogeneous third body layer:

#### 3.2.1 Contact on the upper side of the disc (Preliminary tests)

In this configuration, the pad/disc contact is established with the top surface of the disc as shown in Figure 3.1. The alumina powder – the artificial third body – is spread on the disc surface during the disc rotation.

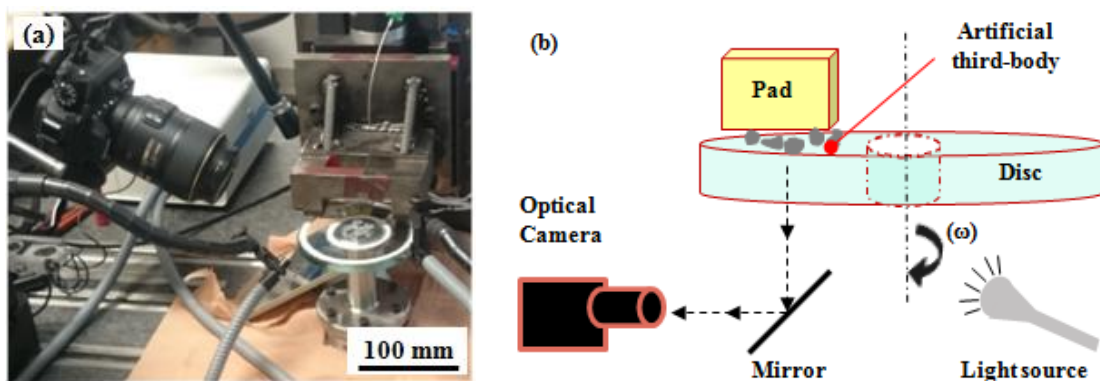


Figure 3.1: Set-up instrumentation for pad contact on the upper side of the disc: (a) general view of instruments; (b) schematic illustration of the optical instrumentation.

The pad is moved towards the disc to establish the contact and capture the powder at the disc/pad interface. This configuration allows the recirculation of most of the particles that escaped from the contact as gravity and the disc rotation bring them back into the contact (Illustrated in section 3.3.2). This recirculation occurs until the contact is fully established i.e. until pad has not reached the pre-defined position. Nonetheless, this configuration presents major drawbacks that hamper further use in this study:

- First of all, observation of the interface through the transparent disc has to be from below the disc. Due to the limited space below the disc, a tilted mirror is

installed below the disc and an optical camera has been adjusted to capture the interface visuals as shown in Figure 3.1.

- Occasionally, due to high vibrations, some of the particles fall from the disc/pad interface onto the mirror surface and reduce the visibility to monitor the interface.
- Another difficulty is to use the torque-meter due to space, as the usage of torque-meter restricts the visualization through the mirror. So, in absence of tangential force data, the friction coefficient calculations were not possible.
- The space requirements below the disc also prevent disc displacement measurements during the experiment as laser sensors could not be used from atop because of the scattering of the alumina particles on the disc.
- Controlling the quantity of powder actually implied in the contact is difficult as the alumina powder is spread on the disc while the disc is rotating.

### **3.2.2 Contact on the underside of the disc (main tests):**

In this configuration, the pad/disc contact has been established on the underside of the disc as shown in Figure 3.2. Contrary to the previous configuration (explained in section 3.2.1), the powder has been spread on the pad surface instead of the disc, before the disc rotation.

This configuration eliminates the main difficulties encountered by the first configuration (contact on the upper side of the disc).

- Direct observation can be made with the optical instruments, no mirror is needed.
- The optical path cannot be disturbed by alumina (or other) particles.
- The torque-meter can be used below the disc as shown in Figure 3.2. Then this configuration allows us to calculate the friction coefficient at every instant of the experiment.
- As shown in Figure 3.2, it is possible to use the laser sensors. By placing above the disc at different angular positions, the disc undulation and the out-of-plane

disc displacement (slight bending due to normal load) can be measured before as well as during the experiment.

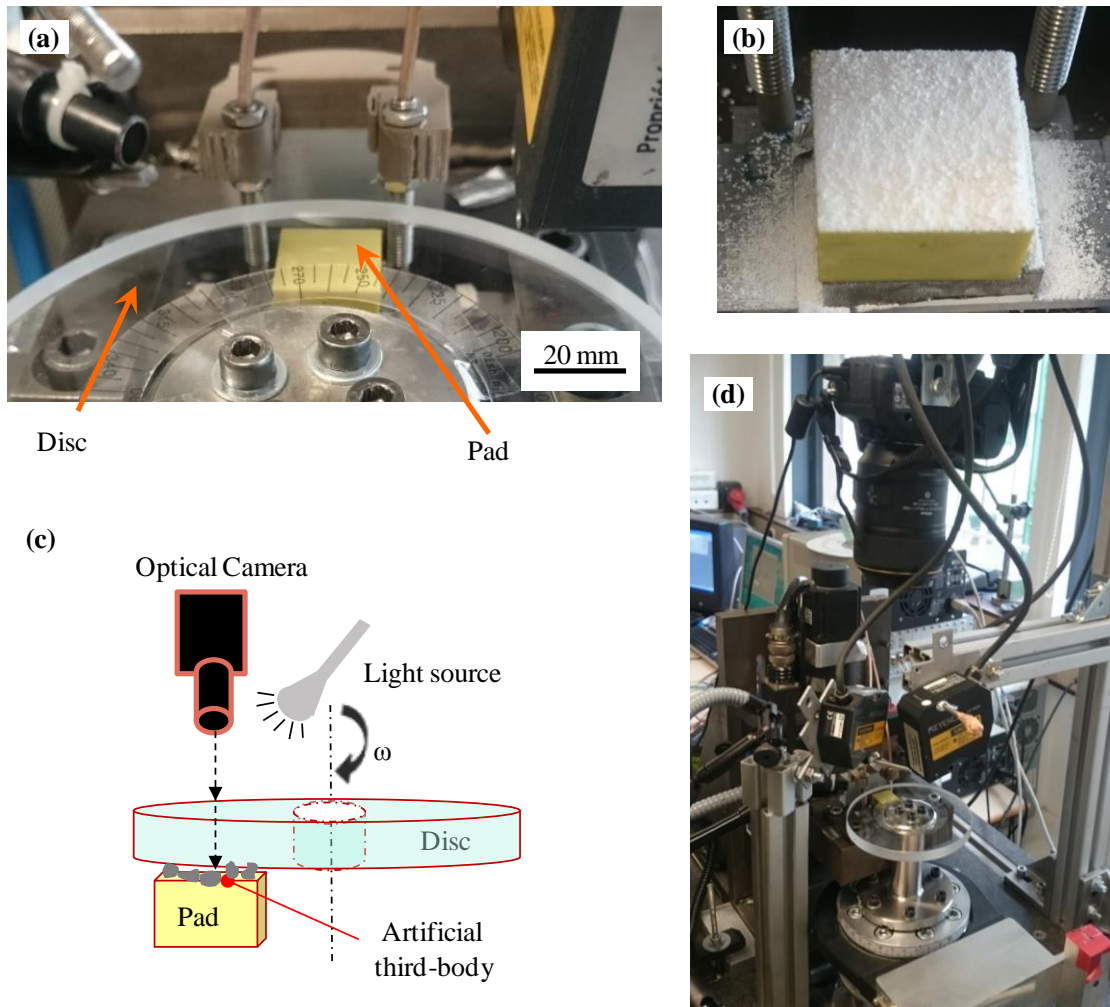


Figure 3.2: Set-up instrumentation for pad contact on the underside of the disc: **(a)** disc/pad interface; **(b)** powder spread on the pad surface before experiment; **(c)** schematic illustration of the optical instrumentation; **(d)** general view of instruments used to capture the experimental data.

- The quantity of powder is also controlled better (see section 3.4 of this chapter with the leveling of the powder layer and just after with compression).
- In addition, the transparent glass disc is also replaced with quartz disc. As the quartz disc has the more durability to perform more experiments without damage the disc than glass.

The adverse condition of this configuration is the unfavorable gravity effect. In the previous case, the alumina particles could re-circulate with the disc and come again in between the disc/pad interface. In the new configuration, very few alumina particles that get out of contact can re-circulate. In addition, the alumina powder cannot be introduced continually in between the disc/pad gap while the disc is rotating, as was done previously, because the powder has to be put on the pad, and not on the disc. The very small gap (100-200 microns) that is left during the final approach of the pad prevents any reproducible introduction of the powder. Therefore, in this case, the first step is the introduction of the powder on the pad, the second step is the rotation of the disc and ultimately the capture of the artificial third body at the interface.

As these two configurations will be used many times in the following study, the following names will be employed in the text:

- Configuration 1 - Contact on the upper surface of the disc.
- Configuration 2 - Contact on the under surface of the disc.

The next section aims at discussing experimental parameters to define criteria allowing to choose one of these two testing configurations.

### **3.3 Parametric analysis towards criteria for experimental configuration selection**

#### **3.3.1 Trapping of the third body**

The alumina powder is spread manually on the disc or the pad, depending upon the configuration used. In both configurations, capturing the powder at the interface between disc and pad is an intricate task. Actually, the first difficulty proves to be parallelism between the flat pad and the flat disc. This configuration always leads to ‘no or very little’ powder captured. To enhance the amount of powder that is trapped in the contact, two techniques have been tried: (1) by modifying the leading-edge design and (2) by tilting the pad.



### 3.3.1.1 Leading-edge design

With respect to configuration 1, Figure 3.3, (a) pictures represent the interface of an experiment made with a normal, sharp-edged pad, (b) pictures correspond to an experiment made with a rounded leading-edge of the pad. In each case, picture (1) represents the interface before spreading the powder on the disc; picture (2) the interface after spreading the powder and in process of closing the contact, and picture (3) the interface after the contact is closed.

From the Figure 3.3(a3), it is observed that a very small amount of powder is captured. Figure 3.3(a2) shows that the sharp leading edge of the pad restricts the quantity of powder that enters the interface. On the contrary, a slight alteration of the leading edge of the pad strongly increases the incoming amount of powder in the interface, as shown by the Figure 3.3(b) and a large amount of powder is captured in the interface while the contact is closed as shown in Figure 3.3(b3).

Figure 3.3(c1) shows the disc/pad contact distribution using a pressure film (without powder and before the friction test). Blue color in the picture represents the contact and black represents the pad valley. It is observed that the disc/pad contact is uniform at all the sides of the pad surface except at the pad center. The pad center is slightly inwards due to some manufacturing defect. This defect has given a boon to the experiment as it blocks the first cluster of powder and makes the primary plateaus. Following that first event, all the third-body particles are able to accumulate behind the primary plateaus.

Removing the sharp leading edge works well to capture a sufficient amount of powder in the interface, but it has its limitations. It does not have the repeatability factor because it strongly depends on the defects of the pad surface. Pads that present the same manufacturing or clamping defect that makes the previously mentioned pad valleys would be needed to block the powder at interface.

The same problem also arises with experimental configuration 2. Consequently, another strategy is required to capture a large amount of powder during the disc/pad contact closing which should work for both experimental configurations.

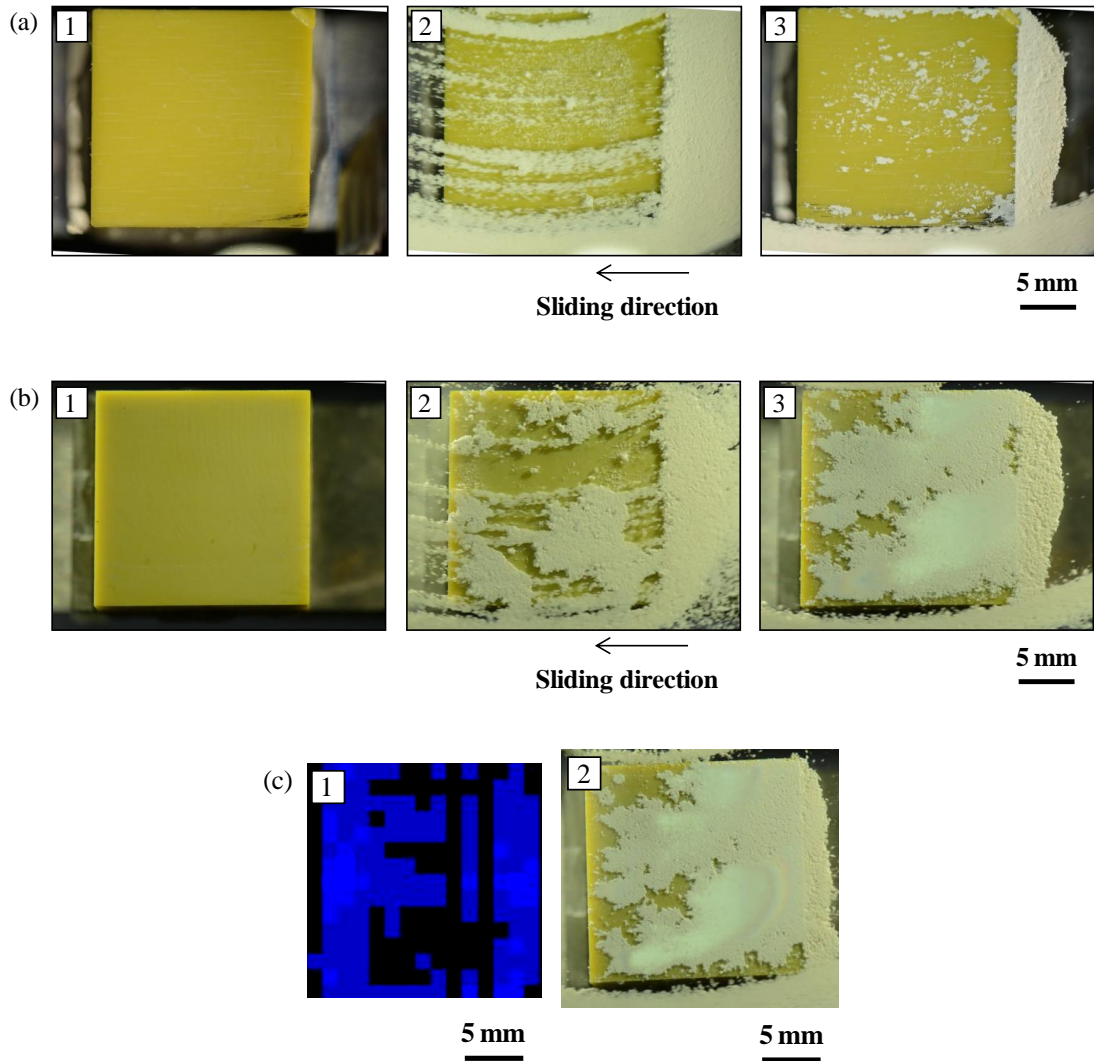


Figure 3.3: Optical view of the disc/pad interface during the powder deposition and approach phases in configuration 1 (contact above the disc): **(a)** Standard run with sharp edged pad at the entrance that restricts the flow of third body; **(b)** Experiment with slightly rounded edge at the entrance that allows the flow of third body; **(c<sub>1</sub>)** disc/pad contact distribution (shown in blue) without powder and before the friction test and **(c<sub>2</sub>)** powder captured at the pad valley zones.

### 3.3.1.2 Pad tilt

The previous paragraph showed the difficulty to capture the third body in between the first bodies while making the disc/pad contact. Actually, the reasons that explain this difficulty are different in the two configurations, the geometry of the system being a predominant factor.

a) **For configuration 1:** the tangential deformation of the pad support under frictional torque at the leading edge of the pad (Massi et al. 2007) leads to an inward tilt of the pad at the leading edge during friction, thus preventing the powder to go in-between the disc/pad interface as represented schematically in Figure 3.4(a). (a1) and (a2) represent the opened contact without friction and closed contact with friction. Obviously, the solution to this tilting pad problem is to deliberately tilt the pad at an outward angle, before the experiment. The angle should be in such a way that the leading side of the pad is slightly open whereas the trailing side is slightly closed as shown in Figure 3.4(b). In this way, the pad captures the powder and locks the contact as the pad translates towards the disc in the same way that was observed with a rounded leading edge in the previous paragraph. Moreover, tilting the pad is a more reproducible way to capture the powder than rounding the edge, as it does not depend on the manufacturing defect of the pad.

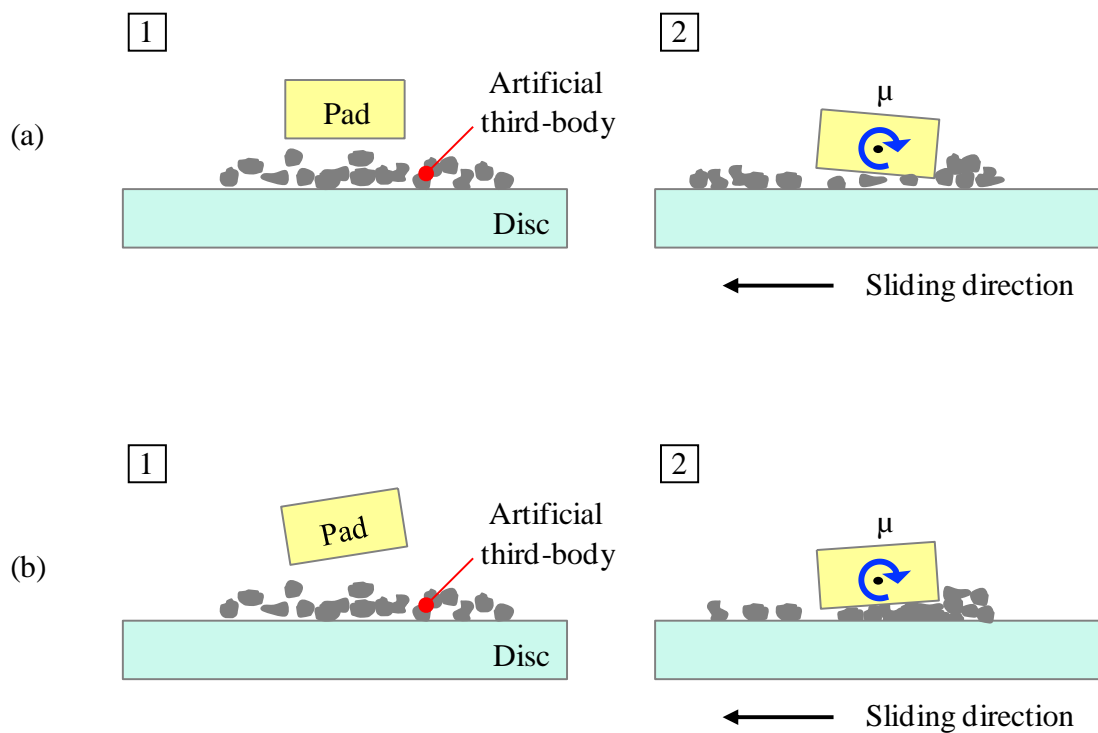


Figure 3.4: Schematic diagrams for capturing the artificial third body in configuration 1: (a) pad surface parallel to the disc surface; (b) Tilted pad with respect to the disc surface; (1) open contact area, (2) closed contact area.

b) **For configuration 2:** Contrary to configuration 1, here, the main difficulty to trap the powder between the parallel surfaces is not the slight tilt of the pad due to the frictional torque. Indeed, as soon as the top layer of the powder (spread on the pad) touches the rotating disc surface, all the powder comes out from the interface because of the electrostatic force or of adhesion. It is explained in Figure 3.5(a1) and (a2) which schematically represent open and closed contact without friction in configuration 2. The solution for this case is also to deliberately tilt the pad to make a wedge for the powder flow. When the top surface of the powder layer approaches the rotating disc, the powder (just at the trailing edge) comes out from the contact along with the rotating disc and the remaining powder is trapped in the contact interface due to the wedge as illustrated in Figure 3.5(b).

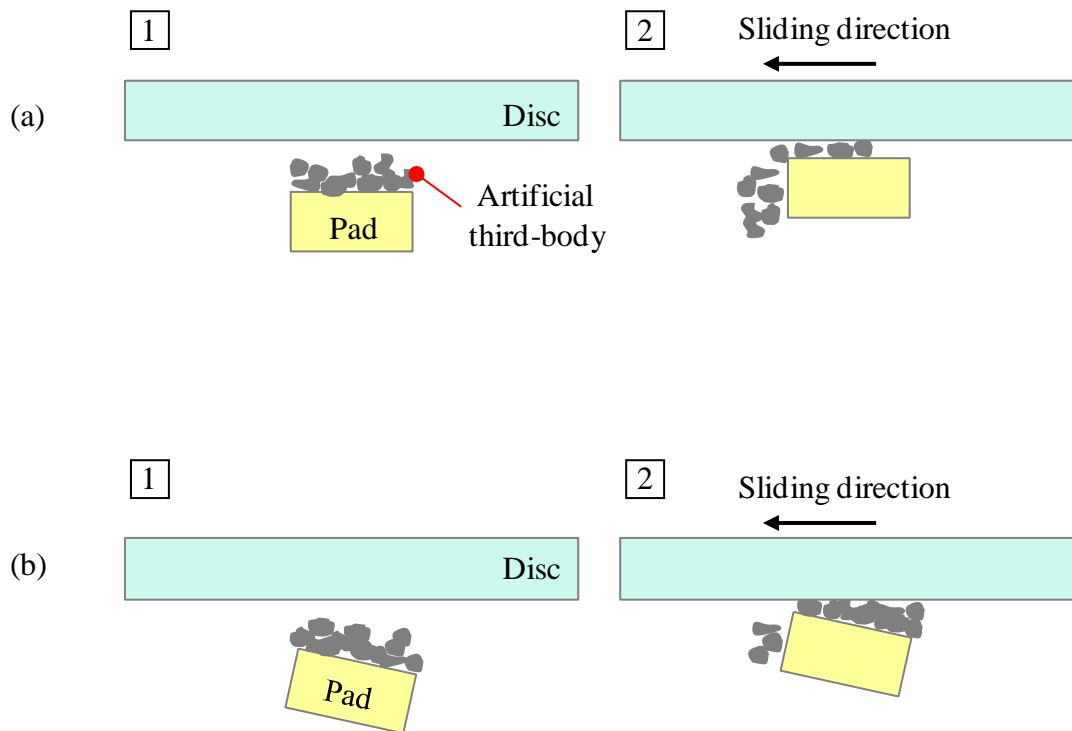


Figure 3.5: Schematic diagrams for capturing the artificial third body in configuration 2: **(a)** pad surface parallel to the disc surface; **(b)** Tilted pad with respect to the disc surface; (1) open contact area, (2) closed contact area.

In the following experiments, an initial tilt of 40 microns has been given to the pad in the sliding direction, so that it can restrict the path of artificial third body. As a reminder, the undulation of the disc is lower than 7  $\mu\text{m}$ . Figures 6 and 7 show (1) the

initial disc/pad contact distribution (blue in color) without powder, and (2) an optical picture of the powder captured in the interface respectively for configurations 1 and 2. For each figure, (a) and (b) respectively correspond to the parallel test and to the tilted pad test. The results show without ambiguity that tilting the pad allows the alumina powder to be captured in sufficient quantity.

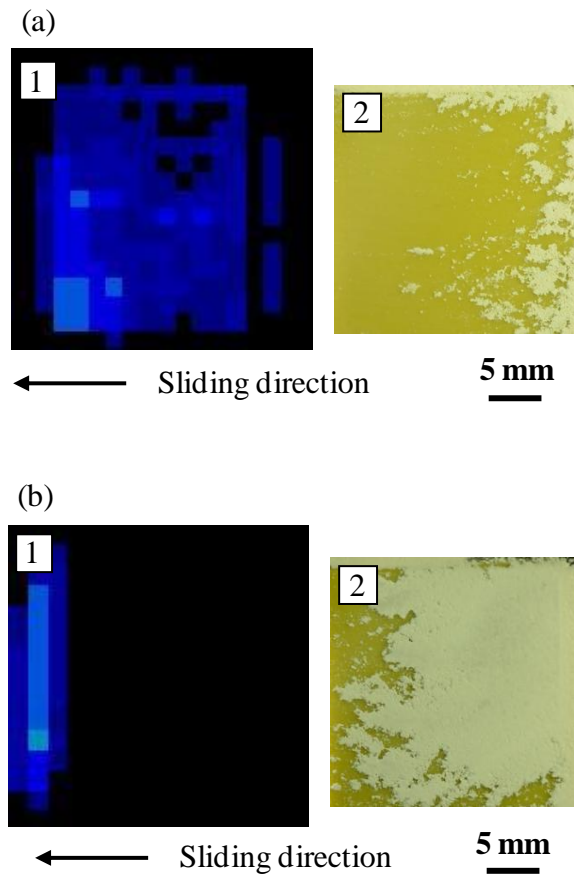


Figure 3.6: Configuration 1: **(a)** pad surface parallel to the disc surface; **(b)** pad is tilted with respect to the disc surface. (1) disc/pad contact distribution (blue in color) without powder, before the experiment and (2) the captured powder in the interface in the respective cases.

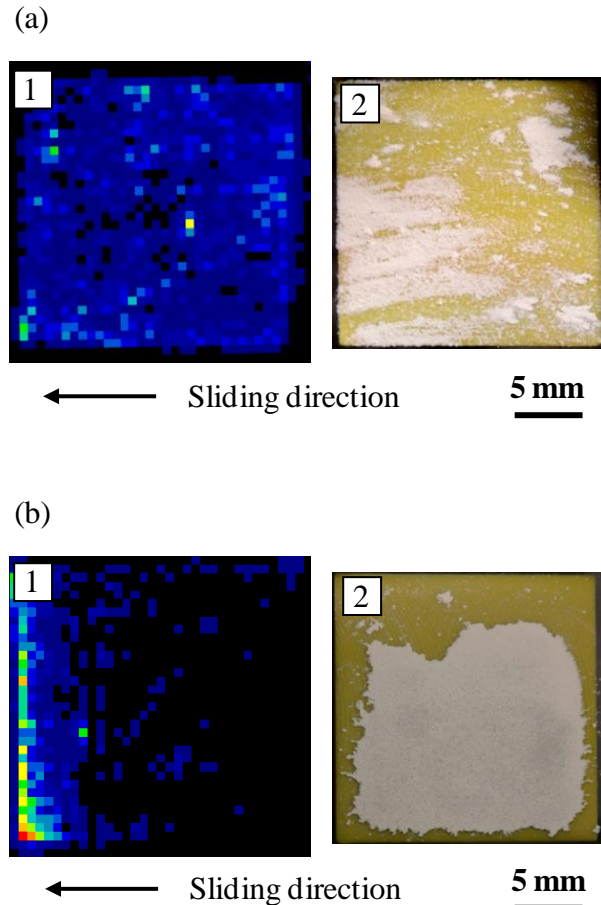


Figure 3.7: Configuration 2: **(a)** pad surface parallel to the disc surface; **(b)** pad is tilted with respect to the disc surface. (1) disc/pad contact distribution (except black color) without powder, before the experiment and (2) the captured powder in the interface in the respective cases.

### 3.3.2 Effect of the third-body recirculation flow

**In configuration 1**, the recirculation flow of the third body along with the disc plays a vital role to capture enough amount of third body at the disc/pad interface. Figure 3.8(1) shows the powder spread on the disc. After spreading the powder on the rotating disc, the pad is allowed to translate towards the disc. While the pad is getting closer to make a contact with the disc, at first, very few particles are captured between the disc and the pad because of the gap between them as shown in Figure 3.8(2). As the pad is getting closer to the disc, more and more powder gets trapped at the interface (at the pad center) as shown in Figure 3.8(3). Due to the recirculation of the disc, some powder particles disengage from the center and establish more primary

plateaus at other locations of the pad as shown in Figure 3.8(4). The escaped particles, which are not trapped in the contact, re-circulate with the disc and accumulate behind the previously trapped particles (primary plateaus) as shown in Figure 3.8(5). Still, many particles escape from these parts, via regions either where no particles are yet trapped or where there is still a gap between the disc and the pad. This trapping process continues until the contact is closed as shown in Figure 3.8(6). At this stage, very few particles are in re-circulation. It is difficult to observe the outgoing particles at the exit of the contact but the accumulation of these re-circulating particles at the entrance is quite visible.

On the contrary, **in configuration 2**, recirculation is not observed because the third body that escapes from the interface falls down due to the gravitational effect.

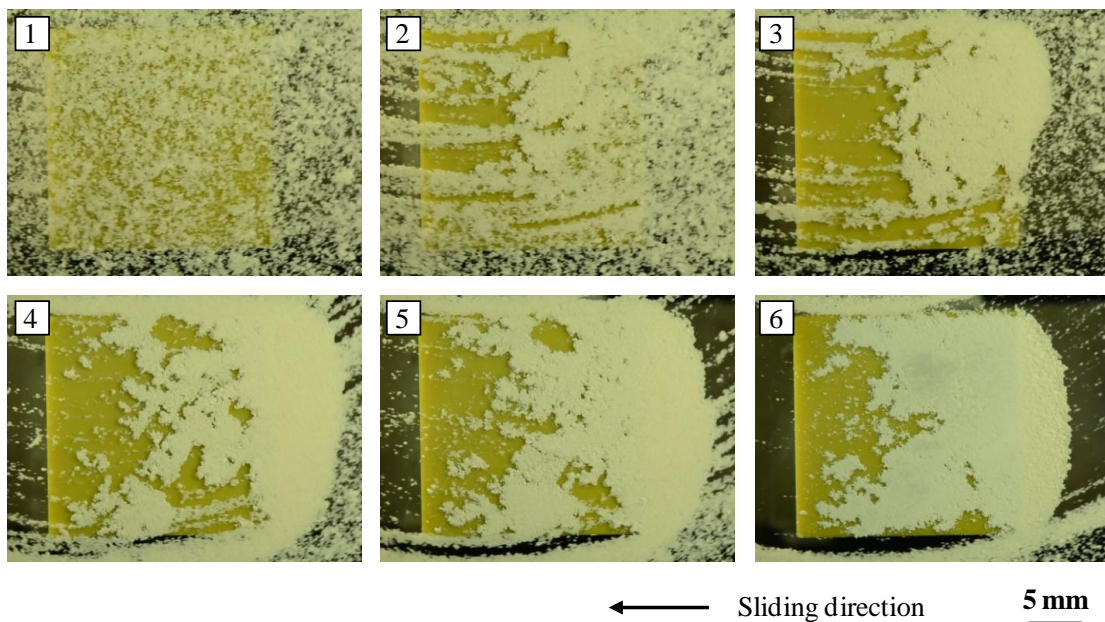


Figure 3.8: Optical pictures of the recirculation flow of the artificial third body during the approach phase of the pad in configuration 1. The third body visibly accumulates by forming primary plateaus.

### 3.3.3 Effect of the amount of third body

- a) **For configuration 1**: Five experiments (with or without pad tilt) with different amounts of powder (large or small) spread on the rotating disc before the experiments are presented in Table 3.1, Table 3.2 and Table 3.3. The tables also

show the different pad orientations used in the experiments namely; (i) no tilt, (ii) tilt in sliding as well as radial direction and (iii) tilt in sliding direction only.

Table 3.1 provides the experimental details regarding the physical states of the disc and the pad, qualitative amount of powder spread on rotating disc and the noise occurrence. Column 2 of Table 3.2, represents the disc/pad contact distribution without third body (before experiment, at 50 N normal load). Column 3 shows optical images of the amount of powder spread on the rotating disc before contact, which can be qualitatively evaluated. The qualitative amount of powder captured in the interface and contact localization can be observed from column 4. Column 5 of Table 3.2 gives information regarding the noise occurrence and the relative spectrum for noise frequencies are presented in column 2 of Table 3.3.

Experiment 1 was performed without pad tilt and with a small amount of powder on the rotating disc. It has captured a sufficient amount of artificial third body, so that the system leads to squeal. The load bearing area can be observed in image as the bright zone, shown in column 4 of Table 3.2. Nonetheless, as explained previously, the lack of reproducibility of this plain solution prevents it from further use.

Experiment 2 (small amount of powder) and experiment 3 (large amount of powder) have been performed with a tilted pad (tilt in sliding as well as radial direction). It can be depicted from the disc/pad contact distribution in column 2 of Table 3.2. It results into a very small amount of powder captured and hence, no noise occurred. This configuration has to be improved.

The disc/pad contact distributions in column 2 for experiments 4 and 5 illustrate that the tilted pads are totally aligned (tilt in sliding direction only): the contact is only at the trailing edge and is uniform on the whole width of the pad. The two experiments are different in terms of powder spread on the disc and similar in terms of capturing the powder and the load bearing areas. In addition, the noise frequencies are similar: 4,600 Hz for experiment 4 and 4,500 Hz for experiment 5 shown in column 2 of Table 3.3. However, this frequency is different from the one measured in experiment 1 (6,000 Hz). This difference may



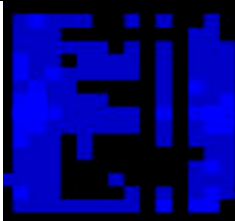
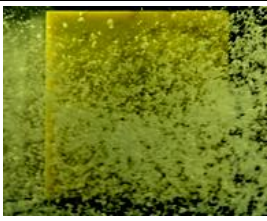
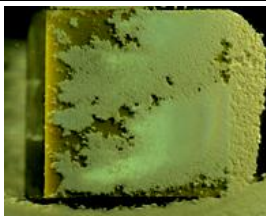
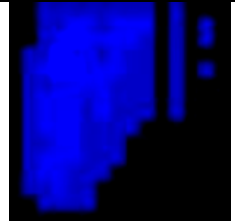
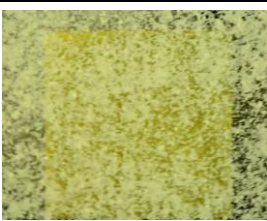
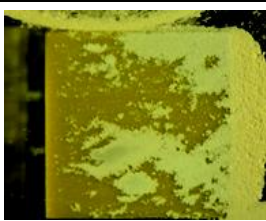
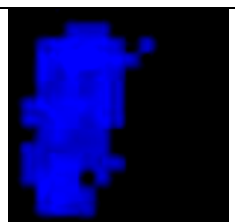

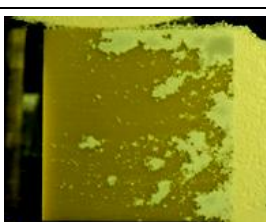
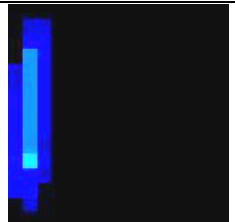
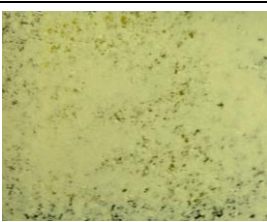
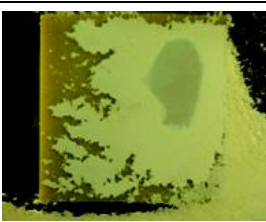
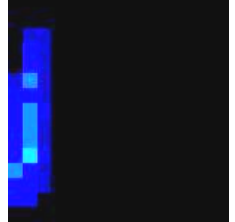

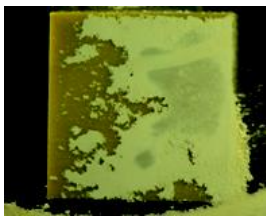
be attributed to the distribution of the captured third body at the interface that leads to much different load bearing areas.

It can be concluded that the quantity of powder spread on the rotating disc does not have much effect on the experimental results in terms of powder captured and noise occurrence. It all depends upon the quantity of powder that is captured at the disc/pad interface and the load bearing area as capturing of powder is random process. One can set parameters and arrangements for the process of capturing the powder such as tilting the pad, but a quantitative approach of the amount of artificial third body to be captured and a mastering of the exact zones where the load bearing areas will set is clearly delusional.

Table 3.1: Experimental details: physical conditions of disc and pad; amount of powder spread on rotating disc of 5 different experiments of configuration 1.

Exp no.	Disc (New / Old)	Pad (New / Old)	Pad tilt (No tilt / Sliding and radial direction / Sliding direction only)	Amount of powder spread on rotating disc (Low / High)	Noise occurrence
Exp 1	New	New	No tilt	Low	Yes
Exp 2	Old	New	Sliding and radial direction	Low	No
Exp 3	Old	Old	Sliding and radial direction	High	No
Exp 4	Old	New	Sliding direction only	High	Yes
Exp 5	Old	Old	Sliding direction only	Low	Yes

Table 3.2: In relation to the Table 3.1, disc/pad contact distribution, amount of powder spread on rotating disc and amount of powder captured in the interface for configuration 1.

Exp no.	Disc/pad contact distribution without third body (before experiment)	Amount of powder spread on rotating disc (qualitative)	Amount of powder captured in the interface (qualitative), and contact localization	Noise occurrence
Exp 1				Yes, spectrum shown in Table 3.3
Exp 2				No
Exp 3				No
Exp 4				Yes, spectrum shown in Table 3.3
Exp 5				Yes, spectrum shown in Table 3.3

Trailing side

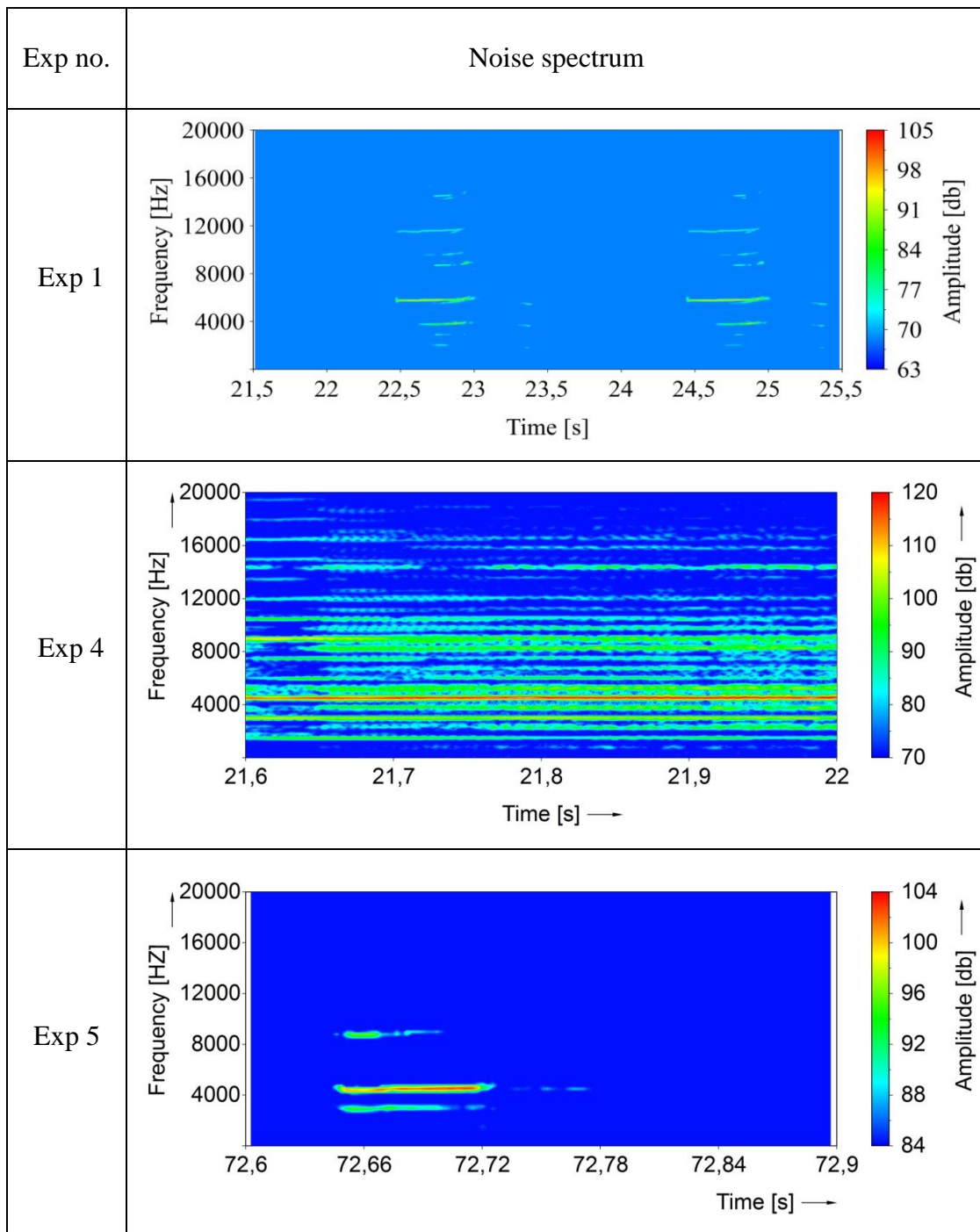


Sliding direction

**5 mm**  

---

Table 3.3: In relation to the Table 3.2, noise spectrum of 3 experiments.



- a) **For configuration 2:** Three experiments (with pad tilt in sliding direction only) with different amounts of powder (large or small) spread on the rotating disc before the experiments are presented in Table 3.4, Table 3.5 and Table 3.6. The amount of powder captured and their corresponding noise spectrum are shown in

the Tables. Here, it is mentioned that the sliding direction shown in Table 3.5 and onwards, for configuration 2, is opposite to the pictures in Table 3.2 for configuration 1.

Similar to configuration 1 as explained above, Table 3.4 provides the experimental details regarding the physical states of the disc and the pad, amount of powder spread on rotating disc and the noise occurrence. Column 2 of Table 3.5 represents the disc/pad contact distribution without third body (before experiment at 50 N normal load). Column 3 shows the amount of powder (qualitatively) spread on the pad before the experiment. The qualitative amount of powder captured in the interface and contact localization can be observed from column 4. Column 5 of Table 3.5 gives information regarding the noise occurrence and the relative spectrum for noise frequencies is presented in column 2 of Table 3.6.

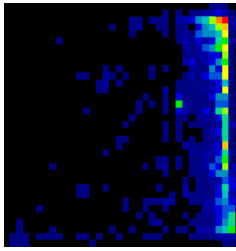

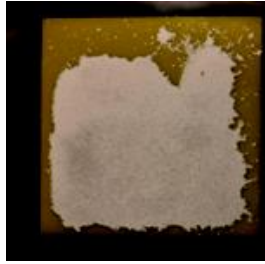
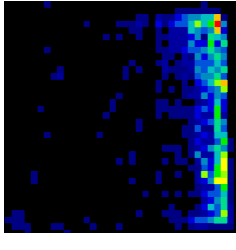

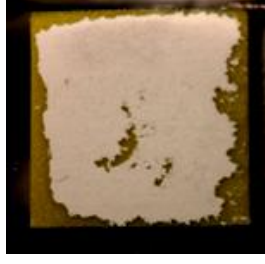
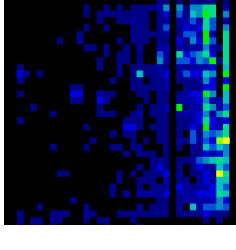

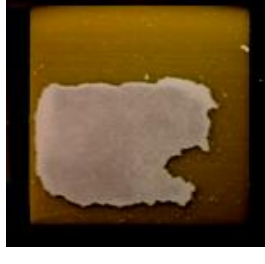
The disc/pad contact distributions in column 2 for experiments 1, 2 and 3 illustrate that the tilted pads are totally aligned (the contact is only at the trailing edge and it is uniform). As can be seen in column 3, the smallest quantity of powder spread on the pad is in experiment 1, while the largest amount is in experiment 3. Still, all three experiments are almost identical in terms of capturing the powder and of noise occurrence. The noise frequencies are similar in all the experiments, (i) 16,000 Hz for experiment 1, (ii) 16,500 Hz for experiment 2 and (iii) 16,100 Hz for experiment 3 as shown in column 2 of Table 3.6.

It can be concluded that – as in configuration 1 – in configuration 2 also, the quantity of powder spread on the pad does not have much effect on the experimental results in terms of captured powder and noise occurrence.

Table 3.4: Experimental details: physical conditions of disc and pad; amount of powder spread on rotating disc of 3 different experiments of configuration 2.

Exp no.	Disc (New / Old)	Pad (New / Old)	Pad tilt (No tilt / Sliding direction only)	Amount of powder spread on rotating disc (Low /Medium / High)	Noise occurrence
Exp 1	Old	New	Sliding direction only	Low	Yes
Exp 2	Old	New	Sliding direction only	Medium	Yes
Exp 3	New	New	Sliding direction only	High	Yes

Table 3.5: In relation to the Table 3.4, Disc/pad contact distribution, amount of powder spread on the pad and amount of powder captured in the interface for configuration 2.

Exp no.	Disc/pad contact distribution without third body (before experiment at 50 N load)	Amount of powder spread on rotating disc (qualitative)	Amount of powder captured in the interface (qualitative) and contact localization	Noise occurrence
Exp 1				Yes, spectrum shown in Table 3.6
Exp 2				Yes, spectrum shown in Table 3.6
Exp 3				Yes, spectrum shown in Table 3.6

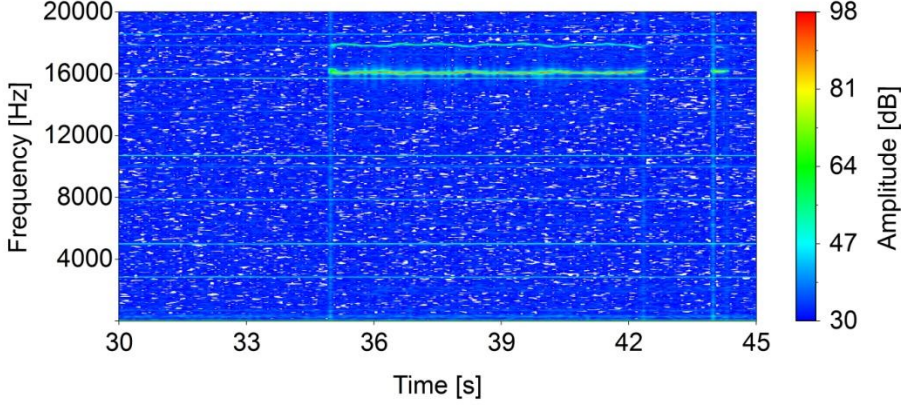
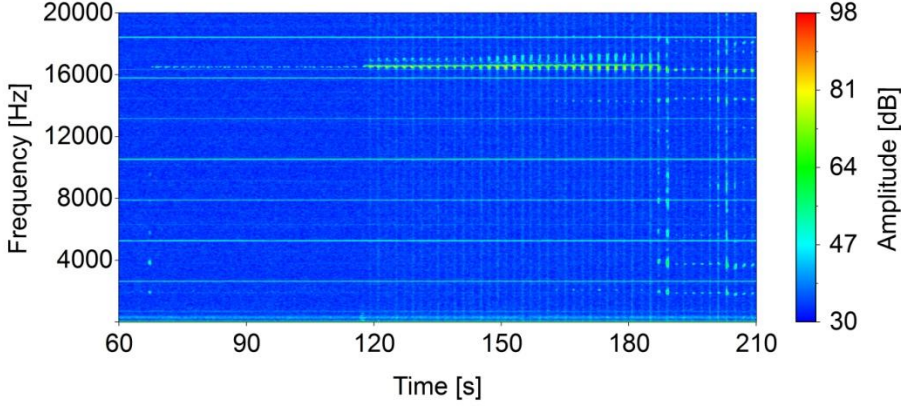
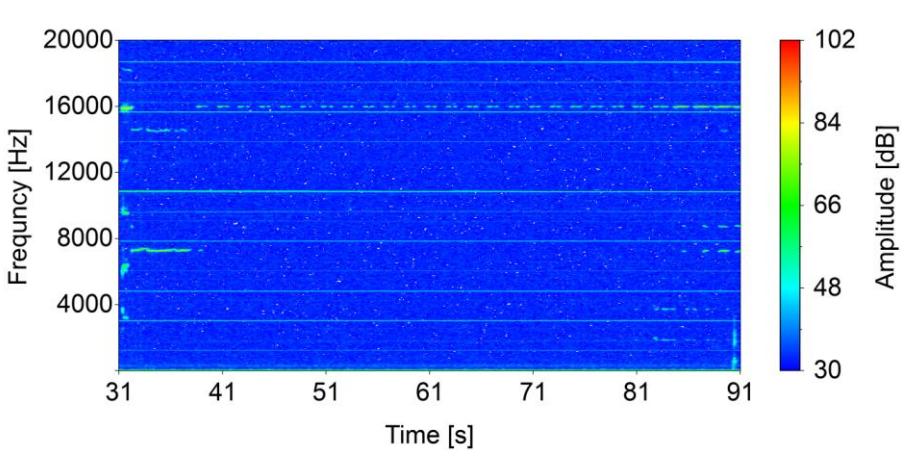
Trailing side

Sliding direction  $\longrightarrow$

5 mm

The sliding direction for configuration 2 is opposite to the pictures of configuration 1.

Table 3.6: In relation to the Table 3.5, noise spectrum of 3 experiments.

Exp no.	Noise spectrum
Exp 1	 <p>20000 16000 12000 8000 4000</p> <p>Frequency [Hz]</p> <p>30 33 36 39 42 45</p> <p>Time [s]</p> <p>98 81 64 47 30</p> <p>Amplitude [dB]</p>
Exp 2	 <p>20000 16000 12000 8000 4000</p> <p>Frequency [Hz]</p> <p>60 90 120 150 180 210</p> <p>Time [s]</p> <p>98 81 64 47 30</p> <p>Amplitude [dB]</p>
Exp 3	 <p>20000 16000 12000 8000 4000</p> <p>Frequency [Hz]</p> <p>31 41 51 61 71 81 91</p> <p>Time [s]</p> <p>102 84 66 48 30</p> <p>Amplitude [dB]</p>

### **3.3.4 Test repeatability**

A repeatable test is defined in our study as a test in which a sufficient amount of artificial third-body is trapped during the approach of the pad, is maintained in the interface during the test and further leads to noise occurrence.

Conclusions from the five different experiments with configuration 1 (see above in section 3.3.3 and the relative data shown in Table 3.2) were in favor of experiments 4 and 5, where the contact distribution is at the end of the trailing side. This configuration always traps the third body and leads to occurrences of squeal. These two tests also show the similar behavior in terms of noise frequencies. In experiment 1, the powder is also captured, but not due to the tilt but to the pad valleys. Although it captured enough powder to produce squeal, this test is not repeatable as the pad valleys are defined by the manufacturing or clamping defects.

The remaining two experiments (2 and 3), in which the contact distribution is not at the end of the trailing side, are not able to trap enough artificial third-body due to the absence of wedge to anchor the flow of third body and no noise appears in these experiments.

Similarly, all three experiments with a tilted pad in configuration 2 (section 3.3.3 and the relative data shown in Table 3.5) are consistent in trapping alumina powder, maintaining it in the contact during friction and producing squeal.

Hence, all the experiments in which the artificial third body well trapped at the disc/pad interface are prone to squeal. This trapping of the third body is consistently achieved by tilting the pad to make a wedge for the intervention of the flow of third body. Therefore, it can be said that tilting the pad provides the repeatability to obtain the noise by trapping the third body.

## **3.4 Synthesis of the protocols for experimental configuration 2**

Based upon the results of the previous part on parametric study it is concluded that the experimental configuration 2 is better than the configuration 1 in terms of capturing the artificial third-body in the disc/pad interface and most importantly, the disc displacement sensors along with the torque-meter can be installed. Therefore,



experimental configuration 2 (pad and contact under the disc) is retained for the remaining of the study.

Actually, in this configuration, the technique to capture the third body in the interface was improved by more than just tilting the pad. To avoid powder ejection from the contact by the rotation of the disc, it was decided to modify the approach protocol by comparison with configuration 1. The pad is tilted beforehand at an angle in the sliding direction. That is to say that the leading side is slightly open whereas the trailing side is slightly closed. However, once the pad was adjusted (tilt), the experiment was conducted by following three successive steps, namely:

- i. Leveling of artificial third body
- ii. Compaction of third body
- iii. The main friction test itself

The leveling is done by disc rotation and vertical translation of the pad towards the disc. Compaction is prepared by pad translation the pad only without disc rotation. Once leveling and compaction are fulfilled, the friction test begins. It is performed, again, by both disc rotation and vertical translation of the pad towards the disc. In all the above steps, the pad is stopped at a pre-established disc/pad gap but at three different levels as presented in Table 3.7. Here, ‘R’ stands for ‘rotation of the disc’ and ‘T’ for ‘translation of the pad’.

Five experiments are illustrated in Table 3.7, Table 3.8 and Table 3.9 to establish clearly the final protocol.

Table 3.8 shows the respective optical images of the artificial third-body distribution just before the tests and after each step of the tests protocol. Table 3.9 shows the noise spectrum of the only 2 experiments out of 5 that produced squeal.

As shown in Table 3.7, for the experiments without the pad tilt, a 600  $\mu\text{m}$  gap between the disc and the pad has been chosen for the leveling of the artificial third body. For step 2 and step 3, different combinations are used in different tests. Test 1 and test 2 did not manage to trap the third body in the interface as the optical images show in Table 3.8. The disc/pad gap combination for all three steps of the protocol for test 3 is able to capture the third-body but as soon as friction-induced vibrations








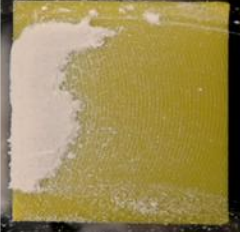










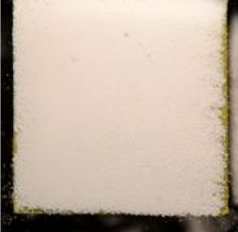

occur, the captured third-body is not able to provide a stable plateau to bear the load, as shown in Table 3.8. The relative spectrum is shown in Table 3.9. It shows that a single squeal event occurs after about 42 s of test. It appears from this experiment that the compaction of the powder is an important condition for this study. In this case, compaction of the alumina third body is not sufficient to maintain it in a vibrating contact. Consequently, this behavior is too unstable to allow further study, as strong vibrations are sought after in this study.

As the protocol for tests without pad tilt does not retain the third-body in the interface throughout the test and therefore is not able to produce squeal, it is decided to set this three-step protocol with a pad tilt (test 4 and 5). Here, the leveling (step 1) is done at a 350- $\mu\text{m}$  gap and the friction test (step 3) is done when the gap reaches 100  $\mu\text{m}$ . The only difference between test 4 and 5 is the difference in the gap at step 2 (compaction). Test 4 works well in terms of retaining the third body in the interface throughout the test but was not able to produce squeal. The optical image during the friction test (step 3) is shown in Table 3.8. To improve test 4, it is decided to increase the third body compaction (in step 2) by decreasing the gap from 150 to 125  $\mu\text{m}$ . This new protocol allows capturing and retaining the third body throughout the test and producing squeal. The spectrum of test 5 is shown in Table 3.9. The noise frequency in the first half of the test was 16,200 Hz until a change occurs at the interface. Thereafter, the frequencies are 1,600 Hz and its harmonics until the test is stopped.

Table 3.7. Synthesis of the protocols for the configuration 2.

Test no.	Pad tilt	Disc/pad gap ( $\mu\text{m}$ ), step (1) 'R' & 'T'	Disc/pad gap ( $\mu\text{m}$ ), step (2) 'T' only	Disc/pad gap ( $\mu\text{m}$ ), step (3) 'R' & 'T'	Third body captured	Noise occurrence
Test 1	No	600	400	300	No	No
Test 2	No	600	350	300	No	No
Test 3	No	600	350	200	Yes	Yes, spectrum shown in Table 3.9
Test 4	Yes	350	150	100	Yes	No
Test 5	Yes	350	125	100	Yes	Yes, spectrum shown in Table 3.9

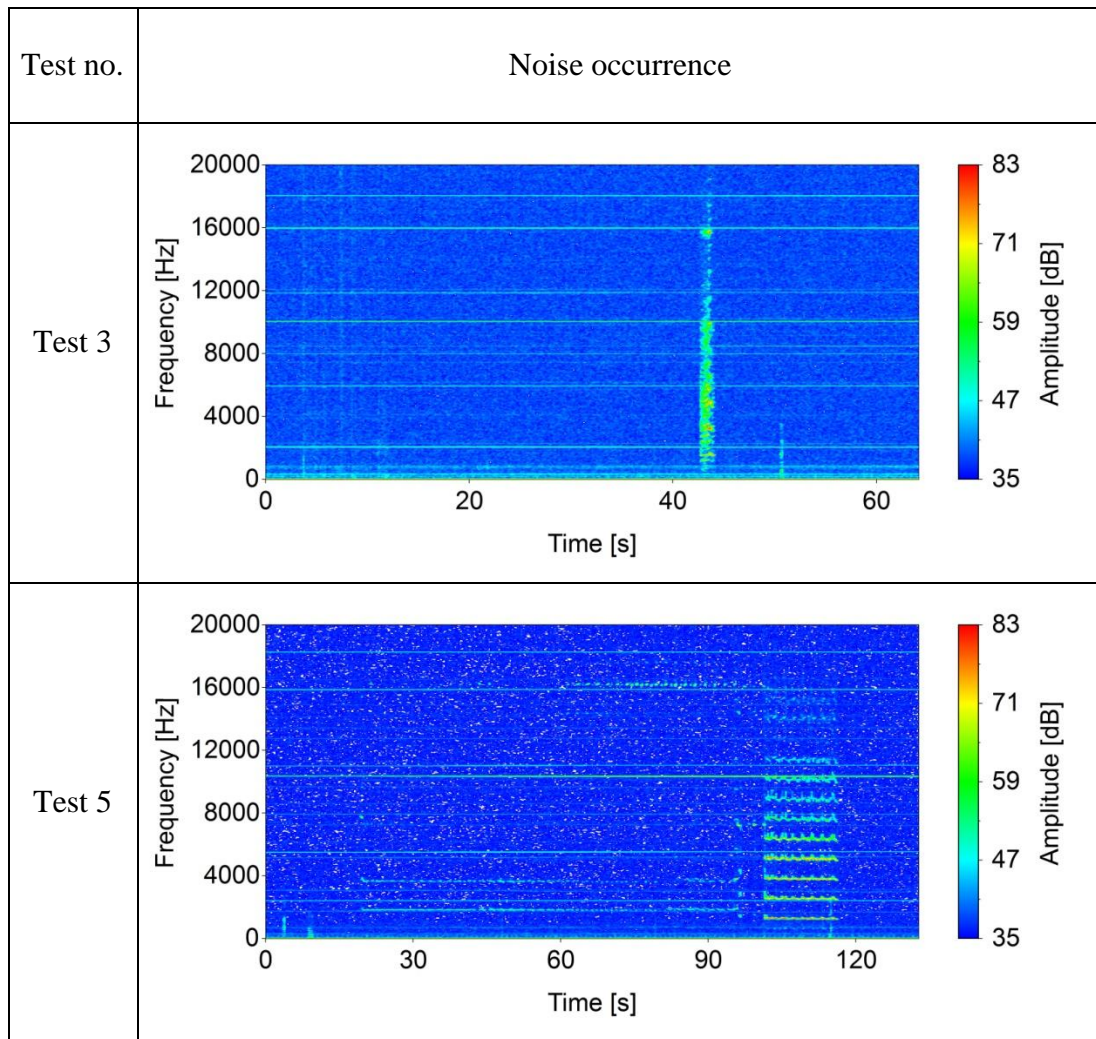
Table 3.8: In relation to the Table 3.7, optical images of the artificial third-body distribution just before the tests and after each step of the protocol for the respective tests.

Test no.	Artificial third body spread before the experiment	Artificial third body after leveling (Step 1)	Artificial third body after compaction (Step 2)	Artificial third body during the friction test (Step 3)
Test 1				
Test 2				
Test 3				
Test 4				
Test 5				

Sliding direction →

5 mm

Table 3.9: In relation to Table 3.7, noise spectrum of experiments 3 (no tilt) and 5 (tilt).



### 3.5 Conclusions

Two types of experimental configurations have been presented. The pros and cons of these configurations, in terms of set-up and instrumentation, show that a contact on the underside of the disc (configuration 2) has to be preferred over a contact on the upper side of the disc (configuration 1).

As explained in chapter 2, a layer of artificial third body is needed to provoke squeal consistently. This chapter showed that trapping the third-body and maintaining it in the contact were two different problems. The experiments presented in this chapter proved tilting the pad to open the contact at the leading edge and to close it at

the trailing edge works for both configurations. The parametric study for two configurations show that the amount of powder spread before experiment does not have much effect. Instead, everything depends upon the amount of powder captured in the interface, which is random. Nonetheless, more consistency was achieved in trapping a sufficient amount of third body to create a dense load-bearing area that seems to be the condition to squeal. Problems linked with the recirculation of third body along with disc rotation are eliminated in case of configuration 2.

Finally, the geometry of the setup in configuration 2 allows for more instrumentation and a direct observation of the contact.

In the end, configuration 2 is considered better than configuration 1. The synthesis of the protocol for configuration 2 has been presented (in three steps) and concluded that the protocol of test 5 is the most consistent in terms of retaining the third-body in the interface and of producing squeal. In the next chapter the detailed procedure, its execution and results & discussion are presented.

---

## **CHAPTER 4: TOWARDS THE EARLY STAGE OF SQUEAL**

---

## 4 Towards the early stage of squeal

---

Two test configurations have been discussed in the previous chapters. The techniques used to trap the artificial third body at the disc/pad interface and the effects of different parameters in the two experimental configurations are discussed. The complete set of parameters of the final experiment is thus determined. This chapter deals with the final detailed protocol and the execution of the experiment.

To better understand the third body flow and associated physical mechanisms in the contact during the different phases (different noise intensities), optical images were extracted from the *in-situ* observation recorded by the optical camera. In a first approach, the images are interpreted in term of behavior of third body (compaction, flow, fragmentation...), then using a digital image processing, additional data concerning the actual load-bearing area and its time variation was obtained from the images.

### 4.1 System behavior

The schematic diagram, shown in Figure 4.1, illustrates how the elastic thin plate drives the system to accommodate the pad-disc contact while the disc is stationary or rotating:

- a) The pad and the disc are not in contact and the thin plate remains straight.
- b) The pad along with the rigid block is moved towards the stationary disc and the bending of the thin plate ensures the normal loading of the flat contact between the third-body layer and the disc.
- c) The disc is rotating and the sliding friction changes the bending of the thin plate, involving a tilt of the pad that has to be accommodated by the third-body layer.
- d) In practice, the disc rotation is not perfect, resulting in an apparent undulation of the friction surface and in a cyclic variation of the normal and tangential contact loading that changes the bending of the thin plate.



As a result, the rotational undulation of the disc enables the cyclic opening and closing of the contact interface, in terms of thickness as well as tilt, which the third-body layer has to accommodate. This interesting driving effect implies a dynamic of the bearing capacity achieved by the third-body layer, whether in location or extent. The accommodation of these contact variations results in internal flows of the third body, modifying its compaction and extent in the apparent contact area.

Displacement sensors help to follow the kinematic of the system: out-of plane displacement measurements at the backside of the pad and the disc can be used as indicators of the variation of the pad-disc clearance, where the third body accumulates both in thickness and slope in the sliding direction.

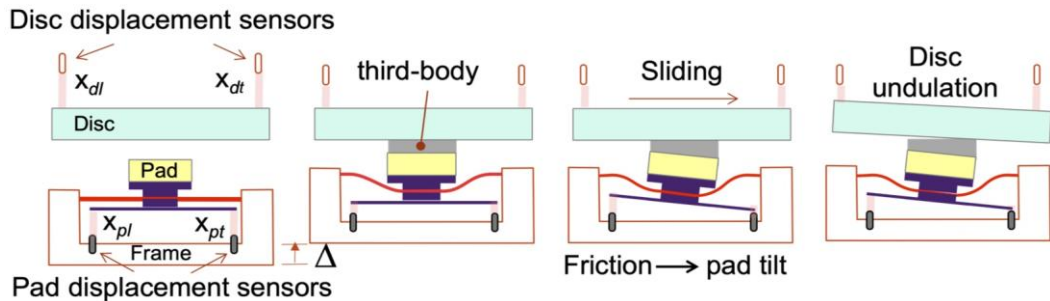


Figure 4.1: Pad-disc contact accommodation: (a) open contact; (b) contact closed, third-body layer bearing the load applied by the thin-plate bending; (c) contact closed, sliding friction involving a pad tilt allowed by the thin-plate bending; (d) contact closed, rotational undulation of the disc involving cyclic variation of the pad-disc clearance in thickness and tilt.

## 4.2 Experimental procedure

Preliminary tests (illustrated in chapter 3) showed clearly that having the pad parallel to the disc prevents trapping enough powder in the interface. Indeed, in this case, powder is ejected from the contact, as soon as the disc touches the powder during its rotation. To avoid this problem, it was decided to slightly compact the powder and tilt the pad before the test with an angle of 0.1 degree in the sliding direction.

To this end, a pressure film was used, before spreading the powder on the pad, to visualize the disc/pad contact distribution, and fine adjustments are then made by

inserting thin spacers (aluminum foil, 40  $\mu\text{m}$  thick) between the steel plate and the pad in order to master the contact distribution. Figure 4.2 shows a typical disc/pad contact distribution, (a) homogeneous before tilting the pad, and (b) concentrated on the trailing edge after tilting the pad.

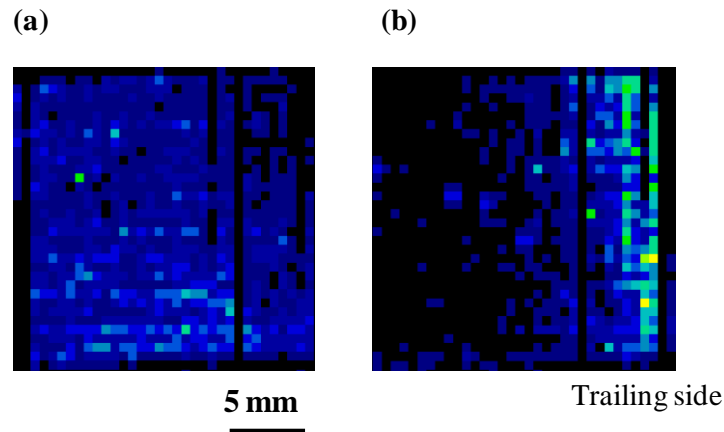


Figure 4.2: Pressure film measurements of the disc/pad contact distribution: (a) without pad tilting; (b) with pad tilting (pressure film measurement: low to high pressure from dark to light).

It should be recalled here that, in this experiment, to apply the normal load the pad is moved up to be in contact with the disc. For this reason, the reference distance of all calibrations is related to the bottom surface of the disc. The initial clearance between the trailing side of the pad surface and the sliding surface of the disc was fixed to 800  $\mu\text{m}$  for all tests.

Once the pad was adjusted (with 0.1 degree tilt), the experiment was conducted following three successive steps as explained in chapter 3, e.g. leveling of artificial third body, compaction of third body and the main friction test:

- Step 1: The leveling step aims at having a uniform thickness of the artificial third body on the surface of the pad. It consists in (i) spraying the powder on the pad surface (initially located at 800  $\mu\text{m}$  under the bottom surface of the disc), (ii) translating the pad in the normal direction toward the rotating disc until a clearance of 350  $\mu\text{m}$  is reached and maintaining the system in this position for a short time (1 second), (iii) and finally translating the pad back to the initial

position of 800  $\mu\text{m}$ . At the end of this step a homogeneous thickness of powdery third body layer is achieved.

- Step 2: Compaction is a vital step to ensure adequate trapping of powder inside the contact. It consists in compressing the leveled layer of third body in the contact by translating the pad toward the disc from its initial position from 800  $\mu\text{m}$  to 125  $\mu\text{m}$  without disc rotation. At the end of this step, the pad is again translated back to its initial position at 800  $\mu\text{m}$ .
- Step 3: Once leveling and compaction are fulfilled, the friction test can begin by rotating the disc at 30 rpm, then translating the pad vertically from its initial position to 100  $\mu\text{m}$  in order to establish the contact with the rotating disc. The main test duration was around 60 seconds before ending it by opening the contact then stopping the rotation. It should be noticed that the bearing contact is fully supported by the trapped third body layer and that there is no direct contact between the first bodies (pad and disc).

The friction tests were performed under disc rotation speed of 30 rpm (corresponding to a linear sliding speed of 0.14 m/s in the mid friction track). All tests were performed under room temperature of 20-22  $^{\circ}\text{C}$  and a relative humidity ranging between 35-40%.

## **4.3 Results and discussion**

### **4.3.1 Normal load and sound pressure**

As mention above, in the present work, the occurrence of squeal with presence of an artificial inert third body (alumina powder) was investigated experimentally. In this section, only results obtained during step 3 are presented. Figure 4.3 shows the time variation of the normal load, measured by the eddy current sensors, and the sound pressure recorded by a microphone located close to the contact. The typical behavior during the friction experiment can be divided into three successive stages: Stage{a} (30 s) corresponds to the upwards translation of the pad from initial position (800  $\mu\text{m}$ ) to the initial contact of the compacted third-body layer with the sliding surface of the disc. During this first stage no normal load is obtained. Stage{b} corresponds to the fast increase of the normal load due to the compression of the

third-body layer while the pad is reaching its final predefined position (100  $\mu\text{m}$ ). Stage{c} corresponds to the time period of the sliding-friction experiment during which no external actions are undertaken except the disc rotation. Indeed, during this last stage, all changes in friction conditions from one disc revolution to another are due to dynamic variation of the third-body layer, which constitutes the exclusive load-bearing area of the contact.

In stage{c} the variation of the normal load can be explained by two contributions. On the one hand, the near-periodic fluctuation of the load, at the same frequency of that of the disc rotation, is induced by the disc undulation. On the other hand, considering the mean value of the cyclic fluctuation, a slight and gradual change of the average normal load can be observed, increasing until  $t \sim 83$  s, before decreasing until the end of the test. This evolution of the load to the change of the third-body layer is attributed and discussed in the next section.

As can be seen in the time-variation graph of sound pressure and frequency-time, a high sound pressure is registered in stage{b} and continued in regressive manner into early stage{c1} correlated with both high (16 kHz) and low (7.5 kHz) frequencies. Then, during stage{c2}, except relatively small and isolated peaks correlated with high frequency (16 kHz), the sound pressure vanished and a quasi-steady state is established. Towards the end of the test, stage{c3}, there is a re-increase of sound pressure, along with high (16 kHz) and low (7.5 kHz) frequencies.

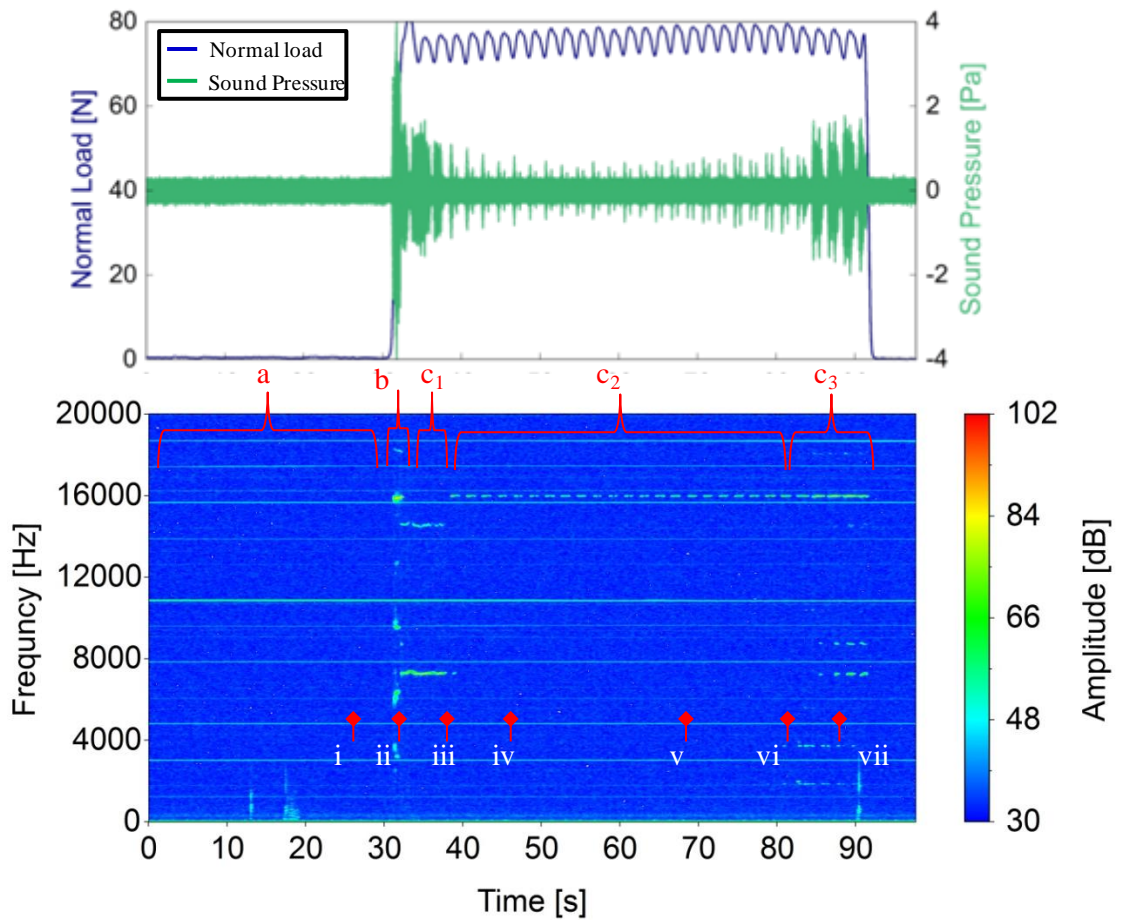


Figure 4.3: Temporal analysis of the experiment: variation of the normal load and the sound pressure, and frequency-time diagram of the noise emission.

To better understand the third-body flows and associated physical mechanisms in the contact during the different phases (noise emissions), a selection of scenes, extracted from the *in-situ* observation recorded by the optical camera, are presented on Figure 4.4. On these pictures, the leading side of the contact area is on the right; the trailing side on the left; the upper side corresponds to the outer perimeter and the lower side to the inner perimeter of the contact area with respect to the disc rotation. Each scene corresponds to a particular instant of the test chronology. The numbering of the pictures, from (i) to (vii) in chronological order, is indicated on the time-frequency diagram in order to correlate the evolution of the load-bearing area with acoustic events.

The first scene(i) corresponds to the end of stage{a} showing the early contact between the rotating disc and the third-body layer deposited on the pad. The, next scene(ii) corresponds to stage{b} in which high-intensity noises occur (see correlation with sound pressure graph in Figure 4.3 ). This noise event is related to the initial compaction of the third-body layer along with high flows of third body. Scene(iii), taken at the end of stage{c1}, shows that, due to the high-amplitude vibrations occurring in the contact during this stage, the third-body layer is partially destroyed and removed from the external perimeter of the contact area. As will be seen in section 4, the contact was mainly located inside the friction track during the test. Thus, the third-body layer, which was loosely compressed on the outside of the friction track, could not be maintained during this period of vibration. . All scenes of the “quasi steady-state” period (stage{c2}, from iv to vi) show clearly that a certain stabilization of the third-body layer is reached and no more notable variation occurs in the contact at this macroscopic scale. Looking at scene (vii) during the second noisy event (stage{c3} toward the end of the experiment), high intensity vibrations were not able to destabilize so much the third-body layer. However, a fragmentation of the third-body layer along the leading side of the contact area can be noticed (Figure 4.5). The video shows that the third body does not stick on the pad anymore at the contact entrance, but is maintained in contact by the load-bearing area downstream.

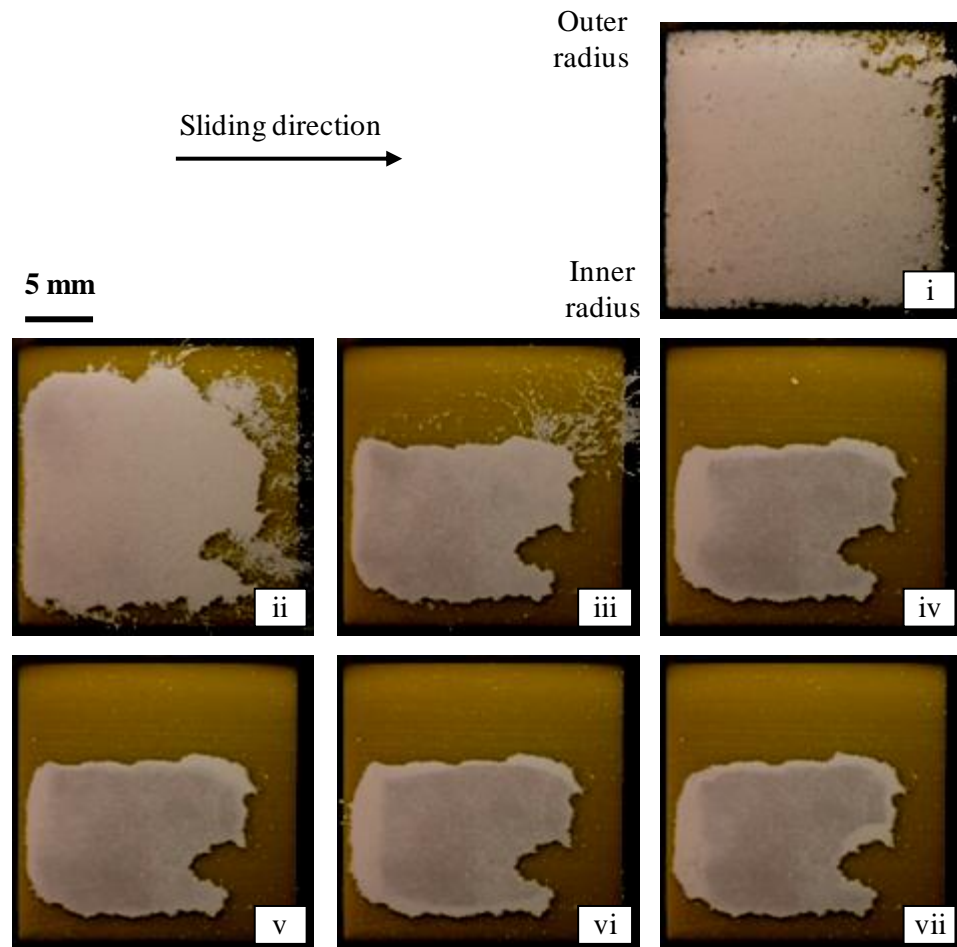


Figure 4.4: Successive scenes of the apparent contact area related to particular times, (i) to (vii), in the test chronology, as shown in Figure 4.3.

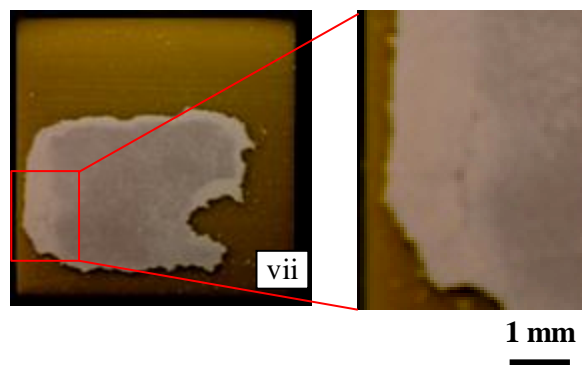


Figure 4.5: Contact scene during the last noisy event of the experiment (stage c3): fragmentation and de-cohesion of the third-body layer along the leading side of the contact area.

### 4.3.2 Friction and pad tilt

Figure 4.6 presents the time variation of the friction coefficient and of the dynamic pad tilt during the contacting period of the experiment; the normal load is recalled as a reminder. As previously discussed, the contact was concentrated in the inner part of the friction track during the test, with little variation in the radial position of the contact location. The friction coefficient was determined from the torque measurement, considering the variation in the radius of application of the resulting contact forces to be negligible. The friction coefficient was determined by arbitrarily considering the average radius in the calculation.

Concerning the slope of the pad, the figure shows the changes in the tilt from an arbitrary zero-reference at the time of first contact (beginning of stage {c1}). The tilt is indicated as an out-of-plane displacement corresponding to the opening or closing of the pad surface at the trailing edge relative to the leading edge. The tilt evolves cyclically in accordance with the normal force, logically opening the pad surface at the trailing edge while the normal load and the friction force increase.

Considering the friction, up to  $t = 45$  s (stage {b}, stage {c1} and beginning of the quasi steady-state stage {c2} of Figure 4.3), the friction coefficient is fluctuating in accordance with the disc revolutions. The average friction decreases during this time period and then increases thereafter, during the quasi-steady-state stage {c2} (from  $t = 45$  s to  $t = 80$  s). One can notice that the friction and the pad tilt fluctuate together as well as the regular decrease in the amplitude of the friction fluctuation during this period.



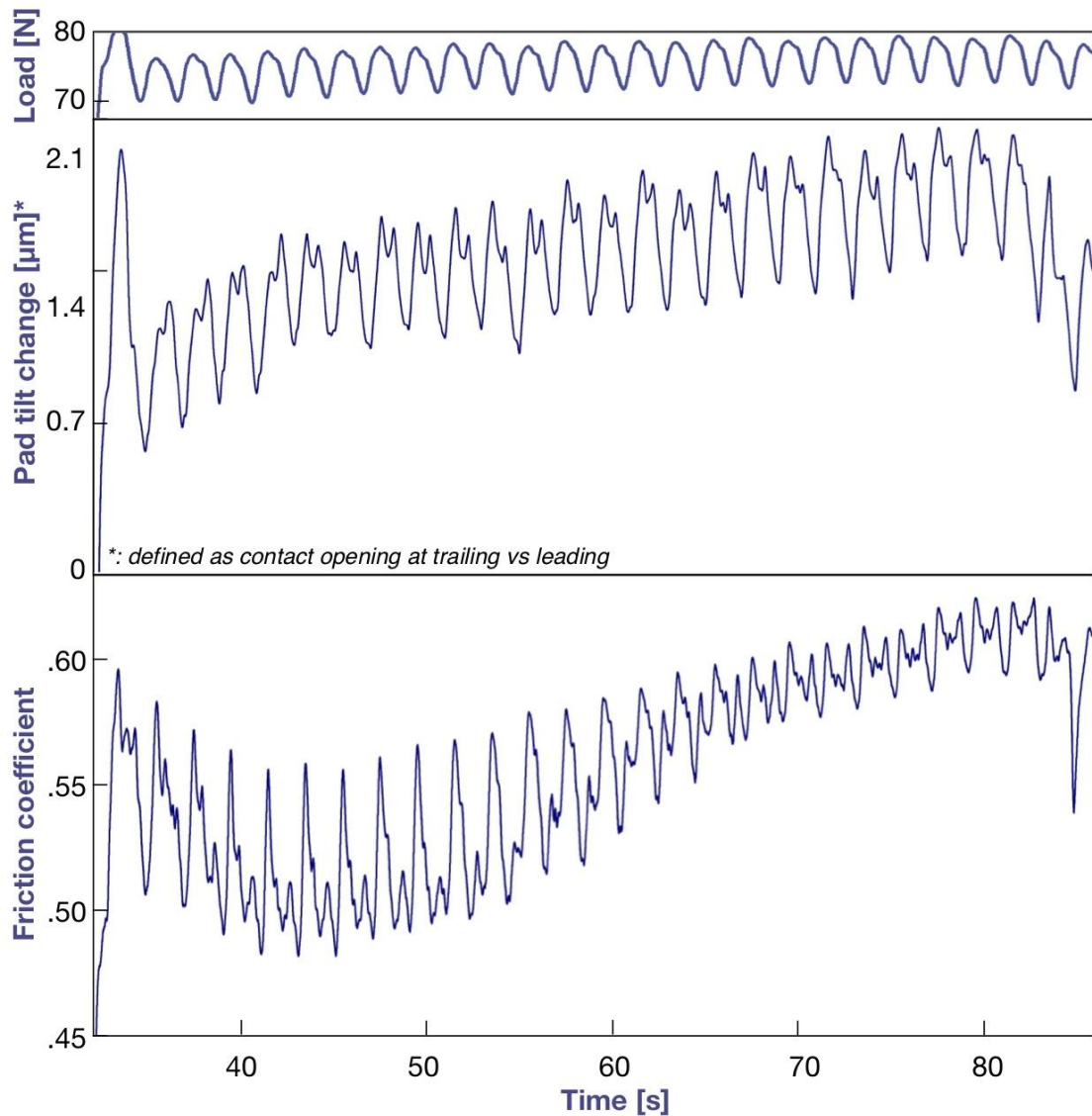


Figure 4.6: Variation of friction and pad tilt as a function of time.

To explain this behavior one should consider the fact that the contact is fully carried out through the third-body, without any contact between the first bodies. As widely admitted by the tribology community, friction between mating surfaces results from several contributions (e.g. mechanical (deformation), adhesive and so on). In our case, it is considered that the friction results from the combination of velocity accommodation in the bulk of the third-body layer and the sliding of the disc on the third-body layer. Thus, during the increase in the force following the compression of the third body (stage{c1}), the high amplitude of the vibration favors the redistribution of the third body in the interface. The internal flows of the third body

thus contribute significantly to the velocity accommodation while homogenizing the load bearing area. This is associated with the decrease in friction during this stage.

To clarify the cyclic behavior, the evolution of the load-bearing area at each revolution of the disc is considered. Figure 4.7 shows the location of the load-bearing area in the apparent contact area for 3 cycles as a function of the tilt of the pad. On each picture a) to e), one can identify the load-bearing area in dark while the third-body layer surrounding in white corresponds to open area where no contact occurs between the third-body layer and the disc (also shown in Figure 4.11, with digital image analysis). It can be noticed that the load-bearing area moves with each revolution from leading to trailing, depending on the opening and closing of the pad tilt. When the pad tilt is low, the contact area moves towards the leading edge, and when the pad tilt is high, the contact area is located towards the trailing edge. This movement of the contact area is made possible by the ability of the third-body layer to accommodate the load-bearing capacity, i.e. by the ability of the third body to flow into the interface. One can consider that the third-body internal flows essentially follow the sliding from leading to trailing, which is then facilitated when the contact is open towards the trailing edge, and conversely, is more difficult when the contact is closed. We understand the friction fluctuations with this possibility of the third body to flow more or less freely in the interface. A similar argument can be proposed to explain the decrease in friction fluctuation. By successive flows, cycle after cycle, the third body is redistributed in the interface in order to homogenize the load bearing capacity. This redistribution of the third body tends to reduce its mobility when the contact is open downstream, and increase it when the contact closes.

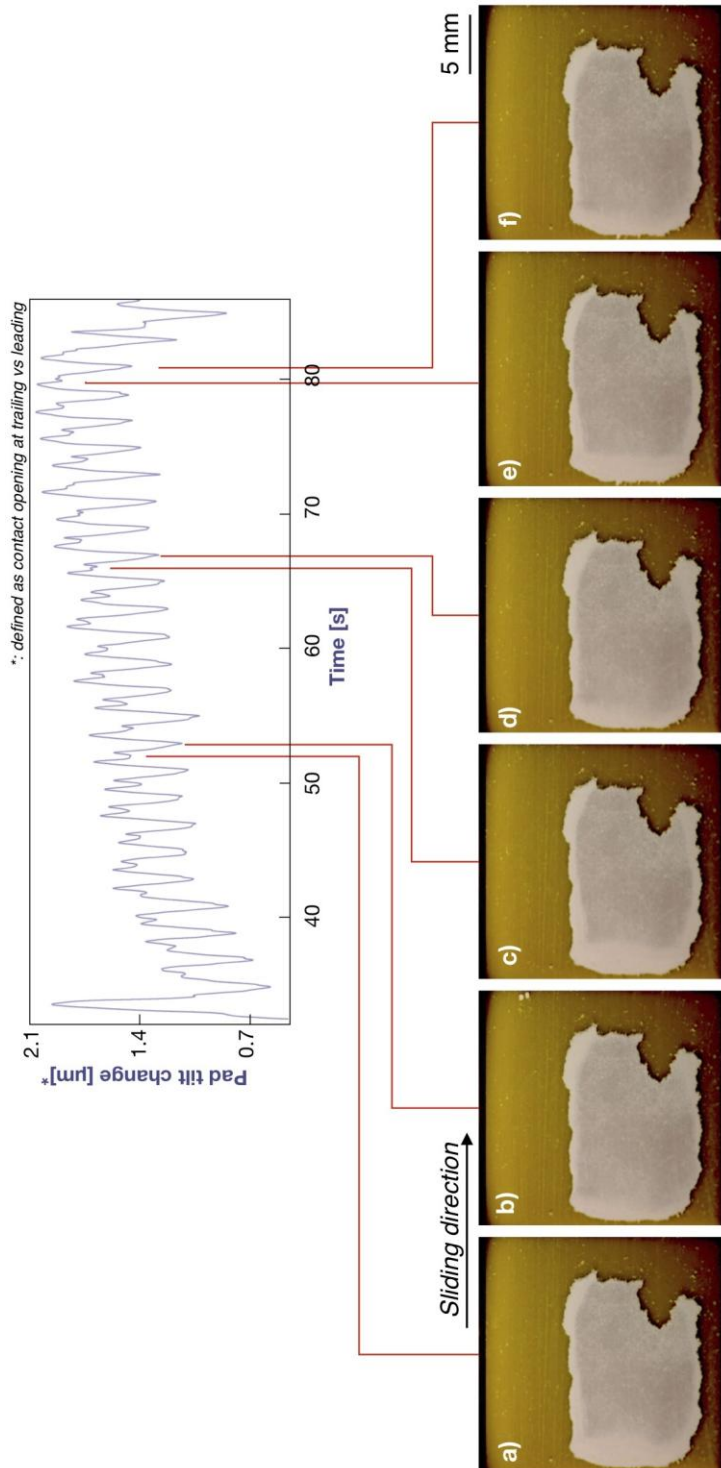


Figure 4.7: Cyclic mobility of the load-bearing area: a), c), e) towards the leading when the pad tilt is opening, b), d) f) towards the trailing when the pad tilt is closing.

The rise of the average friction value can be associated with the progressive redistribution of third body particles in the interface. Under normal load, these particle flows promote the compaction of the third-body layer, and the homogeneity of the surface of interaction with the disc. One can consider that reducing the surface porosity of the powdery third body increases the “adhesive” interactions between the third-body layer and the quartz disc surface.

It should be clarified here that changes in contact conditions occur at the micro-scale, which is far below the resolution of the used *in-situ* optical observation instrument.

#### **4.4 Characterization of the third-body layer**

In order to follow the evolution of the third body in terms of compaction and porosity, post-friction characterizations have been conducted using 3D optical profilometer (Wyko NT1100, Veeco, Tucson, USA) and FIB-SEM. To do so, at the end of the friction test, the contact was opened and the pad carefully removed with its adhering third-body layer for post-friction characterizations. Zones to be characterized were chosen based on optical images taken during the friction test.

Figure 4.8(i) represents the optical image of pad with third-body layer captured during the friction test. This image is transformed in to a digital colored image to distinguish the grey level of third-body layer. The high to low grey level of third-body layer in Figure 4.8(i) is shown as dark to light scale (145 to 205 color scale) in Figure 4.8(ii). Two characteristic zones (see illustration in Figure 4.8(ii), shown as black rectangles) have hence been selected; zone (a) corresponding to the “dark” part considered to be fully in the load-bearing area during the whole test duration and zone (b) corresponding to an area that underwent periodical changes in contact condition between “dark” and “bright” as a function of the cyclic contact loading induced by the disc undulation.

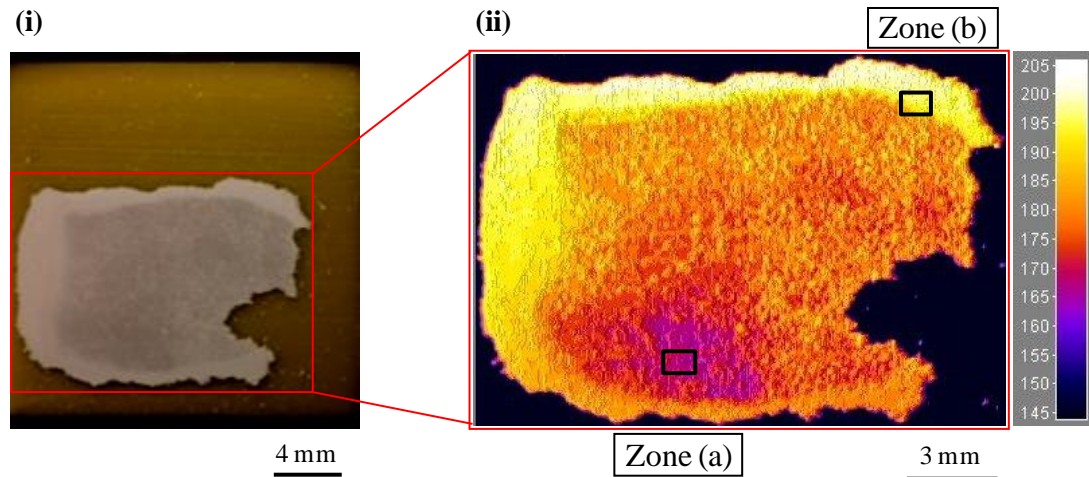


Figure 4.8: **(i)** Optical image of pad with third-body layer illustrated the load-bearing area as dark part, captured during the friction test; **(ii)** Colored image of the third-body layer to distinguish the grey level.

Figure 4.9(i) and Figure 4.9(ii) show the topography of the third body layer in zones (a) and (b), respectively. Comparison of roughness parameters obtained by 3D optical profilometer taken in the relative zones shows clearly that the dark part (zone a) is highly compacted and more smooth when compared to zone (b) (see Average Roughness  $R_a$  in Table 4.1). The particular high values of Core Roughness Depth ( $R_k$ ), and Reduced Valley Depth ( $R_{vk}$ ) parameters in zone (b) indicate clearly that the third-body layer presents opened porosities (in the form of valley) leading thus to less compressed third-body layer in this bright zone (b) compared to the dark zone (a). The same also confirmed by bearing ratio graph presented in Table 4.1. The bearing ratio is the ratio of the intersecting area of a plane (i.e. parallel to the mean plane) passing through the surface at a given height to the cross sectional area of the evaluation region. The bearing Ratio Curve (or Abbot Firestone Curve) is established by evaluating it at various levels from the highest peak to the lowest valley. These results tend to confirm that the “dark” parts observed in the optical images taken during friction correspond to the load-bearing area characterized by denser third-body layer.

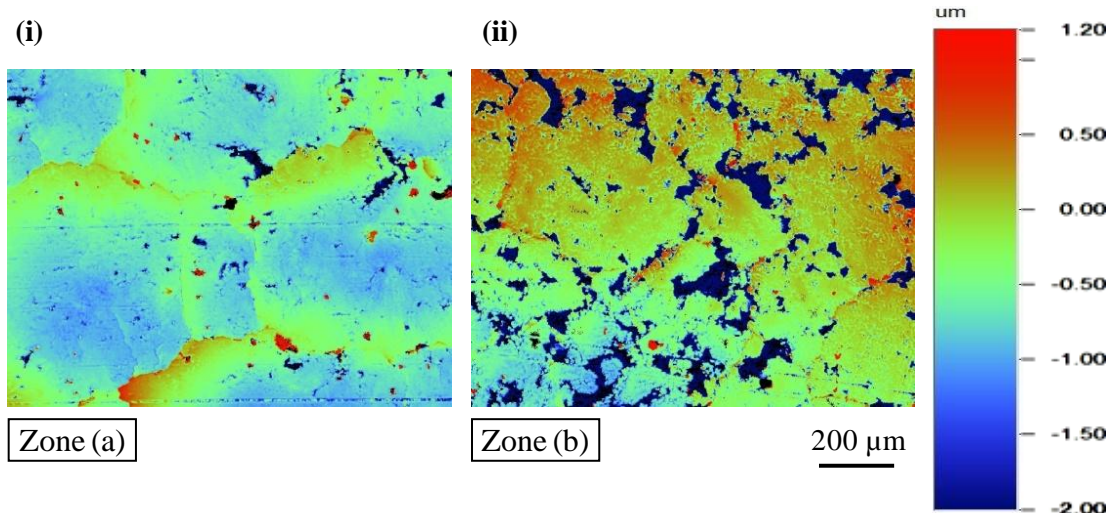
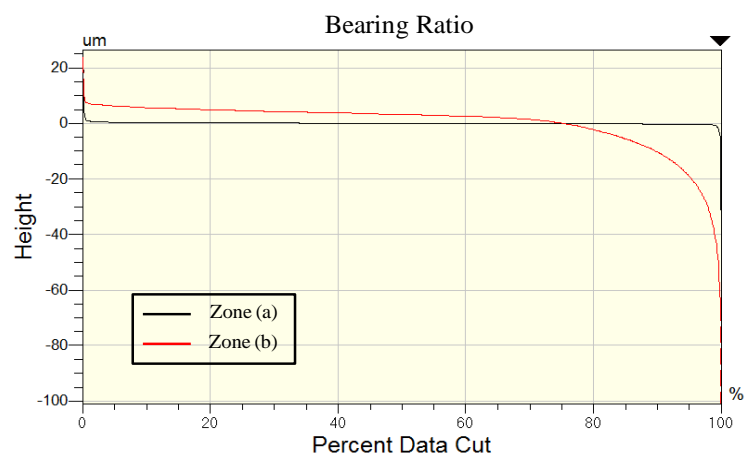


Figure 4.9: 3D optical profilometer images of (i) zone ‘a’; (ii) zone ‘b’

Table 4.1. Roughness parameters obtained by 3D optical profilometer for zone (a) and zone (b)

Parameters (in $\mu\text{m}$ )	Zone (a)	Zone (b)
$R_a$	0.21	5.80
$R_z$	39.9	105
$R_k$	0.43	5.87
$R_{pk}$	0.73	1.70
$R_{vk}$	1.07	23.3



To compare the internal compaction of the third-body layers in zones (a) and (b), mentioned here-above, FIB-SEM characterizations were also done on cross sections prepared perpendicularly to the friction surface. These observations show clearly that the topmost layers ( $\sim 3 \mu\text{m}$ ) of the third-body are much more compacted in area ‘a<sub>1</sub>’ than area ‘b<sub>1</sub>’ as shown in Figure 4.10(i) and (ii). In addition, zone (b) contains much more closed porosities compared to zone (a) as shown in area ‘b<sub>2</sub>’, in which the

boundary between two clusters and a void can be easily identified (see Figure 4.10(ii)).

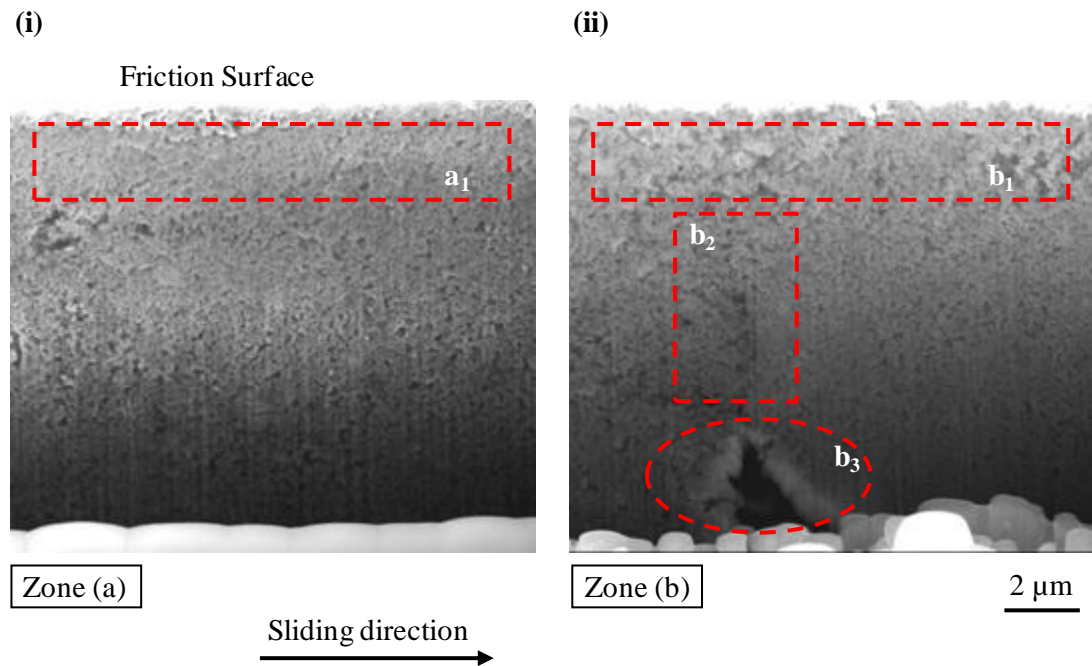


Figure 4.10: FIB-SEM characterizations of (i) zone 'a'; (ii) zone 'b'

#### 4.5 Noise appearances vs third-body layer change

Considering the variations of the load-bearing area during a revolution of the disc, it is observed that it moves cyclically according to the pad tilt. Digital Image Analysis has been done to see its extent, looking for the proportion of the dark zone inside the total surface of the third body, i.e. the proportion of the macroscopic load-bearing surface.

Figure 4.11 presents an estimation of the extent of the load-bearing area at two particular instants of three cycles (presented in Figure 4.7) of the disc revolution, when the pad tilt is low & the loading is high, and when the pad tilt is high & the loading is low. The results show a 5% increase in load-bearing area, from 73% to 78%.

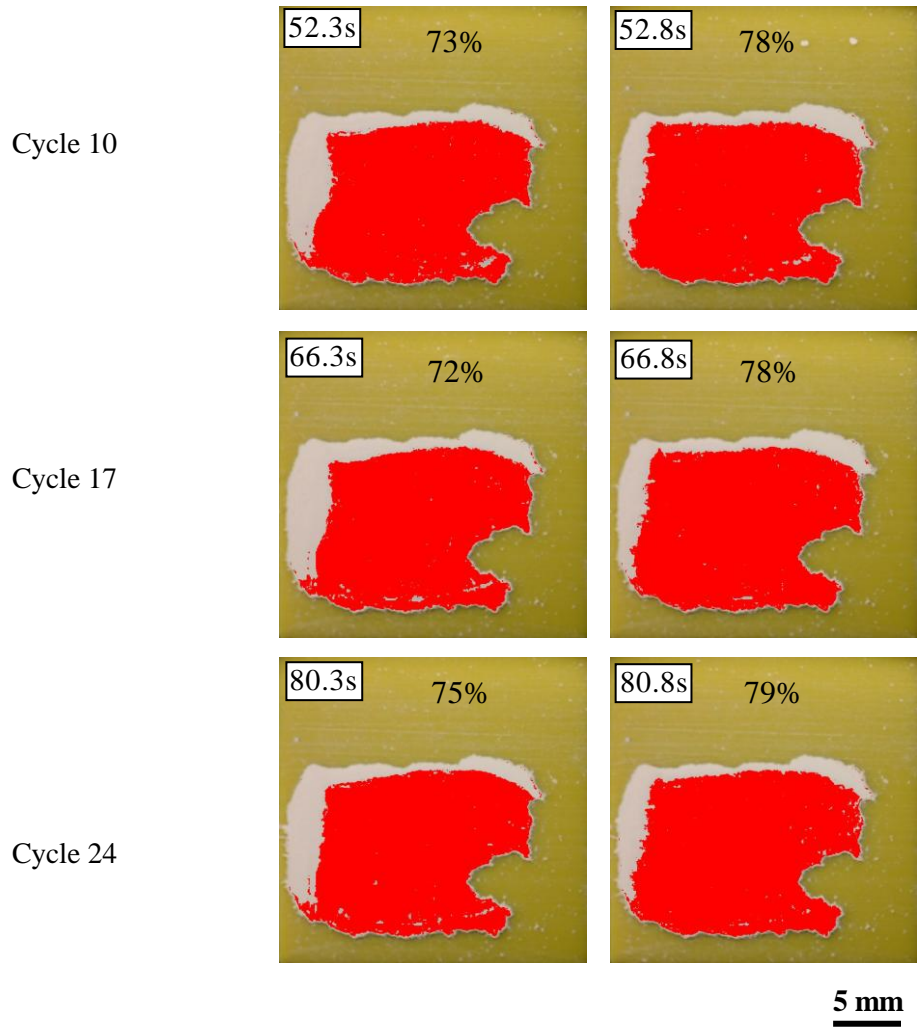


Figure 4.11: Measurements of the load-bearing extent using Digital Image Analysis, at high ( $t = 52.3, 66.3$  &  $80.3$  s) and low ( $t = 52.8, 66.8$  &  $80.8$  s) pad tilt. Results are indicated in fraction of the total extent of the third-body layer.

The measurement has been applied to all images of the video for one complete revolution of the disc. The results are presented in Figure 4.12, for correlation with the high frequency noise events (at 16 kHz) observed during the quasi steady-state stage. These noise occurrences indicate the initiation of vibration in the contact, which can be a precursor to the squealing that occurs at the end of the test. In Figure 4.12, the periods of noise emission are highlighted in green on the tilt curve (in mauve color). The tilt curve corresponds to the tilt change between the pad and the disc, assuming a zero-reference tilt between the two surfaces at the instant of the first



contact. The disc undulation (out-of-plane displacement) and the friction coefficient are recalled for correlation. The curve in light blue indicates the evolution of the fraction of the load-bearing area for one cycle. Two noise events appear for each disc revolution. It is interesting to notice that the occurrences of these noise events appear while the load bearing area reaches a certain proportion of the third-body layer. Below this threshold (in this case, approximately 78%), the contact remains silent. Above this threshold, squeal appears.

Conversely, one can notice that there may be a correlation with friction. In the case of occurrence ‘a’ the friction is low while in the case of occurrence ‘b’, friction is high. Also, it may be correlated with the maxima of the friction curve peaks.

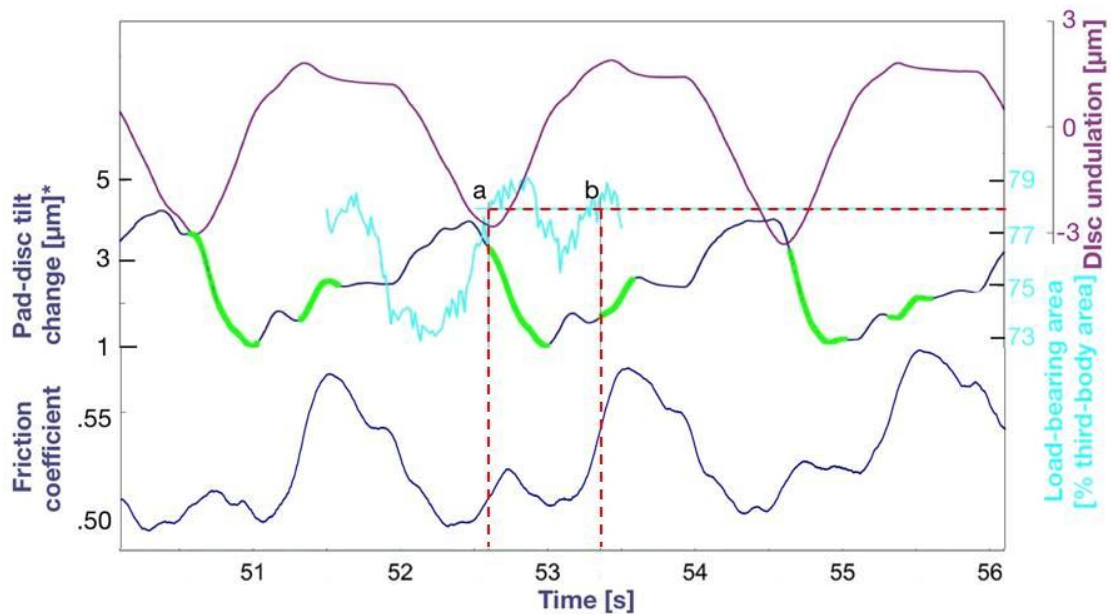


Figure 4.12: Correlation between noise emission and load-bearing area extent. (Blue curve in the bottom is the friction coefficient; pad-disc tilt change in mauve color; noise events in green are placed on it; light blue for 2s is the fraction of load-bearing area; on the top, disc undulation in purple).

Considering on Figure 4.3 the time-frequency diagram, one can remark that the high-frequency noise events occur cyclically throughout the quasi steady-state stage {c2}. These noise occurrences are more intense and last longer over time. One could correlate this with the extent of the load-bearing area exceeding the threshold previously shown for cycle after cycle.

Let us consider the second squeal event that occurs at the end of the test during stage {c3}. As shown in Figure 4.3, the force exerted by the pad seems to be of the same order during stage {c3} as during stage {b}, however with small cyclic fluctuations, due to the cyclic loading induced by the disc undulation. Looking at the last part of the test, suddenly the 7.5 kHz frequency appears at ~85 s (Figure 4.13) which is the beginning of the high frequency squeal vibrations with high amplitude (see Figure 4.3). To understand this, a focus on the stage {c<sub>2</sub>} ‘quasi steady-state’ needs to be made.

From the noise spectrum, it can be observed that a first occurrence of a 4 kHz noise starts at ~ 81 s, followed by several and increasing noise occurrences with frequencies 2 kHz and 4 kHz, while the final squeal event appears after 2 cycles of disc rotation. One can notice that the first 4 kHz noise occurrence appears simultaneously with one of the cyclic high frequency noise events occurring at 16 kHz.

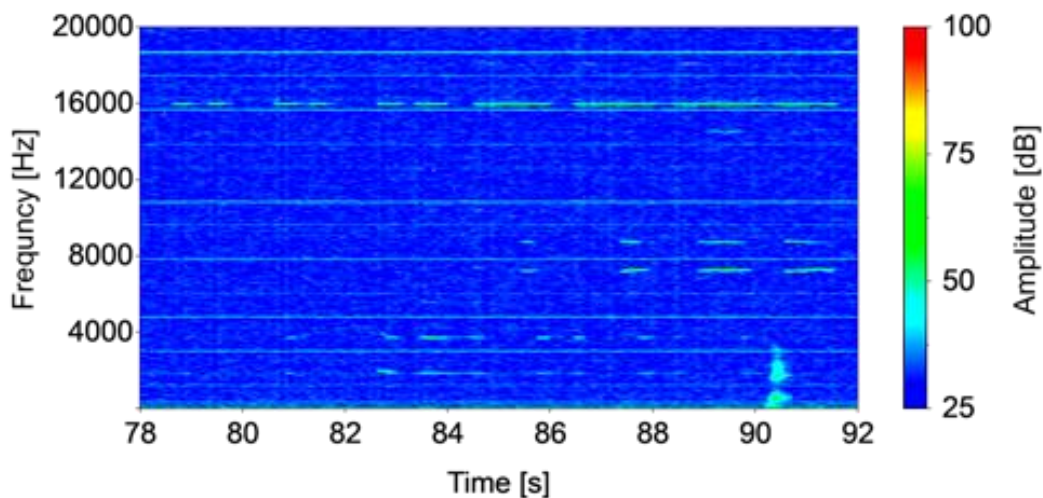


Figure 4.13: Frequency-time diagram corresponding to stage {c<sub>3</sub>} of the friction experiment (see in Figure 4.3).

Except for this synchronization, the authors were not able to distinguish any other remarkable event that could explain the last squeal occurrence. From the video monitoring of the load-bearing scene, the normal load and noise graphs, the tribological system evolves slowly. The average friction is increasing during the quasi steady-state stage, in correlation with the increase of the pad tilt, shown in Figure 4.6.

It is observed that this change can be linked to the increasing homogeneity and the extent of the friction area.

## 4.6 Conclusions

The present work aims at following experimentally the evolution of third-body layer along with the load bearing area. This information is essential for a better understanding of the origin of early stage of squeal occurrence. To do so, a simplified experimental test-rig used to allow the instrumentation of operational conditions leading to the occurrence of squeal during friction tests. Furthermore, in order to simplify the tribological circuit, an alumina powder has been used as an artificial inert third body. An experiment with final protocol of three steps is performed. To better understand the third-body flows and associated physical mechanisms in the contact during the different phases (noise emissions), the in-situ observation recorded by the optical camera. Post-friction characterizations have been conducted for two different zones of the third-body layer. Temporal analysis of variation of the normal load, pad tilt change, friction coefficient and the noise emission of the experiment has been presented.

Based upon above results and post-friction characterization, it is concluded that the internal flows of the third body contribute significantly to homogenizing the load bearing area. Some correlations between average friction variation, compaction of the third-body layer, and the homogeneity of the surface interaction with the disc can be formulated. The roughness parameters and cross-sectional FIB-SEM images of the post-friction characterized zones is presented. It suggests that the continuous velocity accommodation leads to more compaction of the third-body layer and smooth frictional surface than the other by reducing the porosities. Thus reducing the surface porosity, the third body increases the “adhesive” interaction between the third-body layer and disc surface that leads to increase the friction coefficient. Furthermore, the friction coefficient is fluctuating in accordance with the disc revolutions.

Also, due to disc undulation, the load-bearing area is changing continually and well observed by dark zone (due to the light source) of the captured optical images. The dark part facilitates to calculate the macroscopic load-bearing area. The analysis suggests that as soon as the load-bearing area reaches a certain proportion of the third-

body layer, noise appears. The contact becomes silent below this threshold, while there may be a correlation in terms of friction.

---

## **CONCLUSIONS AND PERSPECTIVES**

---

# Conclusions and Perspectives

---

## CONCLUSIONS

Objective of this work is to deal with the occurrence of squeal which is a complex problem involving strongly interdisciplinary issues. An adequate approach is to combine both tribological and dynamic analyses. One challenge is to identify contact accommodation mechanisms at a macroscopic scale involves the internal flows of third-body particles at a microscopic scale. These mechanisms correspond to the so-called third-body plateaus in the case of real braking systems. The main research consent of this study is to better understand the third body flow and associated physical mechanisms in the contact during the different phases (different noise intensities) and to explore the strategy to develop a friction experiment that should allow the in-situ observation of the contact interface and to follow its time-space variation. The study includes the investigation experimentally the behavior of the granular third-body layer in load bearing and how it evolves during sliding friction from silent to noisy situations.

For this, an artificial the third body consists of alumina particles has been introduced inside a flat pin-on-disc interface. The pad and the disc are completely separated by third-body layer. The fluctuations of the flat contact which are due to the relative out-of-plane displacements of moving parts are continuously accommodate by this third-body layer. The time-evolution of the contact area is monitored by an optical camera through a transparent disc. Except for the disc rotation, no external action is applied to the tribosystem during the friction tests. For this, two types of experimental configurations have been designed. The difficulty arises to trap the third-body and maintaining it in the contact throughout the experiment and of course, while system is under vibrations. Tilting the pad to open the contact at the leading edge and to close it at the trailing edge solved the problem for both of the experimental configurations. The experimental configuration with a contact on the underside of the disc has been preferred over experimental configuration with contact on the upper side of the disc to perform the final test. Based upon the experiments of both configurations, the main results are as follows:

The tribosystem which is initially silent remains silent as long as there is no change in the frictional contact interface. The introduction of an artificial third body changes the dynamics of the tribosystem and led it to squeal. The occurrence of squeal is apparently linked to the change in the redistribution of third-body particles in the interface, which strongly influences the location of the load-bearing area. The cyclic squealing is alternatively towards the leading or the trailing edge in the sliding direction. The key points of the developed experiment are the pad tilt to trap third body particles, the compaction of these particles before the test, the resulting repeatability of the experiments in terms of maintaining the third-body layer throughout the test along with squeal occurrence and the light source that helps to follow the macroscopic load bearing area.

The internal flows of the third body contribute significantly to homogenizing the load bearing area by the velocity accommodation. Some correlations between average friction variation, compaction of the third-body layer, and the homogeneity of the surface interaction with the disc can be formulated.

To characterize the evolution of the third body in terms of compaction and porosity, post-friction characterizations have been conducted by choosing two different zone of the third body-layer. Two zones corresponding to be fully in the load-bearing area during the whole test duration and corresponding to an area that underwent periodically due to the disc undulation. The roughness parameters and cross-sectional FIB-SEM images suggested that the zone which was fully in load-bearing during whole test is more compacted and have a very smooth frictional surface due to the continuous velocity accommodation.

Also, due to disc undulation, the load-bearing area is changing continually and in-situ observed by dark zone of the captured optical images. The macroscopic load-bearing area can be calculated by Digital Image Analysis of the area of dark zones. The analysis suggests that as soon as the load-bearing area reaches a certain proportion of the third-body layer, noise appears. The contact becomes silent below this threshold, while there may be a correlation in terms of friction.

In conclusion the developed experiment is reproducible and reliable to observe the *in-situ* frictional contact interface and to follow the evolution of third-body layer that leads the system to squeal.

## **PERSPECTIVES**

The presented work highlights the need to further analyze the videos to quantify the compaction and load-bearing area during the friction test. For this, the resolution of the measurement must also allow information to be obtained at different scales (from macro- to meso-). Digital image correlation would be beneficial in the identification of third body flows.

Also, a quantitative analysis of *in-situ* evolution of third-body layer thickness and its stiffness will be the next step. The experimentation needs to be developed in order to handle up the quantification of the flows: quantity of powder to be introduced in the interface and the recirculation flows.

The experimental analysis also needs a multi-scale model that would couple a macro-scale numerical model with a contact interface model that has to consider the local load-bearing area, the granular environment at a much smaller scale. For this, a further characterization of the 3rd body is required, in terms of physicochemical properties, size, morphologies, and stiffness.

Future work may include other experiments by using different kind of artificial third body powders to see the influence of particles size and of the self-organization of the load-bearing area on squeal occurrences.

On the other hand, several factors that have been maintained constant throughout the study, such as temperature or humidity, may have an influence on the load-bearing area and the occurrence of squeal. Adding these factors are one of the future prospects of this work that could lead to a better understanding of the physics of squeal.



---

## **BIBLIOGRAPHY**

---

# BIBLIOGRAPHY

---

- Akay, Adnan. 2002. "Acoustics of Friction." *The Journal of the Acoustical Society of America* 111 (4): 1525. <https://doi.org/10.1121/1.1456514>.
- Axén, N., and S. Jacobson. 1994. "A Model for the Abrasive Wear Resistance of Multiphase Materials." *Wear* 174 (1–2): 187–99. [https://doi.org/10.1016/0043-1648\(94\)90101-5](https://doi.org/10.1016/0043-1648(94)90101-5).
- Bergman, Filip, Mikael Eriksson, and Staffan Jacobson. 1999. "Influence of Disc Topography on Generation of Brake Squeal." *Wear* 225–229 (April): 621–28. [https://doi.org/10.1016/S0043-1648\(99\)00064-2](https://doi.org/10.1016/S0043-1648(99)00064-2).
- Berthier, Yves. 1996. "Maurice Godet's Third Body." *Tribology Series* 31 (January): 21–30. [https://doi.org/10.1016/S0167-8922\(08\)70766-1](https://doi.org/10.1016/S0167-8922(08)70766-1).
- Berthier, Yves. 2001. "SECTION 8.2 - Background on Friction and Wear." In *Handbook of Materials Behavior Models*, edited by JEAN LEMAITRE, 676–99. Burlington: Academic Press. <https://doi.org/https://doi.org/10.1016/B978-012443341-0/50074-0>.
- Bonnay, K., V. Magnier, J.F. Brunel, P. Dufrénoy, and G. De Saxcé. 2015. "Influence of Geometry Imperfections on Squeal Noise Linked to Mode Lock-In." *International Journal of Solids and Structures* 75–76: 99–108. <https://doi.org/10.1016/j.ijsolstr.2015.08.004>.
- Brunel, J.F., P. Dufrénoy, M. Naït, J.L. Muñoz, and F. Demilly. 2006. "Transient Models for Curve Squeal Noise." *Journal of Sound and Vibration* 293 (3–5): 758–65. <https://doi.org/10.1016/j.jsv.2005.12.003>.
- Cho, M. H., K. H. Cho, S. J. Kim, D. H. Kim, and H. Jang. 2005. "The Role of Transfer Layers on Friction Characteristics in the Sliding Interface between Friction Materials against Gray Iron Brake Disks." *Tribology Letters* 20 (2): 101–8. <https://doi.org/10.1007/s11249-005-8299-6>.
- Conglin, Dong, Mo Jiliang, Yuan Chengqing, Bai Xiuqin, and Yu Tian. 2019. "Vibration and Noise Behaviors During Stick – Slip Friction." *Tribology Letters*. <https://doi.org/10.1007/s11249-019-1216-1>.

- Cristol-Bulthé, A.-L., Yannick Desplanques, and G. Degallaix. 2007. “Coupling between Friction Physical Mechanisms and Transient Thermal Phenomena Involved in Pad–Disc Contact during Railway Braking.” *Wear* 263 (7–12): 1230–42. <https://doi.org/10.1016/j.wear.2006.12.052>.
- Cristol-Bulthé, A.-L., Yannick Desplanques, Gérard Degallaix, and Yves Berthier. 2008. “Mechanical and Chemical Investigation of the Temperature Influence on the Tribological Mechanisms Occurring in OMC/Cast Iron Friction Contact.” *Wear* 264 (9–10): 815–25. <https://doi.org/10.1016/j.wear.2006.12.080>.
- Davin, Edouard, Anne-lise Cristol, Jean-françois Brunel, and Yannick Desplanques. 2019. “Wear Mechanisms Alteration at Braking Interface through Atmosphere Modification.” *Wear* 426–427 (September 2018): 1094–1101. <https://doi.org/10.1016/j.wear.2019.01.057>.
- Desplanques, Yannick, and Gérard Degallaix. 2008a. “Interactions between Third-Body Flows and Localisation Phenomena during Railway High-Energy Stop Braking.” *SAE Int. J. Passeng. Cars – Mech. Syst.* 1 (1): 1267–75. <https://doi.org/10.4271/2008-01-2583>.
- Desplanques, Yannick, and Gérard Degallaix. 2008b. “Interactions between Third-Body Flows and Localisation Phenomena during Railway High-Energy Stop Braking” 1 (1): 1267–75. <https://doi.org/10.4271/2008-01-2583>.
- Desplanques, Yannick, and Gérard Degallaix. 2009a. “Genesis of the Third-Body at the Pad-Disc Interface : Case Study Of Sintered Metal Matrix Composite Lining Material” 2 (2): 25–32.
- Desplanques, Yannick, and Gérard Degallaix. 2009b. “Genesis of the Third-Body at the Pad-Disc Interface: Case Study Of Sintered Metal Matrix Composite Lining Material.” *SAE Int. J. Mater. Manf.* 2 (2): 25–32. <https://doi.org/10.4271/2009-01-3053>.
- Dmitriev, a. I., and W. Österle. 2013. “Modelling the Sliding Behaviour of Tribofilms Forming During Automotive Braking: Impact of Loading Parameters and Property Range of Constituents.” *Tribology Letters* 53 (1): 337–51. <https://doi.org/10.1007/s11249-013-0274-z>.

- Duboc, Martin, J.F. Brunel, and Philippe Dufrénoy. 2013. “Etude Multi-Échelle Du Crissement : Dispositif Expérimental et Éléments de Compréhension.” Université Lille 1.
- Dufrénoy, P., G. Bodovillé, and G. Degallaix. 2002. “Damage Mechanisms and Thermomechanical Loading of Brake Discs.” *European Structural Integrity Society* 29 (C): 167–76. [https://doi.org/10.1016/S1566-1369\(02\)80073-5](https://doi.org/10.1016/S1566-1369(02)80073-5).
- Eriksson, Mikael, Filip Bergman, and Staffan Jacobson. 1999. “Surface Characterisation of Brake Pads after Running under Silent and Squealing Conditions.” *Wear* 232 (2): 163–67. [https://doi.org/10.1016/S0043-1648\(99\)00141-6](https://doi.org/10.1016/S0043-1648(99)00141-6).
- Eriksson, Mikael, Filip Bergman, and Staffan Jacobson. 2002. “On the Nature of Tribological Contact in Automotive Brakes.” *Wear* 252 (November 1999): 26–36.
- Eriksson, Mikael, and S Jacobson. 2001. “Friction Behaviour and Squeal Generation of Disc Brakes at Low Speeds.” <https://doi.org/10.1243/0954407011528789>.
- Eriksson, Mikael, and Staffan Jacobson. 2000. “Tribological Surfaces of Organic Brake Pads.” *Tribology International* 33 (12): 817–27. [https://doi.org/10.1016/S0301-679X\(00\)00127-4](https://doi.org/10.1016/S0301-679X(00)00127-4).
- Eriksson, Mikael, John Lord, and Staffan Jacobson. 2001. “Wear and Contact Conditions of Brake Pads: Dynamical in Situ Studies of Pad on Glass.” *Wear* 249 (3–4): 272–78. [https://doi.org/10.1016/S0043-1648\(01\)00573-7](https://doi.org/10.1016/S0043-1648(01)00573-7).
- Fieldhouse, John D, and Peter Newcomb. 1993. “The Application of Holographic Interferometry to the Study of Disc Brake Noise.” In *International Congress & Exposition*. SAE International. <https://doi.org/https://doi.org/10.4271/930805>.
- Giannini, Oliviero, Adnan Akay, and Francesco Massi. 2006. “Experimental Analysis of Brake Squeal Noise on a Laboratory Brake Setup.” *Journal of Sound and Vibration* 292 (1–2): 1–20. <https://doi.org/10.1016/j.jsv.2005.05.032>.
- Godet, Maurice. 1984. “The Third-Body Approach: A Mechanical View of Wear.” *Wear* 100 (1–3): 437–52. [https://doi.org/10.1016/0043-1648\(84\)90025-5](https://doi.org/10.1016/0043-1648(84)90025-5).

- Hetzler, H., and K. Willner. 2012. "On the Influence of Contact Tribology on Brake Squeal." *Tribology International* 46 (1): 237–46. <https://doi.org/10.1016/j.triboint.2011.05.019>.
- Heussaff, a., L. Dubar, T. Tison, M. Watremez, and R.F. Nunes. 2012. "A Methodology for the Modelling of the Variability of Brake Lining Surfaces." *Wear* 289 (June): 145–59. <https://doi.org/10.1016/j.wear.2012.04.002>.
- Hoffmann, Norbert, Michael Fischer, Ralph Allgaier, and Lothar Gaul. 2002. "A Minimal Model for Studying Properties of the Mode-Coupling Type Instability in Friction Induced Oscillations." *Mechanics Research Communications* 29 (4): 197–205. [https://doi.org/10.1016/S0093-6413\(02\)00254-9](https://doi.org/10.1016/S0093-6413(02)00254-9).
- Jacko, M. G., P. H. S. Tsang, and S. K. Rhee. 1989. "Wear Debris Compaction and Friction Film Formation of Polymer Composites." *Wear* 133 (1): 23–38. [https://doi.org/10.1016/0043-1648\(89\)90110-5](https://doi.org/10.1016/0043-1648(89)90110-5).
- Kasem, H., P. Dufrénoy, Y. Desplanques, M. Siroux, and B. Desmet. 2011. "On the Use of Calcium Fluoride as an Infrared-Transparent First Body for in Situ Temperature Measurements in Sliding Contact." *Tribology Letters* 42 (1): 27–36. <https://doi.org/10.1007/s11249-010-9745-7>.
- Kasem, Haytam, Sylvie Bonnamy, Yves Berthier, and Pascale Jacquemard. 2010. "Characterization of Surface Grooves and Scratches Induced by Friction of C/C Composites at Low and High Temperatures." *Tribology International* 43 (11): 1951–59. <https://doi.org/10.1016/j.triboint.2010.03.004>.
- Kasem, Haytam, Sylvie Bonnamy, Bernard Rousseau, Henriette Estrade-Szwarckopf, Yves Berthier, and Pascale Jacquemard. 2007. "Interdependence between Wear Process, Size of Detached Particles and CO<sub>2</sub> production during Carbon/Carbon Composite Friction." *Wear* 263 (7-12 SPEC. ISS.): 1220–29. <https://doi.org/10.1016/j.wear.2007.01.077>.
- Kinkaid, N.M., O.M. O'Reilly, and P. Papadopoulos. 2003. "Automotive Disc Brake Squeal." *Journal of Sound and Vibration* 267 (1): 105–66. [https://doi.org/10.1016/S0022-460X\(02\)01573-0](https://doi.org/10.1016/S0022-460X(02)01573-0).
- Krick, Brandon A., Jennifer R. Vail, Bo N.J. Persson, and W. Gregory Sawyer. 2012.

- “Optical in Situ Micro Tribometer for Analysis of Real Contact Area for Contact Mechanics, Adhesion, and Sliding Experiments.” *Tribology Letters* 45 (1): 185–94. <https://doi.org/10.1007/s11249-011-9870-y>.
- Lee, Kwangjin, and J R Barber. 1994. “An Experimental Investigation of Frictionally-Excited Thermoelastic Instability in Automotive Disk Brakes Under a Drag Brake Application.” *Journal of Tribology* 116 (3): 409–14. <http://dx.doi.org/10.1115/1.2928855>.
- Lee, Sangmok, and Ho Jang. 2018. “Effect of Plateau Distribution on Friction Instability of Brake Friction Materials.” *Wear* 400–401 (June 2017): 1–9. <https://doi.org/10.1016/j.wear.2017.12.015>.
- Lee, Seongjoo, ShinWook Kim, ShinWan Kim, and Seong Rhee. 2015. “Characterization of Disc Wear Particles Transferred to the NAO Pad Surface: Brake Squeal.” SAE International . <https://doi.org/10.4271/2015-01-2684>.
- Loyer, A., J.-J. Sinou, O. Chiello, and X. Lorang. 2012. “Study of Nonlinear Behaviors and Modal Reductions for Friction Destabilized Systems. Application to an Elastic Layer.” *Journal of Sound and Vibration* 331 (5): 1011–41. <https://doi.org/10.1016/J.JSV.2011.10.018>.
- Magnier, V., J.F. Brunel, and P. Dufrénoy. 2014. “Impact of Contact Stiffness Heterogeneities on Friction-Induced Vibration.” *International Journal of Solids and Structures* 51 (9): 1662–69. <https://doi.org/10.1016/j.ijsolstr.2014.01.005>.
- Magnier, V., D. Naidoo Ramasami, J. F. Brunel, P. Dufrénoy, and T. Chancelier. 2017. “History Effect on Squeal with a Mesoscopic Approach to Friction Materials.” *Tribology International* 115 (June): 600–607. <https://doi.org/10.1016/j.triboint.2017.06.031>.
- Massi, Francesco, Laurent Baillet, Oliviero Giannini, and Aldo Sestieri. 2007. “Brake Squeal: Linear and Nonlinear Numerical Approaches.” *Mechanical Systems and Signal Processing* 21 (6): 2374–93. <https://doi.org/10.1016/j.ymsp.2006.12.008>.
- Massi, Francesco, Yves Berthier, and Laurent Baillet. 2008. “Contact Surface Topography and System Dynamics of Brake Squeal.” *Wear* 265 (11–12): 1784–92. <https://doi.org/10.1016/j.wear.2008.04.049>.

- Massi, Francesco, Oliviero Giannini, and Laurent Baillet. 2006a. "Brake Squeal as Dynamic Instability: An Experimental Investigation." *The Journal of the Acoustical Society of America* 120 (3): 1388. <https://doi.org/10.1121/1.2228745>.
- Massi, Francesco, Oliviero Giannini, and Laurent Baillet. 2006b. "Brake Squeal as Dynamic Instability: An Experimental Investigation." *The Journal of the Acoustical Society of America* 120 (3): 1388–98. <https://doi.org/10.1121/1.2228745>.
- Mills, H. R. 1938. "Brake Squeak." *Technical Report*.
- Mo, J.L., Z.G. Wang, G.X. Chen, T.M. Shao, M.H. Zhu, and Z.R. Zhou. 2013. "The Effect of Groove-Textured Surface on Friction and Wear and Friction-Induced Vibration and Noise." *Wear* 301 (1–2): 671–81. <https://doi.org/10.1016/j.wear.2013.01.082>.
- Mortelette, L, J F Brunel, X Boidin, Y Desplanques, P Dufrénoy, and L Smeets. 2009. "Impact of Mineral Fibres on Brake Squeal Occurrences." SAE International . <https://doi.org/10.4271/2009-01-3050>.
- Müller, M., and G.P. Ostermeyer. 2007. "A Cellular Automaton Model to Describe the Three-Dimensional Friction and Wear Mechanism of Brake Systems." *Wear* 263 (7–12): 1175–88. <https://doi.org/10.1016/j.wear.2006.12.022>.
- North, M. R. 1976. "Disc Brake Squeal." In *Proceedings of the Conference on Braking of Road Vehicles, Automobile Division, Institution of Mechanical Engineers, Mechanical Engineering Publications Limited, London, England*, 169–76.
- Oberst, Sebastian, and J. C.S. Lai. 2011a. "Statistical Analysis of Brake Squeal Noise." *Journal of Sound and Vibration* 330 (12): 2978–94. <https://doi.org/10.1016/j.jsv.2010.12.021>.
- Oberst, Sebastian, and J.C.S. Lai. 2011b. "Chaos in Brake Squeal Noise." *Journal of Sound and Vibration* 330 (5): 955–75. <https://doi.org/10.1016/j.jsv.2010.09.009>.
- Österle, W., I. Dörfel, C. Prietzel, H. Rooch, A.-L. Cristol-Bulthé, G. Degallaix, and Yannick Desplanques. 2009. "A Comprehensive Microscopic Study of Third Body Formation at the Interface between a Brake Pad and Brake Disc during the

- Final Stage of a Pin-on-Disc Test.” *Wear* 267 (5–8): 781–88.  
<https://doi.org/10.1016/j.wear.2008.11.023>.
- Österle, W., H. Kloß, I. Urban, and a.I. Dmitriev. 2007. “Towards a Better Understanding of Brake Friction Materials.” *Wear* 263 (7–12): 1189–1201.  
<https://doi.org/10.1016/j.wear.2006.12.020>.
- Österle, W., G Orts-gil, T Gross, C Deutsch, R Hinrichs, and M A Z Vasconcellos. 2013. “Impact of High Energy Ball Milling on the Nanostructure of Magnetite – Graphite and Magnetite – Graphite – Molybdenum Disulphide Blends.” *Materials Characterization* 86: 28–38.  
<https://doi.org/10.1016/j.matchar.2013.09.007>.
- Österle, W., and I. Urban. 2004. “Friction Layers and Friction Films on PMC Brake Pads.” *Wear* 257 (1–2): 215–26. <https://doi.org/10.1016/j.wear.2003.12.017>.
- Ostermeyer, G.P., and M. Müller. 2008. “New Insights into the Tribology of Brake Systems.” *Proceedings of the Institution of Mechanical Engineers, Part D: Journal of Automobile Engineering* 222 (7): 1167–1200.  
<https://doi.org/10.1243/09544070JAUTO595>.
- Ouyang, Huajiang, Wayne Nack, Yongbin Yuan, and Frank Chen. 2005. “Numerical Analysis of Automotive Disc Brake Squeal: A Review.” *Int. J. Vehicle Noise and Vibration* 1 (3/4): 207–31. <https://doi.org/10.1504/IJVNV.2005.007524>.
- Ozcan, Soydan, and Peter Filip. 2005. “Microstructure and Wear Mechanisms in C/C Composites.” *Wear* 259 (1–6): 642–50.  
<https://doi.org/10.1016/j.wear.2005.02.112>.
- Papinniemi, Antti, Joseph C.S. Lai, Jiye Zhao, and Lyndon Loader. 2002. “Brake Squeal: A Literature Review.” *Applied Acoustics* 63 (4): 391–400.  
[https://doi.org/10.1016/S0003-682X\(01\)00043-3](https://doi.org/10.1016/S0003-682X(01)00043-3).
- Ramasami, Davis Naidoo, V. Magnier, Jean-françois Brunel, and Philippe Dufrénoy. 2014. “Influence of Friction Material & Test Sequence on Disc Brake Squeal.”
- Rapontchombo, Jessie, Alexandre Mège-Revil, Jean-françois Brunel, Yannick Desplanques, and Philippe Dufrénoy. 2019. “Performances de Garnitures Frittées Métalliques à Basse Teneur En Cuivre Pour Les Applications de Freinage



Ferroviaire Haute Énergie.” Université Lille.

- Renaud, Franck, Gaël Chevallier, Jean-Luc Dion, and Guillaume Taudière. 2012. “Motion Capture of a Pad Measured with Accelerometers during Squeal Noise in a Real Brake System.” *Mechanical Systems and Signal Processing* 33 (November): 155–66. <https://doi.org/10.1016/J.YMSSP.2012.06.027>.
- Renouf, M., H.-P. Cao, and V.-H. Nhu. 2011. “Multiphysical Modeling of Third-Body Rheology.” *Tribology International* 44 (4): 417–25. <https://doi.org/10.1016/j.triboint.2010.11.017>.
- Renouf, Mathieu, Francesco Massi, Nicolas Fillot, and Aurélien Saulot. 2011. “Numerical Tribology of a Dry Contact.” *Tribology International* 44 (7–8): 834–44. <https://doi.org/10.1016/j.triboint.2011.02.008>.
- Renouf, Mathieu, Viet Hung Nhu, Aurélien Saulot, and Francesco Massi. 2014. “First-Body versus Third-Body: Dialogue between an Experiment and a Combined Discrete and Finite Element Approach.” *Journal of Tribology* 136 (2): 1–9. <https://doi.org/10.1115/1.4026062>.
- Rhee, S.K., M.G. Jacko, and P.H.S. Tsang. 1991. “The Role of Friction Film in Friction, Wear and Noise of Automotive Brakes.” *Wear* 146 (1): 89–97. [https://doi.org/10.1016/0043-1648\(91\)90226-K](https://doi.org/10.1016/0043-1648(91)90226-K).
- Richard, David, Ivan Iordanoff, Mathieu Renouf, and Yves Berthier. 2008. “Thermal Study of the Dry Sliding Contact With Third Body Presence.” *Journal of Tribology* 130 (3): 031404. <https://doi.org/10.1115/1.2913540>.
- Sherif, Hany A. 1991. “Effect of Contact Stiffness on the Establishment of Self-Excited Vibrations.” *Wear* 141 (2): 227–34. [https://doi.org/10.1016/0043-1648\(91\)90270-5](https://doi.org/10.1016/0043-1648(91)90270-5).
- Spurr, R T. 1961. “A Theory of Brake Squeal.” *Proceedings of the Institution of Mechanical Engineers: Automobile Division* 15 (1): 33–52. [https://doi.org/10.1243/PIME\\_AUTO\\_1961\\_000\\_009\\_02](https://doi.org/10.1243/PIME_AUTO_1961_000_009_02).
- Sriwiboon, Meechai, Nipon Tiempan, Kritsana Kaewlob, and Seong Rhee. 2016. “Brake Squeal and Wheel Dust vs. Disc Wear.” *SAE International Journal of Materials and Manufacturing* 9 (1): 112–17. <http://www.jstor.org.ressources->

[electroniques.univ-lille.fr/stable/26268810](http://electroniques.univ-lille.fr/stable/26268810).

Suchal, Andrea, J.F. Brunel, Philippe Dufrenoy, and Milos Musil. 2013. "Influence of Thermal Effects on Dynamics of Disc Brakes and Brake Squeal Propensity." Slovak university of technology, Bratislava.

Wang, D.W., J.L. Mo, H. Ouyang, G.X. Chen, M.H. Zhu, and Z.R. Zhou. 2014. "Experimental and Numerical Studies of Friction-Induced Vibration and Noise and the Effects of Groove-Textured Surfaces." *Mechanical Systems and Signal Processing*, February. <https://doi.org/10.1016/j.ymssp.2014.02.007>.

Wang, D.W., J.L. Mo, Z.G. Wang, G.X. Chen, H. Ouyang, and Z.R. Zhou. 2013. "Numerical Study of Friction-Induced Vibration and Noise on Groove-Textured Surface." *Tribology International* 64 (August): 1–7. <https://doi.org/10.1016/j.triboint.2013.02.031>.

# APPENDIX - A

---

## Material roughness

Material roughness of the first bodies i.e. pad and the disc are gained from the measurement on device 3D profilometer.

	Quartz disc	Compressed Polyurethane Resin (CRP) Pad
$R_a$ (average roughness)	~ 4 nm	~ 600 nm

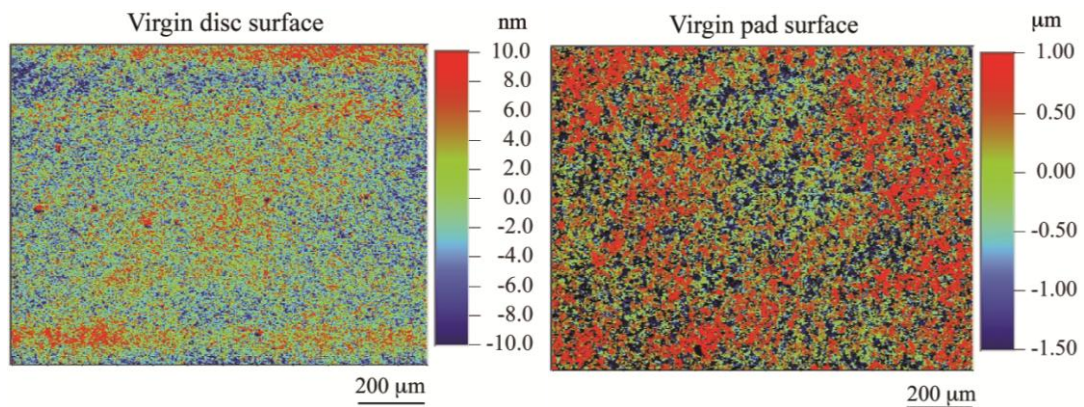


Figure: 3D profilometer images of the virgin disc and the virgin pad.

---

## **RESUME ETENDU**

---

# RESUME ETENDU

---

## CONTEXTE

Le freinage est une fonction essentielle au contrôle de véhicules de transport routiers et ferroviaires, notamment pour en assurer la sécurité. Parmi les différentes technologies de freinage utilisées (friction, courants de Foucault, rhéostatique, etc.), le freinage par friction (considéré comme le plus efficace, notamment en cas d'urgence) est encore le plus utilisé. Bien que les freins à friction aient été considérablement améliorés au fil des ans, certains problèmes fondamentaux liés à leur utilisation restent non résolus. Les plus fréquents de ces problèmes sont la fissuration des disques de frein due à la fatigue thermique (Dufrénoy et al. 2002), les instabilités de friction (K. Lee et al. 1994), l'usure (Österle et al. 2009; Haytam Kasem et al. 2007; Ozcan et al. 2005) et les émissions sonores. En effet, les vibrations induites par les freins à friction conduisent à un large éventail de bruits, classés en fonction de leurs fréquences et de la nature des vibrations (Akay 2002). Parmi ceux-ci, le crissement (Mortelette et al. 2009; Massi et al. 2008) est l'un des plus gênants, tant pour les personnes que pour l'environnement. Etant responsable d'une émission sonore de haute fréquence et de haute pression acoustique (supérieur à 1 kHz et 80 dB), il peut être associé à des vibrations de haute fréquence et de grande amplitude dans des conditions de glissement (Massi et al. 2007). Malgré les progrès significatifs réalisés récemment dans les techniques de traitement, les outils de caractérisation et les algorithmes de calcul, la compréhension fondamentale des conditions physiques conduisant au crissement fait encore défaut, car il est inévitablement affecté par de nombreux facteurs à la fois aux échelles micro et macroscopiques.

D'un point de vue dynamique, le crissement est vu comme une instabilité sous condition de glissement et plusieurs mécanismes de passage à l'instabilité ont été proposés, par exemple la décroissance du frottement avec la vitesse, sprag-slip, flutter instabilities, stick-slip, coiplage de modes (Kinkaid et al. 2003; Ouyang et al. 2005). Bien que ces mécanismes puissent être interdépendants, il est communément admis que l'instabilité vibratoire responsable du crissement est majoritairement due à un phénomène de couplage de modes. La prédiction des modes instables repose couramment sur l'analyse numérique des valeurs propres complexes du système de

freinage (Massi et al. 2008; Giannini et al. 2006). Massi *et al.* ont étudié expérimentalement l'origine du crissement en utilisant un banc d'essai pion-disque. Ils ont montré que les instabilités dynamiques du tribo-système sont la cause principale du crissement des freins (Massi et al. 2006b).

D'un point de vue tribologique, la configuration des surfaces en contact apparaît être au premier ordre dans l'apparition du crissement. Comme le proposent les concepts de troisième corps et de circuit tribologique introduits par Godet (Godet 1984) et Berthier (Berthier 1996), la formation de couches inter-faciales, constituées de particules issues de l'usure, joue un rôle majeur dans le fonctionnement mécanique d'un contact, et son évolution temporelle. Aux échelles méso et microscopiques, Jacko *et al.* ont rapporté que lorsque des films de friction stables sont facilement formés pour un couple de friction donné, un niveau de friction stable et un faible taux d'usure peuvent être maintenus à différentes températures, tant que le film de friction n'est pas détruit (Jacko et al. 1989). En considérant l'interface interne disque / garniture pendant le frottement, certaines études ont montré la formation de plateaux de contact sur la garniture composite, appelés plateaux primaires, tandis que des débris d'usure, appelés plateaux secondaires, s'accumulent et se compactent autour des plateaux primaires (Eriksson, Lord, et al. 2001). Dans la même étude, les auteurs ont montré que lorsque la situation de contact change pendant le frottement, les plateaux de contact secondaires se désintègrent, et une élimination progressive de ces débris compactés se produit. L'évolution spatio-temporelle du contact, la formation de couches de troisième corps stables et les interactions entre les écoulements internes de troisième corps ont été illustrées dans plusieurs études (Desplanques et al. 2008b; 2009b). Dans ce contexte, la complexité de la compréhension du crissement de freinage réside dans le fait que ce crissement dépend des changements de conditions de frottement microscopiques ainsi que du coefficient de frottement macroscopique, eux-mêmes fortement dépendants de la topographie de la surface du disque (Bergman et al. 1999). De plus, de nombreux travaux de recherche ont rapporté une corrélation étroite entre l'usure et l'apparition du crissement dans le système de freinage system (Rhee et al. 1991; Hetzler et al. 2012; Magnier et al. 2017).

Malgré les récentes améliorations significatives des outils d'observation expérimentale du contact glissant, de nombreux chercheurs préfèrent adopter des approches théoriques, c'est-à-dire des méthodes par éléments finis (Richard et al.

2008), des automates cellulaires (Müller et al. 2007; Ostermeyer et al. 2008), ou des automates cellulaires mobiles (Österle et al. 2013; Dmitriev et al. 2013). Ces méthodes théoriques ont été utilisées pour modéliser des tribofilms à l'interface disque / garniture ainsi que pour décrire la topographie de surface. Ces travaux publiés permettent de conclure que le contact est affecté par les phénomènes se produisant d'une part aux petites échelles liées à l'espace (effets de contact microscopiques) et au temps (vibrations haute fréquence), et d'autre part aux grandes échelles (usure, comportement du triplet tribologique et dynamique de l'ensemble du système de freinage). En conséquence, il est clair que le crissement est un problème complexe impliquant des questions fortement interdisciplinaires, qui nécessite une approche adéquate qui doit combiner à la fois des analyses tribologiques et dynamiques.

## **MOTIVATION**

Les études expérimentales « classiques », liées aux problèmes de crissement en particulier et à la tribologie en général, impliquent une observation de la surface usée après frottement. Le défaut de ces observations réside dans le fait qu'après l'ouverture du contact, beaucoup d'informations vitales propres à la dynamique de l'interface sont définitivement perdues. Si l'on veut comprendre le crissement, il est important de pouvoir mesurer *in situ* les paramètres impliqués et de suivre leur variation spatio-temporelle au cours de l'expérience. Ceci est particulièrement vrai si l'on considère en général le circuit tribologique du troisième corps proposé par Berthier (Berthier 1996) et en particulier dans le système de freinage proposé par Desplanques (Desplanques et al. 2009b; Cristol-Bulthé et al. 2007). Il est admis que le circuit tribologique du troisième corps est capable de modifier continuellement la surface de frottement et donc la surface portante. De plus, il est constamment affecté par de nombreux facteurs tels que (i) les sources externes, (ii) les sources internes du troisième corps, y compris l'adhérence et les réactions chimiques, (iii) l'éjection et la réintroduction de particules du troisième corps dans le contact. En considérant tous ces facteurs pour accéder à l'information, il est clair que suivre le circuit tribologique est une tâche très complexe d'un point de vue expérimental, compte tenu de l'inaccessibilité du contact, fermé pendant le frottement.

Par conséquent, une approche réaliste doit être simplifiée autant que possible tout en conservant la possibilité d'introduire d'une manière ou d'une autre un troisième corps contrôlé artificiellement au lieu de subir des particules d'usure naturelles non

contrôlées provenant des premiers corps (c'est-à-dire le patin et le disque). En outre, l'approche doit permettre l'observation *in operando* de l'interface et de suivre sa variation spatio-temporelle. La stratégie consiste à développer une nouvelle expérience basée sur un circuit tribologique élémentaire dont on maîtrise la circulation des particules du troisième corps. Pour réaliser un tel circuit tribologique élémentaire, les matériaux (premier et troisième corps) doivent être choisis de manière à réduire, autant que possible, les couplages physiques et les réactions chimiques à l'interface. En outre, les paramètres opérationnels de l'expérience doivent être choisis de manière à ce que l'usure des premiers corps ait des effets négligeables sur le circuit tribologique et reste suffisamment faible pour maintenir une visibilité adéquate de la zone de contact observée à travers un disque transparent pendant le glissement.

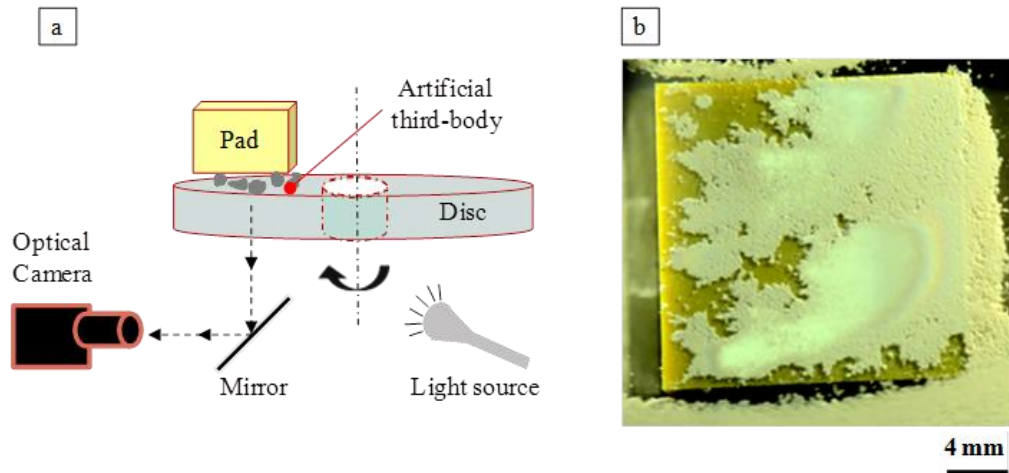
## **STRATÉGIE**

À la lumière de ce qui précède, l'objectif de la thèse est le développement d'une expérience originale permettant d'appréhender le comportement de la couche d'un troisième corps granulaire dans l'aire de portance et la façon dont elle évolue pendant le glissement de situations silencieuses à bruyantes. Pour cette raison, un troisième corps artificiel a été choisi (particules d'alumine chimiquement inertes) capable de former une couche cohésive et épaisse. Ce circuit tribologique a été mis en oeuvre sur un tribomètre élémentaire spécifique permettant de connaître les conditions dynamiques de fonctionnement et de conduire à l'apparition de phases crissements pendant les essais de friction (Duboc et al. 2013).

La thèse présente l'approche expérimentale développée. L'expérience est conçue pour maîtriser le circuit tribologique et pour permettre la surveillance *in operando* de l'aire de contact pendant le glissement. Le banc d'essai a été conçu pour fonctionner avec peu de modes vibratoires et de fréquences susceptibles de couplages afin d'en limiter le nombre et de rendre accessible l'analyse et la compréhension des phénomènes physiques impliqués dans les instabilités vibratoires associées. Enfin, un disque transparent, en verre, a été utilisé pour permettre l'observation optique de l'aire de contact fermée. Une représentation schématique du dispositif expérimental et un exemple d'image capturée pendant l'expérience sont présentés à la figure 1. Le choix du troisième corps et les protocoles expérimentaux définis permettent d'obtenir une couche de troisième corps suffisamment épaisse et large pour l'observation optique de l'aire de portance et le contrôle de ses grandeurs mécaniques. Les conditions d'essai



sont choisies de telle manière que le frottement n'endommage pas les premiers corps et qu'il y ait très peu ou approximativement pas d'usure.



## RÉSULTATS

Deux configurations expérimentales ont été explorées, capable de relever la difficulté à piéger le troisième corps et à le maintenir en contact tout au long de l'expérience, notamment lorsque le système est soumis à des vibrations. L'inclinaison du patin, pour ouvrir le contact au bord d'attaque et de le fermer au bord de fuite, le battement hors plan du disque, la quantité et la rhéologie du troisième corps et l'amplitude de sa compaction sont des éléments expérimentaux clé. L'expérience est menée avec une instrumentation cinématique, dynamique et acoustique nécessaire à connaître l'évolution des vibrations du système en adéquation avec l'évolution de la couche de troisième corps. Pendant l'essai, le patin et le disque sont totalement séparés, sans contact direct entre leur surface, c'est la couche du troisième corps qui a l'entière responsabilité de l'aire de contact avec la surface plane du disque. Les fluctuations de l'aire plane de contact, qui sont consécutives aux déplacements relatifs des premiers corps, sont continuellement accommodées par la couche de troisième corps. L'évolution temporelle de l'aire de contact est enregistrée par une caméra

optique à travers le disque transparent. À l'exception de la rotation du disque, aucune action extérieure n'est appliquée au tribosystème pendant l'essai, la charge normale du contact et sa variation étant notamment induites par l'élasticité du montage.

La figure 2 présente l'analyse temporelle d'une expérience, en termes de variation de la charge normale, de la pression sonore, et de fréquences des émissions sonores. La figure 3 montre des scènes successives de l'aire de contact, associés à des moments particuliers, (i) à (vii), de la chronologie de l'essai.

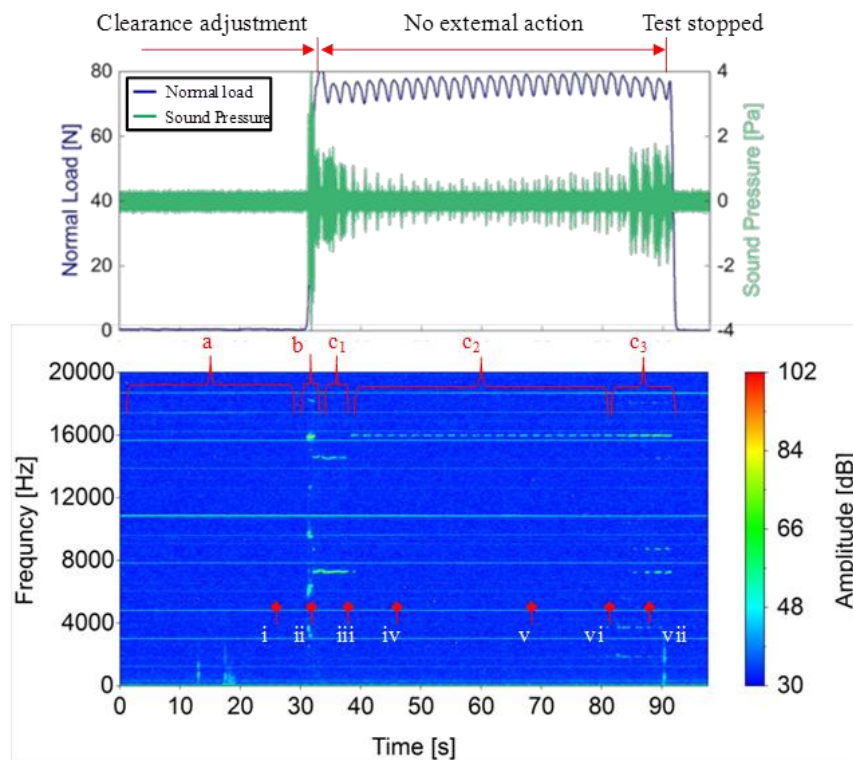


Figure 2. Analyse temporelle de l'expérience : variation de la charge normale et de la pression sonore, et diagramme fréquence-temps de l'émission sonore.

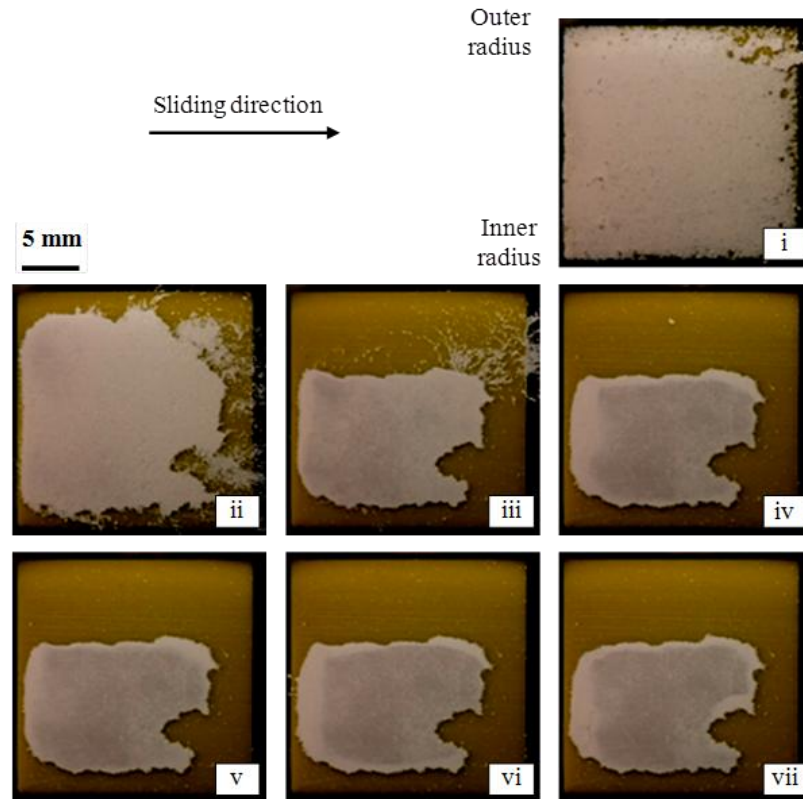


Figure 3. Scènes successives de l'aire de contact liées à des moments particuliers, (i) à (vii), dans la chronologie de l'essai présenté en figure 2 (sens de glissement du disque de la gauche vers la droite).

L'analyse des essais a montré que l'émission sonore est associée aux cycles de rotation et qu'elle concorde à la fluctuation cyclique de la charge normale, elle-même liée au battement du disque. L'émission sonore montre une lente évolution des occurrences de bruit, cycle après cycle, de manière concordante à l'évolution de plusieurs facteurs tribologiques et de leur fluctuation (aire et localisation de la portance, ouverture de contact, frottement) avant l'apparition du crissement.

L'analyse de l'interface a porté essentiellement sur la couche de troisième corps en relation avec l'historique locale de la portance. La fluctuation de la surface de contact est étudiée cycle après cycle par analyse d'images numériques, en termes d'étendue et de position dans l'aire apparente de contact, en relation avec la cinématique relative des premiers corps et les forces de contact. La surface portante se déplace ainsi lors d'une révolution du disque, de façon cyclique en fonction des ouvertures et fermetures du contact, le moteur de ce phénomène étant le battement micrométrique du disque. Une analyse quantitative de la variation de l'aire de portance a été réalisée. La figure 4 montre en exemple la fraction de l'aire apparente

de contact (constituée de l'ensemble du troisième corps compacté) qui contribue à la portance, pour 2 conditions d'ouverture de contact exprimées au bord de fuite, selon la position angulaire du disque en rotation. L'analyse a montré que l'ouverture du contact conduit à une baisse de la charge et du frottement.

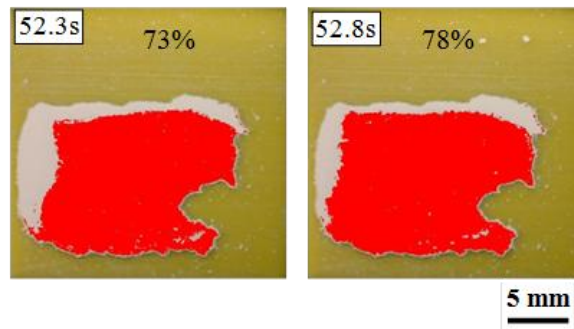


Figure 4. Mesure par analyse d'images de l'étendue de la portance, à ouverture de contact élevée à gauche, faible à droite (résultats en fraction de l'étendue totale de la couche de troisième corps, sens de glissement du disque de la gauche vers la droite).

La densification du troisième corps a été étudiée en profilométrie, en termes de porosité de surface et en profondeur au voisinage de la surface, en microscopie électronique à balayage de coupes FIB, les zones d'intérêt ayant été choisies selon l'historique locale de la portance. Les résultats montrent d'une part une densification du troisième corps d'autant plus grande que l'on est au voisinage de la surface en contact avec le disque, qui est interprété comme un écoulement et une réorganisation du troisième corps du au frottement dans le sens de glissement. D'autre part, la densification se manifeste plus en profondeur, selon l'historique de la localisation de la portance, donc de la charge locale, qui est interprétée par un écoulement normal et transverse du milieu granulaire. Ainsi, nous avons interprété les variations du frottement aux capacités du troisième corps à l'écouler, la fermeture du contact, bloquant les degrés de liberté des particules de troisième corps, conduisant à une élévation du frottement.

La figure 5 synthétise la corrélation entre l'aire de la portance (en fraction de l'aire apparent en bleu ciel), le frottement, l'ouverture du contact, le battement du disque et les émissions sonores de haute fréquence (à 16 kHz, périodes en vert sur la courbe d'ouverture de contact) observés pendant la lente phase évolutive du contact précurseur du crissement. Il est intéressant de noter que chaque occurrence de ces événements sonores apparait lorsque l'aire de portance atteint une valeur seuil (78%

de l'air apparente de contact dans l'exemple), le contact étant silencieux en dessous de ce seuil. L'occurrence sonore intervient alors que le frottement augmente, en cohérence avec l'augmentation de l'aire de contact, sans que l'on puisse associer une valeur seuil de frottement. Il est plus difficile d'établir un lien entre l'évolution du frottement et la disparition d'une occurrence de bruit.

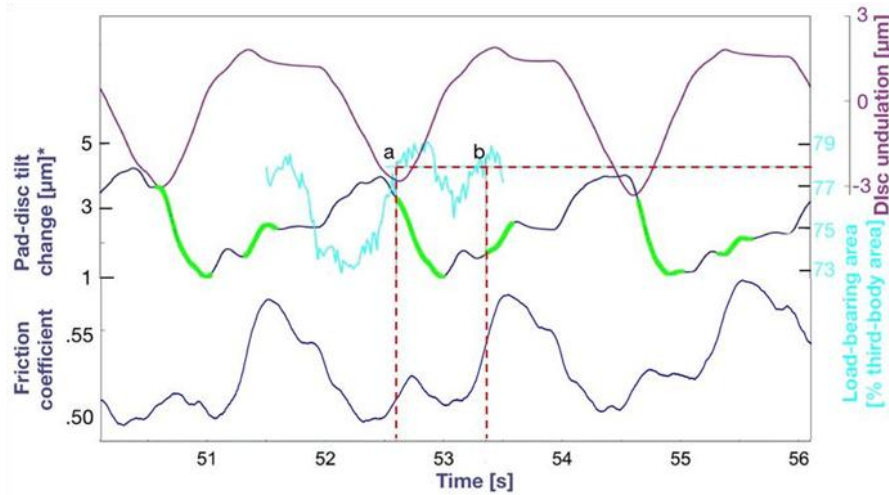


Figure 5. Corrélation entre les occurrences d'émission sonore (en vert) et l'étendue de l'aire de portance (en bleu ciel). (coefficient de frottement en bas en bleu sombre; ouverture du contact au milieu en bleu sombre, battement du disque en haut en violet).

## CONCLUSIONS

Ces travaux visent à étudier les conditions d'apparition de l'instabilité de crissement en lien avec les phénomènes mis en jeu au sein du circuit tribologique. En ce sens, une expérimentation élémentaire est développée, permettant de suivre la mise en place du circuit tribologique jusqu'à l'apparition du crissement.

Le tribosystème ainsi proposé, initialement silencieux, reste silencieux tant qu'aucun changement significatif n'est observé dans l'interface de contact par friction. L'introduction d'un troisième corps artificiel modifie la dynamique du tribosystème et l'amène à crisser. L'apparition du crissement est manifestement liée à la redistribution des particules du troisième corps dans l'interface, ce qui influence fortement l'aire de portance.

Les flux internes du troisième corps contribuent de manière significative à redistribution et à l'homogénéisation de l'aire de portance par l'accommodation de la vitesse. Il est possible de formuler certaines corrélations entre la variation moyenne du

frottement, le compactage de la couche de troisième corps et l'homogénéité de l'interaction de la surface avec le disque, confirmée par les analyses post-mortem (MEB-FIB, profilométrie).

En conclusion, l'expérience développée est reproductible et fiable pour observer *in situ* le contact frottant à son interface et pour suivre l'évolution de la couche de troisième corps qui conduit le système au crissement.

## **PERSPECTIVES**

Le travail présenté souligne la nécessité d'analyser plus avant les observations *in operando* de l'aire de contact afin de quantifier le compactage et la surface portante pendant le glissement. La résolution de la mesure doit également permettre d'obtenir des informations à différentes échelles (macroscopique à mésoscopique). La corrélation des images numériques serait utile pour l'identification des flux de troisième corps. Par ailleurs, une analyse quantitative de l'évolution *in situ* de l'épaisseur de la couche du troisième corps et de sa rigidité constituera la prochaine étape, par un traitement des données de déplacement et des efforts mesurés sur le dispositif. L'expérimentation doit être développée afin d'aborder la quantification des flux : quantité de poudre à introduire dans l'interface et flux de recirculation.

Les investigations futures pourraient inclure d'autres expériences en utilisant différents types de poudres artificielles du troisième corps pour appréhender l'influence de la taille des particules et de l'auto-organisation de la zone de charge sur l'apparition du crissement. D'autre part, plusieurs facteurs qui ont été maintenus constants tout au long de l'étude, tels que la température ou l'humidité, peuvent avoir une influence sur la surface portante

En complément une modélisation multi-échelle couplant un modèle numérique à macro-échelle avec un modèle d'interface de contact permettra d'investiguer l'effet des paramètres clés de l'apparition du crissement. Pour cela, une caractérisation plus poussée du troisième corps est nécessaire, en termes de propriétés de morphologies et de rigidité.

## **Résumé**

### **Etude expérimentale de la relation entre l'occurrence de bruit et l'aire de portance dans un contact sec glissant**

Les freins à friction peuvent induire des vibrations et du bruit, notamment le crissement, qui constitue un enjeu de santé publique majeur. Le crissement résulte d'une instabilité dynamique, responsable de vibrations de grande amplitude et d'émissions sonores intenses. Si le phénomène est bien connu en soi, l'origine des occurrences de crissement demeure mal comprise. Il est reconnu que le crissement est lié à de nombreux facteurs, parmi eux notamment l'usure des organes de friction. La nature multi-échelle des couplages physiques, la complexité des matériaux de friction et la nature fermée du contact, sont cependant autant d'obstacles à la compréhension de son apparition. Ce travail expérimental s'appuie sur la tribologie à trois corps et la notion de circuit tribologique pour explorer les mécanismes source de crissement, considérant que les écoulements du troisième corps modifient continuellement les surfaces de frottement et donc l'aire de portance pendant le glissement. L'objectif des travaux est d'examiner le lien entre l'évolution du troisième corps, celle du triplet tribologique et l'apparition du bruit en condition de frottement sec. Pour cela, un tribomètre élémentaire, dédié à l'analyse vibratoire d'un contact est utilisé, l'expérimentation permettant l'observation de l'interface à travers un disque transparent et un contrôle du circuit tribologique par l'usage d'un troisième corps artificiel et d'une configuration de contact appropriée. Les résultats montrent en particulier que l'apparition du crissement est fortement liée à la densification et à la redistribution de la couche de troisième corps dans le contact au cours du glissement.

## **Mots-clefs**

Crissement de frein, Vibrations induites par le frottement, Circuit tribologique, circulation de troisième corps

## **Abstract**

### **Experimental investigation of the relationship between noise occurrence and the load-bearing area in dry sliding contact**

Friction brakes can induce vibrations and noise, including squealing, which is a major public health concern. Squeal results from dynamic instabilities, leading to high amplitude vibrations and intense noise emissions. Although the phenomenon is well known, the origin of squealing occurrences remains poorly understood. It is recognized that squealing is related to many factors, including the wear of the friction parts. However, the multi-scale nature of physical couplings, the complexity of friction materials and the closed nature of contact are all obstacles to understanding its appearance. This experimental work is based on the third-body approach and the notion of a tribological circuit to explore the mechanisms originating squeal, considering that flows of third body at the interface continuously change the friction surfaces and thus the load-bearing area during the slip. The objective of the work is to examine the link between the change of the third body, that of the tribological triplet and the appearance of noise in dry friction conditions. For this purpose, an elementary tribometer dedicated to the analysis of contact vibrations is used, the experiment allowing a monitoring of the interface through a transparent disc and a control of the tribological circuit by the use of an artificial third body and an appropriate contact configuration. The results show in particular that the appearance of squealing is strongly related to the densification and redistribution of the third-body layer in the contact during sliding.

## **Keywords**

Brake squeal, Friction induced vibrations, Tribological circuit, Third-body flows